The Effect of Growth Method on GaN Films and Their Interfaces with CdTe and CdS

David Gouldey

Thesis submitted the faculty of the Virginia Polytechnic Institute and State University in partial fulfillment of the requirements for the degree of

Master of Science
In
Materials Science and Engineering

Robert Hendricks, Chair
William Reynolds
Wolfram Jaegermann (TU-Darmstadt)
Dimitris Pavlidis (TU-Darmstadt)

December 15, 2010
Blacksburg, VA

Keywords: Gallium nitride, wide-band gap semiconductors, cadmium sulfide, cadmium telluride, MOCVD

The Effect of Growth Method on GaN Films and Their Interfaces with CdTe and CdS

David Gouldey

ABSTRACT

This work has analyzed the complex interfaces of GaN and InGaN grown by sputter deposition and GaN grown by metal-organic chemical vapor deposition (MOCVD) with CdTe and CdS. First, the GaN and InGaN films were characterized by AFM and XRD, and it has been shown that the MOCVD samples have a very smooth surface and are single crystalline with growth in the (002) direction. On the other hand, the sputter deposited samples have rougher surfaces and are polycrystalline. Furthermore, complete interface studies have been performed using in-situ XPS and deposition between GaN grown by sputter deposition and MOCVD and CdTe and CdS to determine the band alignments, conduction and valence band offsets, and Fermi level positions. These interface studies will help determine basic properties to see if these GaN films can be incorporated in a CdTe solar cell to improve its efficiency. It was determined that all the interfaces between the sputtered GaN/InGaN and CdTe/CdS have small conduction band offsets of less than 0.1 eV that do not significantly prevent electron flow across the interface. However, the valence band offsets were much more significant, as they ranged from 0.43 eV to over 1.8 eV. For purposes of the desired positions of the GaN in the CdTe solar cell, the conduction band offsets are much more crucial, and very small conduction band offsets are desired. An interesting effect was that the interfaces between InGaN/CdTe and InGaN/CdS showed In migration into the CdTe and CdS, causing a rise in the Fermi level for the CdTe and CdS, which has been known to worsen the performance of the CdTe solar cell. The MOCVD GaN/CdTe and CdS interfaces showed a slightly higher conduction band offset of about 0.15 eV, but this barrier still should not significantly prevent current flow.

Acknowledgements

There are many people who I would like to thank for guiding me through this challenging and unique project. I owe a great deal of gratitude to Dr. Robert Hendricks at Virginia Tech for not only acting as my graduate committee chair, but also for giving me the wonderful opportunity to study and research at Technische Universität Darmstadt in Darmstadt, Germany. Dr. William Reynolds at Virginia Tech also deserves a big thank you, as his ICTAS facility has led to the partnership between Virginia Tech and TU-Darmstadt.

Prof. Dr. Wolfram Jaegermann and Prof. Dr. Dimitris Pavlidis at TU-Darmstadt provided me with constant support for my project. Also at TU-Darmstadt, Dr. Ganhua Fu helped me become familiar with laboratory techniques and trained me on the DAISY-SOL in the material science building. He provided day-to-day support and spent numerous hours helping me complete my project. Additionally, many thanks to Laurence Considine for the countless hours he spent explaining the MOCVD system in the electrical engineering department at TU-Darmstadt. Dr. Jens-Peter Biethan was also a huge help to me in the electrical engineering department, as he would always answer my day-to-day questions and provide assistance throughout the project.

Without the assistance of the aforementioned people as well as countless others, my project would not have been nearly as successful.

Table of Contents

Acknowledgements iii
List of Figures vii
List of Tables ix
List of Acronyms x
1. Introduction 1
  1.1. Semiconductor Overview 1
    1.1.1. Intrinsic Semiconductors 1
    1.1.2. Doping 3
    1.1.3. Fermi Levels 3
    1.1.4. Band Diagrams 5
    1.1.5. p-n Junctions 5
  1.2. Photovoltaic Devices 7
  1.3. CdTe Photovoltaic Devices 9
  1.4. Thesis Overview 11
2. GaN Background 13
  2.1. Material Properties 13
  2.2. Crystal Structure 14
  2.3. History and Major Breakthroughs 15
  2.4. Fabrication Methods 18
    2.4.1. Metalorganic Chemical Vapor Deposition 18
    2.4.2. Sputter Deposition 21
    2.4.3. Hydride Vapor Phase Epitaxy 23
    2.4.4. Other Deposition Methods 24
3. Experimental Details 25
  3.1. Sample Creation 25
    3.1.1 Sputter Deposition 25
    3.1.2 MOCVD 26
  3.2. Characterization 28
    3.2.1 X-Ray Diffraction (XRD) 28
    3.2.2 Atomic Force Microscopy (AFM) 31
4. Interface Studies 37
  4.1 Methods for Performing Interface Studies 37

4.1.1 X-Ray Photoelectron Spectroscopy (XPS) ... 37
4.1.2 Close Space Sublimation (CSS) ... 38
4.1.3 Structure of Interface Studies ... 38
4.1.4 What is Learned from Interface Studies ... 40
4.1.5 Different Interface Studies ... 44
4.2. Attempts for Contamination-Free MOCVD GaN ... 44
4.2.1 Attempts at removing surface contamination ... 44
4.2.2 MOCVD GaN with SiN cap ... 47
4.3. GaN and CdTe Interfaces ... 51
4.3.1. CdTe onto Sputtered GaN ... 51
4.3.2. CdTe onto MOCVD-GaN ... 54
4.3.3. Sputter Deposited InGaN and CdTe Interface ... 56
4.4. GaN and CdS Interfaces ... 59
4.5.1. CdS on Sputtered GaN ... 59
4.5.2. CdS on MOCVD-GaN ... 62
4.5.3. Sputter Deposited InGaN and CdS Interfaces ... 64
4.7. Interface Study Summary ... 67
5. Conclusions ... 72
6. Future Work ... 73
References: ... 74
Appendix A – Powder diffraction file (PDF) of hexagonal GaN ... 78
Appendix B – AFM pictures of 2 µm and 10 µm squares ... 79
Sputter Deposited GaN ... 79
Sputter Deposited InGaN ... 79
MOCVD GaN ... 80
CdTe on Sputtered GaN ... 80
CdTe on Sputtered InGaN ... 80
CdTe on MOCVD GaN ... 81
CdS on Sputtered GaN ... 81
CdS on Sputtered InGaN ... 81
CdS on MOCVD GaN ... 82
Appendix C – XPS and UPS Data for Interface Studies ... 83
Sputter Deposited GaN and CdTe Interface ... 83

MOCVD GaN and CdTe Interface 84
Sputter Deposited InGaN and CdTe Interface 86
Sputter Deposited GaN and CdS Interface 87
MOCVD-GaN and CdS Interface 89
Sputter Deposited InGaN and CdS Interface 90

List of Figures

Figure 1 - General band diagrams of an intrinsic, n-type, and p-type semiconductor. The band gap (E_g), ionization potential (I_P), electron affinity (χ), and the work function (φ) are shown. 5
Figure 2 - Band diagram for a p-n homojunction with the same concentration of n-type and p-type doping on either side of the interface 6
Figure 3 - Band diagram for a typical p-n heterojunction. Notice the different band bending between the two materials and the conduction band and valence band offsets 7
Figure 4 – The structure of a typical CdTe solar cell. Note, the layers are not to scale 10
Figure 5 – The wurtzite (hexagonal) structure of GaN [1] 14
Figure 6 – The zinc blende (cubic) structure of GaN [1] 15
Figure 7- The effect of increasing In concentration in a GaInN compound on the optical band gap of the material [55] 17
Figure 8 – Basic process flow for an MOCVD system 19
Figure 9 - Basic sputter deposition process 22
Figure 10 – Herb Maruska's HPVE reactor where the first single crystal GaN sample was created [21]. 23
Figure 11 – The DAISY-SOL in the materials science department at TU-Darmstadt, which houses the sputter chamber for the GaN and InGaN, the CSS system for both CdTe and CdS, and the XPS system. 26
Figure 12 – Thomas Swann MOCVD reactor in the electrical engineering department at TU-Darmstadt 27
Figure 13 - Theta 2-theta XRD measurements for sputter deposited GaN 29
Figure 14 - Theta 2-theta XRD measurements for sputter deposited InGaN 30
Figure 15 - Theta 2-theta XRD measurements for MOCVD GaN. While the blue lines are the actual XRD data, the green lines represent the wurtzite GaN peaks from the PDF, and the magenta lines represent the sapphire peaks from the PDF. 31
Figure 16 - AFM pictures of a 5 µm x 5 µm square of sputter deposited GaN (a) and InGaN (b) 32
Figure 17 – AFM picture of a 5 µm x 5 µm square of MOCVD GaN 33
Figure 18 - AFM pictures for a 5 µm x 5 µm square of CdTe on sputtered GaN (a) and sputtered InGaN (b) 34
Figure 19 - AFM pictures for a 5 µm x 5 µm square of CdTe on MOCVD GaN 34
Figure 21 - AFM pictures for a 5 µm x 5 µm square of CdS on MOCVD GaN 35
Figure 20 - AFM pictures for a 5 µm x 5 µm square of CdS on sputtered GaN (a) and sputtered InGaN (b) 35
Figure 22 - Flowchart describing the structure of the interface studies between GaN (or InGaN) and CdS/CdTe 40
Figure 23 - XPS measurements of the valence band to determine the Fermi level position relative to the valence band. Sputtered GaN prior to any CdTe deposition is on the left and CdTe after 32 minutes of deposition is on the right. 41
Figure 24 - Shifting of the XPS measurements for the Ga2p and Cd3d peaks over the course of the interface study to determine the band bending of each material 42
Figure 25 - UPS measurements for the bulk GaN (left) and bulk CdTe (right) and calculations to determine work function of each material 43
Figure 26 – XPS data from MOCVD-grown GaN sample exposed to air 45
Figure 27 – XPS data for the C1s peak of MOCVD-grown GaN, averaged over 20 scans 46
Figure 28 - XPS data for O peaks of MOCVD-grown GaN, averaged over 20 scans 47

Figure 29 – XPS surveys of samples before and after sputtering 48
Figure 30 - XPS measurements of the Si2s peak for GaN with a SiN cap 49
Figure 31 - XPS measurements of the valence band of GaN with a SiN cap 50
Figure 32 - XPS data of O1s peaks for GaN with SiN cap 50
Figure 33 - The XPS peaks of Ga, Te, Cd, and the valence band as the material shifts from bulk GaN (0 minutes CdTe deposition) to bulk CdTe (32 minutes CdTe deposition) 51
Figure 34 - Survey XPS measurements for the entire interface study of sputter deposited GaN and CdTe. Note the simultaneous decrease of the Ga and N peaks while the Te and Cd peaks gradually increase. ... 52
Figure 35 - UPS measurements for CdTe deposited on top of sputter deposited GaN 53
Figure 36 - Band diagram for CdTe deposited onto sputter deposited GaN. The GaN is on the left and the CdTe is on the right 54
Figure 37 - XPS peaks for Ga, Te, Cd, and the valence band as the material shifts from bulk GaN (0 minutes) to bulk CdTe (7 minutes) 55
Figure 38 - Band diagram for CdTe deposited onto MOCVD GaN. The GaN is on the left and the CdTe is on the right. 56
Figure 39 - XPS peaks for Ga, Te, In, Cd, and the valence band as the material shifts from bulk InGaN (0 minutes) to bulk CdTe (32 minutes) 57
Figure 40 - XPS survey data showing the presence of In after the N peak has disappeared 58
Figure 41 - Completed band diagram with Fermi level alignment for sputter deposited InGaN (left) and CdTe (right) 59
Figure 42 - XPS peaks for Ga, Cd, S, and the valence band as the material shifts from bulk GaN (0 min) to bulk CdS (16 min) 60
Figure 43 - Left: The change in Fermi level position for each element as the interface study proceeds. Right: The change in valence band offset between the two materials as the interface study proceeds. 61
Figure 44 - Completed band diagram with Fermi level alignment for sputter deposited GaN (left) and CdS (right) 62
Figure 45 - XPS peaks for Ga, Cd, S, and the valence band as the material shifts from bulk GaN (0 min) to bulk CdS (8 min) 63
Figure 46 - Completed band diagram with Fermi level alignment for sputter deposited GaN (left) and CdS (right). The UPS was not functioning properly during this interface study, so there is no information about the electron affinity or the vacuum levels. 64
Figure 48 - XPS survey data showing the presence of In after the N peak has disappeared 65
Figure 47 - XPS peaks for Ga, In, Cd, S, and the valence band as the material shifts from sputter deposited InGaN (0 min) to CdS (16 min) 65
Figure 49 - Completed band diagram with Fermi level alignment for the sputter deposited InGaN (left) and the CdS (right) 66
Figure 50 - Comparison between the values E_F-E_{VB} for GaN and InGaN. The MOCVD GaN films have the highest Fermi level position position. 68
Figure 51 - Bulk Ga2p peak for sputtered GaN, sputtered InGaN, and MOCVD GaN 69
Figure 52 - E_F-E_{VB} values for CdTe films deposited onto sputter deposited GaN and InGaN as well as MOCVD GaN 70
Figure 53 – E_F-E_{VB} values for CdS films deposited onto sputter deposited GaN and InGaN as well as MOCVD GaN 70
Figure 54 - CdTe coverage of MOCVD grown GaN (left) and sputter deposited GaN (right). 71

List of Tables

Table 1 – Electrical resistivities of selected intrinsic semiconductors and metals.. 2
Table 2 – Electronic properties for selected semiconductors [24].. 13
Table 3 – Timeline of the breakthroughs in GaN history 18
Table 4 - Summary of RMS roughness data acquired from AFM measurements 36
Table 5 - Band gaps of materials used in interface studies determined by optical absorption 43
Table 6 - Summary of interface studies 67

List of Acronyms

AFM	atomic force microscopy
CdTe	cadmium telluride
CdS	cadmium sulfide
DAISY-SOL	Darmstadt Integrated System for Solar Cell Research
GaN	gallium nitride
HVPE	hydride vapor phase epitaxy
InGaN	indium gallium nitride
LED	light-emitting diode
MBE	molecular beam epitaxy
MOCVD	metal organic chemical vapor deposition
MOVPE	metal organic vapor phase epitaxy
PED	pulsed electron deposition
SiN	silicon nitride
TCO	transparent conducting oxide
UPS	ultraviolet photoelectron spectroscopy
XPS	x-ray photoelectron spectroscopy
XRD	x-ray diffraction

1. Introduction

1.1. *Semiconductor Overview*

1.1.1. Intrinsic Semiconductors

Semiconductors are a unique type of material since their electrical properties can be easily controlled through temperature and composition. There are two general types of semiconductors: homogenous and compound. Homogenous semiconductors contain only one element which comes from Group IV on the periodic table, such as silicon (Si) or germanium (Ge). On the other hand, compound semiconductors consist of an alloy of two or more elements that are usually a combination of group III and group V elements (such as GaN, GaAs, AlN) or group II and group VI elements (such as ZnO, ZnTe, CdTe). Semiconductors typically crystallize in the diamond structure if they are homogenous or in the zinc-blende structure if they are compound [1]. These structures have a tetrahedral arrangement of four equidistant neighboring atoms, which is an important feature of semiconductor physics [1].

Semiconductors are characterized by their band gaps. By using quantum mechanics and the Schrödinger equation, it is concluded that the electrons of a material can only exist in certain states or energy levels. The valence band of a material is considered as the state of electrons furthest away from the nuclei while still being fully bonded to the individual atom. The conduction band is the lowest energy state for an electron to break from its bond to an individual atom, so that it can now move freely through the lattice and contribute to electrical conduction. The size of the band gap is a very important property of semiconductor materials, and it is simply the energy difference between the conduction and valence bands. Unlike insulators, with very large, essentially infinite band gaps, or metals, where the conduction band and the valence band often overlap each other, there is a finite separation in semiconductors between the valence bands and the conduction bands. In this band gap, no energy states, e.g. electrons, can exist, which is why the band gap is often referred to as the forbidden gap [2]. At 0 K, the valence band of a semiconductor is completely full and the conduction band completely empty because electrons need some form of external stimulation to jump across the band gap. This is achieved with thermal energy, electrical excitation, or light irradiation. The intrinsic carrier concentration n_i due to thermal energy can be calculated as:

$$n_i = \sqrt{N_C N_V} e^{-E_g/2kT} \quad (1)$$

where N_C is the density of states at the conduction band edge, N_V is the density of states at the valence band edge, E_g is the band gap of the material, k is the Boltzmann constant, and T is the temperature in

Kelvin. Thus, methods to increase the intrinsic carrier concentration include using a material with a lower band gap or raising the operating temperature.

There are two types of band gaps for semiconductors, and they are termed direct and indirect. A direct band gap, like that found in GaN and CdTe, requires only an energy transfer to cause an electron to jump from the valence band to the conduction band. However, in an indirect semiconductor like Si, both a transfer of energy and momentum are usually required to promote an electron across the band gap [1].

When an electron jumps into the conduction band, it leaves behind a formerly neutral atom in the valence band. Since this atom was neutral before it lost a negatively charged electron, it now carries a positive charge equal in magnitude to the charge of an electron. This positive charge is termed a hole, and it also contributes to the electrical conduction of a semiconductor. Because of the hole's positive charge, a neighboring valence band electron will jump to the positive charge to replace the missing electron. The hole now exists in the atom from which the electron jumped. Another electron will transfer from a neighboring atom to fill the positively charged hole, and this process continues indefinitely. Thus, the hole is able to migrate throughout the lattice by the movement of electrons compensating the positive charge of the hole. The electrical conductivity in a semiconductor is described as [3]:

$$\sigma = qn\mu_n + qp\mu_p \tag{2}$$

where q is the magnitude of an electron charge, n is the number of electrons in the conduction band, μ_n is the mobility of an electron in the lattice, p is the number of holes in the valence band, and μ_p is the mobility of a hole in the lattice. In intrinsic semiconductors, n is equal to p, and their product is equal to n_i^2, the square of the intrinsic carrier concentration from equation 1 [1]. However, at room temperature, intrinsic semiconductors are often not conductive enough to be useful in devices. Table 1 lists the electrical resistivities of some intrinsic semiconductors in comparison with some common metals at room temperature, and it is clear that the semiconductors have electrical resistivities that are many orders of magnitude higher than the conductive metals.

Table 1 – Electrical resistivities of selected intrinsic semiconductors and metals

Material	Type	Resistivity (Ω)
Silicon	Semiconductor	2.3×10^{5} [4]
Germanium	Semiconductor	0.53 [5]
Aluminum	Metal	26.55×10^{-9} [6]
Copper	Metal	16.73×10^{-9} [7]

1.1.2. Doping

In order to increase the conductivity of semiconductors, impurity atoms, or dopants, are often introduced into the semiconductor. When dopants are added to the semiconductor material, it is now referred to as an extrinsic semiconductor instead of an intrinsic semiconductor. There are two types of dopants: donors and acceptors. Donors donate electrons to the conduction band whereas acceptors accept electrons, or rather donate holes to the valence band. As aforementioned, atoms in semiconductor lattices are normally tetrahedrally bonded to their nearest neighboring atoms. If a donor atom takes the place of a normal atom, the material now has at least one more electron than is needed to complete the bond, and these extra electrons can move freely through the crystal, allowing them to contribute to electrical conduction. Conversely, if a normal atom is replaced with an acceptor atom, then it has one less electron than is needed to form the tetrahedral bond, and a hole is introduced. As described in the previous section, electrons will continually compensate this positive charge, and the hole migrates throughout the lattice, contributing to electrical conduction [3]. When donors are used as the doping material, then the semiconductor is referred to as n-type, as additional negative charges are supplied to the semiconductor. On the other hand, a material doped with acceptors is termed p-type, since additional positive charges are supplied to the semiconductor. Adding tiny amounts of dopants can drastically increase the conductivity of a semiconductor.

An n-type doping material usually comes from one group to the right of the semiconductor material on the periodic table, such as phosphorous for silicon. Conversely, a p-type doping material usually comes from one group to the left of the semiconductor material on the periodic table, such as boron for silicon. For gallium nitride and other compound semiconductors, the doping materials can often come from other places in the periodic table. Gallium nitride usually takes magnesium or zinc as a p-type dopant and silicon or oxygen as an n-type dopant.

1.1.3. Fermi Levels

Fermi-Dirac statistics can be used to describe the energetic position of electrons in a semiconductor. According to these statistics, the probability of finding an electron at a given energy level in a semiconductor can be approximated by [8]:

$$f(E) = \frac{1}{1+e^{(E-E_F)/k_B T}} \qquad (3)$$

where k_B is the Boltzmann constant (1.38×10^{-23} J/K or 8.62×10^{-5} eV/K) and T is the absolute temperature. E_F is termed the Fermi level and is defined as the energy level of a semiconductor at which the probability of finding an electron is equal to 0.5, as can be seen if E_F is inserted for E into the function [8]. The Fermi level is a very important characteristic of a semiconductor, as its position describes key

aspects of bulk semiconductors as well as interfaces. In intrinsic semiconductors, the Fermi level can be calculated by:

$$E_F = \frac{E_g}{2} + \frac{3k_BT}{4}\ln\frac{m_e^*}{m_h^*} \quad (4)$$

m_e^* is the effective electron mass for that semiconductor and m_h^* is the effective hole mass. Both values can be easily looked up for various semiconductors. It should be noted that the Fermi level generally lies close to the midpoint of the band gap in intrinsic semiconductors. While the Fermi level usually lies inside the band gap, it should be noted that still no electrons are actually located in the forbidden gap [8]. The Fermi level simply gives an idea for the carrier properties of the semiconductor. The closer the Fermi level is to either the conduction band or the valence band, the higher the conductivity of the material. When dopants are added to the semiconductor, they introduce dopant energy states, which lie close to the conduction band for n-type dopants and close to the valence band for p-type dopants. If moderate doping concentrations and temperatures are assumed, then the distance from the conduction band to the Fermi level can be approximated for an n-type semiconductor by:

$$E_{CB} - E_F = k_BT\ln\frac{N_C}{n} \quad (5)$$

Similarly, for a p-type semiconductor, the distance from the Fermi level to the valence band is:

$$E_F - E_{VB} = k_BT\ln\frac{N_V}{p} \quad (6)$$

N_C and N_V are the density of states in the conduction and valence bands respectively. n is the concentration of free electrons and is roughly equal to the concentration of donors in an n-doped semiconductor. p is the concentration of free holes and is roughly equal to the concentration of acceptors in a p-type semiconductor. If the concentration of the dopant is known, then the minority carrier concentrations (holes in n-type material or electrons in p-type material) can be determined by the following charge neutrality condition [8]:

$$np = n_i^2 \quad (7)$$

where n_i is the intrinsic carrier concentration, as calculated from equation 1.

At an interface between a metal and a semiconductor or between two semiconductors, the Fermi levels of the two materials become aligned at thermal equilibrium, causing a band bending in the conduction and valence band of each material that represents a built-in voltage. The Fermi level position is very important to describing the interface.

1.1.4. Band Diagrams

The easiest way to visualize energy levels in semiconductors is to examine band diagrams. Figure 1shows basic band diagrams for intrinsic, n-type, and p-type materials. The vacuum level (E_{Vac}), conduction band energy (E_{CB}), Fermi level (E_F), and valence band energy (E_{VB}) are shown on the left. Values such as the band gap (E_g), ionization potential (I_P), electron affinity (χ), and work function (φ) are shown in the figure. Since Figure 1makes it appear that I_P, for example, is exclusive to the intrinsic semiconductors, it should be noted that the I_P, χ, and φ are related and coexist in all intrinsic, n-type, and p-type semiconductors.

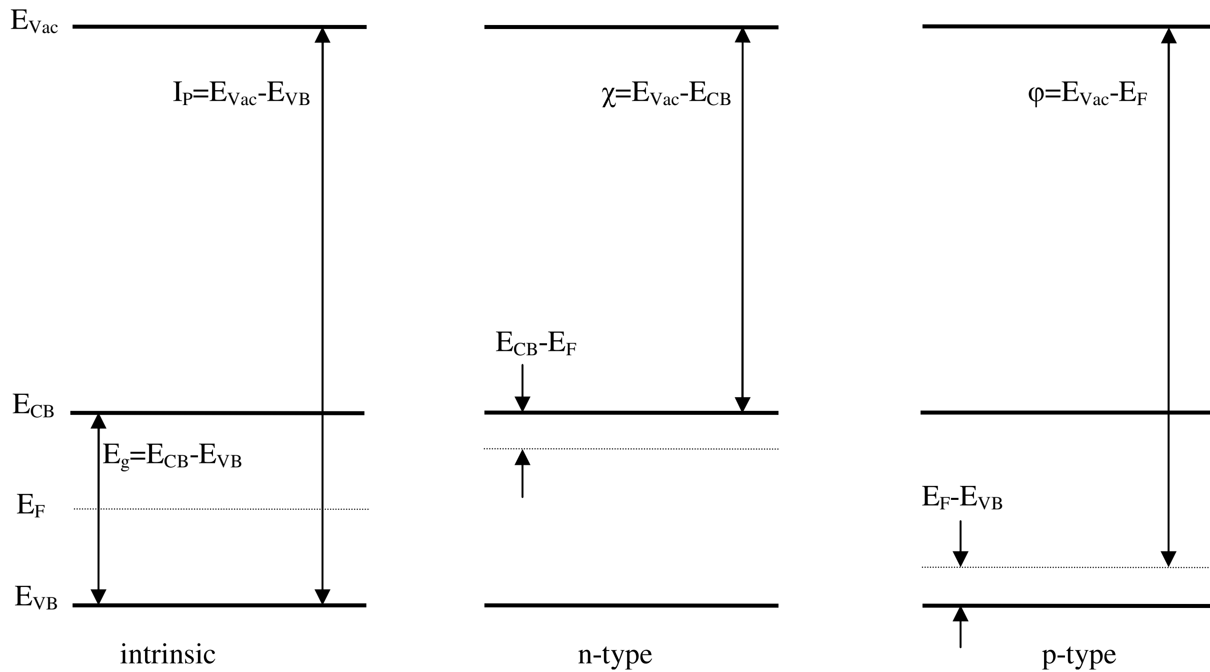

Figure 1 - General band diagrams of an intrinsic, n-type, and p-type semiconductor. The band gap (E_g), ionization potential (I_P), electron affinity (χ), and the work function (φ) are shown.

1.1.5. p-n Junctions

A p-n junction exists when a p-type material and an n-type material are placed in contact with each other, and a p-n homojunction occurs when the same semiconductor material (with different dopants) is used on either side of the junction, or interface. At the p-n junction, there are diffusion currents, as holes diffuse from the p-type region into the n-type region and electrons diffuse from the n-type region into the p-type region due to the concentration gradient. The holes in the n-type region and the electrons in the p-type region are called the minority carriers. As electrons are at lower energies in the n-type material and holes are at lower energies in the p-type material, drift currents also form which flow in the opposite direction to the diffusion currents, meaning the electrons drift from the p-type material to

the n-type material. When no external energy source is applied, the drift current is equal and opposite to the diffusion current, resulting in charge neutrality. However, due to the constant movement of charges from both sets of currents, an internal electric field (qV_{bi}) develops at the junction [9], as is represented by the band bending. This internal field is a result of the Fermi levels becoming equal at the junction. Figure 2 shows the course of the bands for a p-n homojunction.

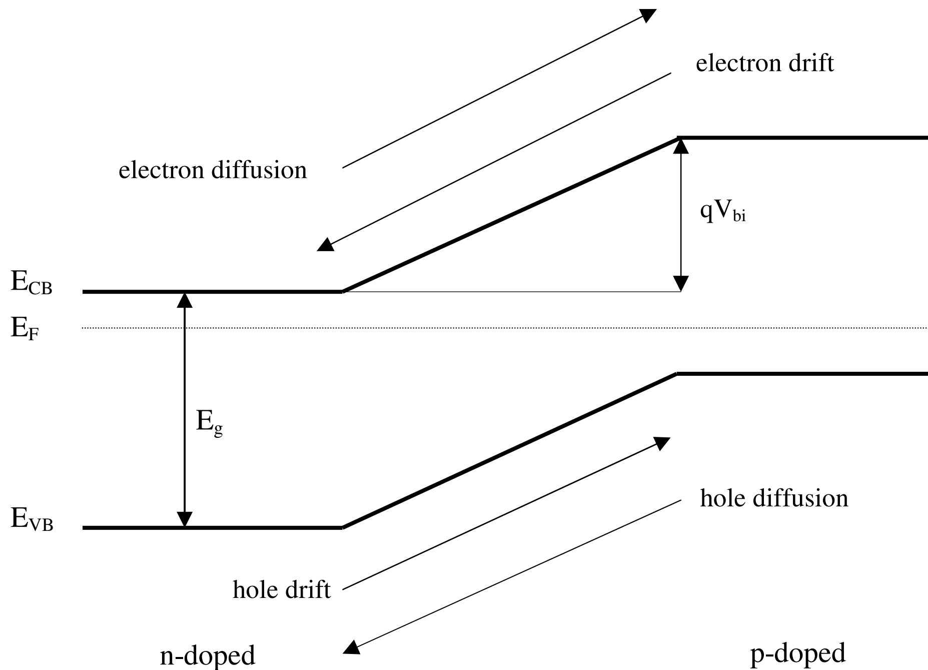

Figure 2 - Band diagram for a p-n homojunction with the same concentration of n-type and p-type doping on either side of the interface

A heterojunction occurs when different semiconductor materials are put in contact with each other. Like in homojunctions, a band bending develops where the p-type material generally bends down and the n-type material generally bends up. However, in p-n heterojunctions, due to differences in band gaps and work functions between the materials, there are often offsets, or barriers, that form in the conduction band and valence band, which inhibit the flow of electrons or the flow of holes across the interface. These offsets are characteristic of the junction of the materials, and do not depend on doping levels. On the other hand, doping levels do influence the work functions of the materials, and thus the amount of band bending [1]. The n-type side of the junction usually bends up, meaning it becomes more p-type at the interface, and the p-type side of the junction bends down, becoming more n-type at the interface. Figure 3 shows a typical p-n heterojunction with different band gaps.

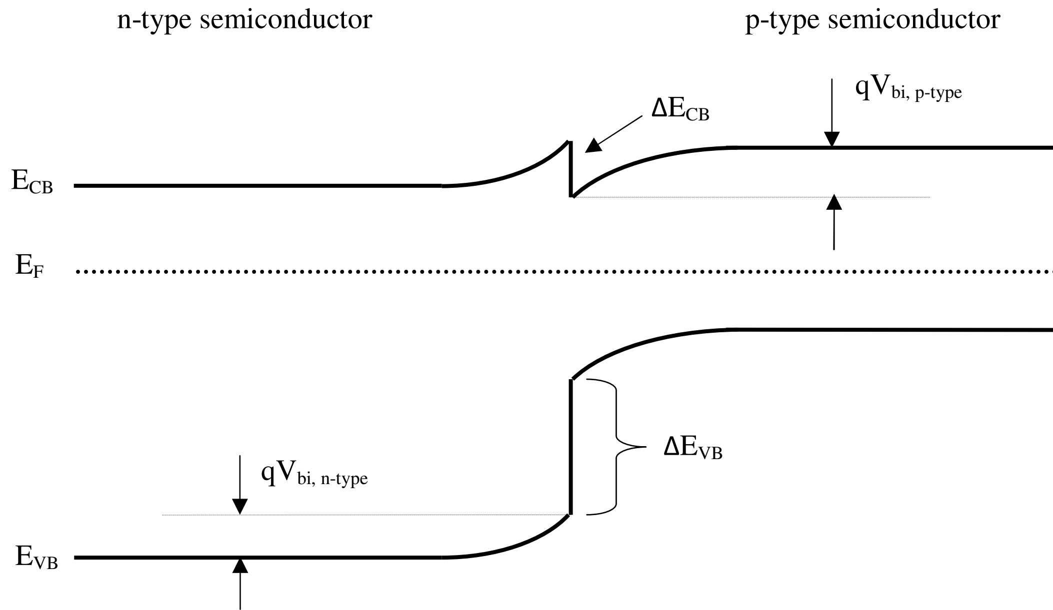

Figure 3 - Band diagram for a typical p-n heterojunction. Notice the different band bending between the two materials and the conduction band and valence band offsets

1.2. Photovoltaic Devices

In addition to integrated circuits and computer chips, a large application for semiconductors is photovoltaic devices, also known as solar cells. Photovoltaics are devices that convert sunlight (or any light source) directly into electricity. The amount of sunlight that illuminates the earth is 14,000 times higher than the amount of energy the world consumes in one year [10]. Between this fact and the emerging movement for renewable, environmentally-friendly energy, the photovoltaics industry continues to expand. For example, in 1998, there were 19 photovoltaic-manufacturing companies in the United States and 21,201 domestic shipments of solar cells and modules. Just nine years later, in 2008, there were 66 photovoltaic manufacturers in the United States and 524,252 domestic shipments [11].

Although the production and commercialization of solar cells is fairly recent, they have a history that dates back to the mid-1800s. In 1839, a French scientist named Edmund Becquerel first discovered the photovoltaic effect, when he noticed a small increase in current was produced when his metal samples was exposed to light. The first genuine solar cell was built out of selenium and described by Charles Fritts in1883 [12]. In 1905, Albert Einstein theoretically explained the photoelectric effect, which causes electrons to eject or emit from the surface of a material when it is struck by incident light [12]. His explanation regarded light as packets or quanta of energy rather than waves, and his theory was later proven mathematically to be valid by Robert Millikan in 1916 [12]. In 1941, Russell Ohl discovered the p-n junction in silicon and patented the first crude silicon photovoltaic device [13]. This was a huge

discovery for the photovoltaic industry as, today, most solar cells are made with silicon. In 1958, the American satellite Vanguard I used solar power for the first time in outer space [12]. Sharp Corporation created the first practical silicon solar cell module in 1963, paving the way for residential and commercial applications [12]. From there, the United States, Germany, and Japan have been the world's leaders in photovoltaic research.

In terms of a semiconductor structure, photovoltaic devices are fairly simple. These devices consist of a basic p-n junction, where one side of an interface is a p-doped semiconductor and the other side is n-doped. When light illuminates the surface of the semiconductor material, the photon energy causes electrons to jump from the valence band to the conduction band in the absorbing material, resulting in electron-hole pairs. The internal electric field caused by the p-n junction separates the minority carriers and draws them across the interface, resulting in a finite current flow. When there are electrical contacts on each side of the junction and a resistance load is applied, the current flows through the load, causing the current to dissipate. Thus, the non-equilibrium current can be captured and used as an energy source [9-10].

The short-circuit current, I_{sc}, is the maximum current that results when a solar cell is illuminated and there is no applied load, meaning the back contact is in direct contact with the front contact. The open-circuit voltage, V_{oc}, is the maximum voltage measured between the front and back contact when the contacts are not connected and no current is flowing. The theoretical optimal power, $P_{opt,}$ which can be produced by the solar cell is thus:

$$P_{opt} = I_{sc} \cdot V_{oc} \tag{8}$$

However, the I-V curve of a solar cell is not perfectly rectangular, and the maximum attained power, P_m, is the product of I_m and V_m. The fill factor, FF, is thus defined as the ratio between P_m and P_{opt} :

$$FF = \frac{P_m}{P_{opt}} = \frac{I_m V_m}{I_{sc} V_{sc}} \tag{9}$$

To achieve the best efficiency, a fill factor of close to one is desired, although a very good polycrystalline film will have a fill factor of close to 80% [9].

The absorption length is the depth into the semiconductor where the intensity of the light drops to 1/e (about 37%) of the initial intensity, or rather, 1-1/e (about 63%) of the light is absorbed by the material, causing the electron-hole pairs to form [9]. A short absorption length is desired so that most of the light can be absorbed using less material. Silicon, however, has a long absorption length, thus a low absorption coefficient, so a relatively large amount of material is required to absorb all of the incoming

light [9]. Therefore, other materials with larger absorption coefficients are currently being researched for solar cells so that thin film solar cells can become a reality.

Probably the most important number for photovoltaic devices is its conversion efficiency, which is defined as the ratio of generated electrical power to the energy of the incident radiation:

$$\eta_{pv} = \frac{Electrical\ output}{Energy\ of\ incident\ light} = \frac{P_m}{P_{light}} = \frac{FF \cdot P_{opt}}{P_{light}} = \frac{FF \cdot I_{sc} \cdot V_{oc}}{P_{light}} \tag{10}$$

Although Sharp has claimed the world record for highest conversion efficiency of a solar cell (35.8%) using a compound solar-cell structure with three p-n junctions [14], the conversion efficiencies are usually much lower for normal solar cells. There are many reasons for low efficiencies. First and foremost, the semiconductor is only able to absorb light with energy greater than the band gap of the material, so a portion of the sunlight spectrum with low energy is immediately unable to be absorbed. Another reason for low efficiency is optical losses that cause the intensity of the light to be lower when it is absorbed by the semiconductor than when it first hits the solar cell. Between reflection, absorption, and refraction at the various layers of the structure, a portion of the incident light does not reach the semiconductor absorbing material. The next reason for lower efficiencies is ohmic losses that result from resistance in the current pathways. Another reason for low efficiencies is due to recombination of electron-hole pairs. The incident light may induce an electron-hole pair, but if it recombines before it reaches the p-n junction, no current is produced. Additionally and most importantly, when incident light with energy much higher than the band gap reaches the semiconductor, the excited electron is promoted to a state well above the conduction band. However, the electron will then relax from the higher energy level into the conduction band, and this excess energy is transferred to phonons and heat instead of providing additional current [10]. Thus, much of the energy of the incoming light is unusable or transferred to other processes, causing the conversion of solar energy to electrical energy to not be very efficient.

1.3. CdTe Photovoltaic Devices

As our intentions are to use the GaN film in cadmium telluride (CdTe) solar cells, it is necessary to have a brief summary of CdTe device technology. There are several advantages of creating photovoltaic devices with CdTe. It has an almost perfect-sized band-gap (1.49 eV) that matches the solar spectrum for optimal photovoltaic conversion efficiency [15]. This means that the peak of the solar energy spectrum has about the same energy as the band gap of the material. Furthermore, CdTe's direct band gap gives it a high absorption coefficient, meaning it can absorb nearly all of the incoming solar radiation in just a couple μm of material [16].

A typical CdTe photovoltaic device has a superstrate structure. A transparent substrate is needed for light to pass through into the photovoltaic structure, and these substrates are usually borosilicate glass [15] or soda-lime glass [16]. On top of the substrate, a transparent conducting oxide (TCO) is required so that light can pass through while still being conductive to act as a front contact. Although newer materials such as Cd_2SnO_4 have been experimented with for a front contact [17], typically the front contact consists of tin-doped indium oxide (ITO) or fluorine-doped tin oxide (FTO) [16]. A thin layer of intrinsic tin oxide (SnO_2) is then deposited to ensure coverage over the ITO or FTO, so that in case of pinholes in the CdS layer, there will not be a direct front contact/CdTe connection. When ITO is used as the front contact, the SnO_2 also prevents In diffusion into the CdS/CdTe. Next, the n-type window layer is required for the p-n junction. Ideally, this layer will be very thin and absorb no light, however the band gap of CdS absorbs a portion of the incident light in the short wavelength region and has almost a 10% lattice mismatch with CdTe [17]. Still, CdS is the most common material used for this purpose. Naturally, the CdTe layer comes next, as this forms the p-portion of the p-n junction since it can be grown to be contain Cd vacancies, making it intrinsically p-doped [16]. The CdTe layer is much thicker than the CdS, and ideally, this is where all of the light is absorbed. Next, the structure is annealed in a $CdCl_2$ atmosphere, which causes the CdS layer to become more n-doped and leads to a strong CdS/CdTe interdiffusion layer, relieving many of the defects and recombination centers due to the lattice mismatch [18]. This interdiffusion step is crucial to producing viable CdTe solar cells. Before the back contact is deposited, a nitric/phosphoric etch is used on the CdTe to remove contaminants and create a Te rich surface. At TU-Darmstadt, a metal (usually Au) is then deposited onto the Te to complete the back contact. Figure 4 shows the order of the layers in a CdTe solar cell.

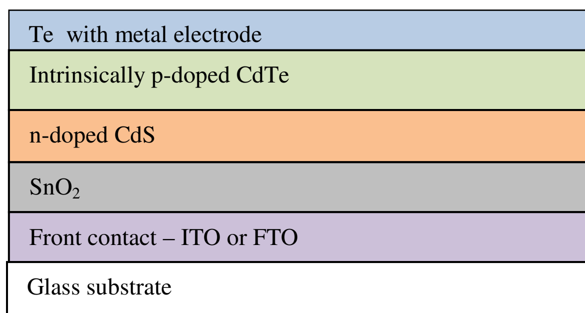

Figure 4 – The structure of a typical CdTe solar cell. Note, the layers are not to scale

It is believed that the first CdTe photovoltaic device was created by Russian scientists in 1960 [19]. Since then, there has been much research performed to optimize the CdTe solar cell. While the highest published efficiency for a CdTe solar cell (16.5%) is attributed to X. Wu at the National Renewable Energy Laboratory [17], recently a joint venture between Sunovia and EPIR Technologies has

claimed an efficiency of 24% using single-crystal CdTe deposited by molecular beam epitaxy onto a silicon substrate [20].

1.4. Thesis Overview

My research has been performed at TU-Darmstadt in Darmstadt, Germany, as part of an international exchange program. My work has been in collaboration with the surface science group in the materials science department and the high frequency electronics group in the electrical engineering department. The surface science group is currently working on several projects, but my research is with a group that is trying to improve the efficiency of cadmium telluride solar cells.

The long-term goal of the project I am working on is to incorporate a GaN or InGaN film into the current CdTe solar cell device. There are two films in the solar cell that could potentially be replaced with GaN, and they are the CdS and the SnO_2 films. As aforementioned, the n-type CdS film has a band gap of about 2.4 eV, so it absorbs some of the incident light before it reaches the CdTe absorber film. GaN has a larger band gap of about 3.39 eV, so it will absorb less of the incoming light. Unfortunately, Dr. Fu has already attempted to create this solar cell, and it yielded poor results, probably because the interdiffusion between CdS and CdTe is necessary. Thus, it would be possible to thin the CdS layer using GaN, but not fully replace it. On the other hand, it is hoped that the SnO_2 film can be replaced with GaN. The SnO_2 film has two functions when an ITO contact is used. First, it acts as a buffer layer between the CdS and ITO to prevent In diffusion into the CdS. Secondly, it ensures that the CdTe is not in contact with the ITO (or FTO if used as the front contact) if the CdS is relatively thin and could have pinholes. If the SnO_2 film is thin enough, electrons can tunnel from the CdS to the ITO front contact. The problem with the SnO_2 is that it is often too conductive, which decreases the shunting resistance in the cell, often causing an increase in the recombination of charge carriers. The hope is that the GaN will be more electrically resistive to improve the performance of the solar cell.

Before the GaN films can be adequately included in a CdTe solar cell, the nature of the GaN films and how they interact with CdS and CdTe must be understood. Therefore, my research has two main goals:

1. To examine the physical differences between GaN grown via sputter deposition and metal-organic chemical vapor deposition (MOCVD)
2. To investigate the interfaces between GaN and CdTe/CdS using photoelectron spectroscopy for potential applications in CdTe solar cells

To achieve these goals, three different types of samples were created: sputter deposited GaN, sputter deposited InGaN, and MOCVD-grown GaN. These samples were then characterized by atomic force microscopy (AFM) to understand the surface roughness and x-ray diffraction (XRD) to check the crystalline properties of the samples. After characterization, interface studies were performed using x-ray photoelectron spectroscopy (XPS) and ultraviolet photoelectron spectroscopy (UPS) between the GaN samples and both CdTe and CdS. These techniques yield information about composition, band bending, and the Fermi level positions of both semiconductors at the interface. Each sample of GaN and InGaN underwent an interface study with CdTe and CdS, and the results were examined and compared.

As aforementioned, this work has been split between the materials science department and the electrical engineering department at TU-Darmstadt. The materials science department houses the XPS, AFM, XRD, and the sputter deposition tool for GaN/InGaN. The XPS, the sputter deposition tool, and the close space sublimation chambers for CdTe and CdS deposition are integrated into a system known as the Darmstadt Integrated SYstem for SOLar cell research, or DAISY-SOL. The DAISY-SOL is a wonderful device, as it enables both deposition and characterization to be performed in an ultra-high vacuum environment, preventing contamination of samples. Meanwhile, the MOCVD GaN samples were grown in the electrical engineering department. I have had the opportunity to meet and work with very helpful and knowledgeable people in both groups.

This paper begins with a very basic overview of semiconductor materials, photovoltaic devices, and cadmium telluride solar cells. The next section reviews the properties, history, major breakthroughs, and deposition of gallium nitride. Following all of the background research, the methods and results of the comparison between the MOCVD-grown GaN and the sputter deposited GaN are presented. Next, the interface studies are fully explained and presented. Following is a brief section that examines what conclusions can be drawn from this research. Finally, there is a short section on what needs to be done in the future for this project.

2. GaN Background

2.1. Material Properties

Since this project revolves around the deposition and implementation of gallium nitride in a CdTe solar cell, a brief review of GaN is offered to give an understanding of its properties and limitations. GaN is a III-V compound semiconductor, as the gallium comes from group III in the periodic table and nitrogen comes from group V. James Tietjen of Radio Corporation of America (RCA) first realized in the late 1960s that single-crystal GaN could yield a blue light-emitting diode (LED) [21]. As first reported by Maruska in 1969, GaN has a wurtzite (hexagonal) structure with lattice constants a=3.189 Å and c=5.185 Å, and a direct band gap of 3.39 eV at room temperature [22], classifying it as a wide-band gap semiconductor. Direct band gap semiconductors are desirable in applications such as solar cells or LEDs because they have a much higher probability of optical transition than indirect semiconductors for both the absorption and emission of photons [23].

Table 2 shows some important electronic properties for certain semiconductors [24]. Due to its wide band gap, GaN has a low intrinsic carrier concentration (n_i) of about 1.9 x 10^{-10} cm^{-3}, an electron mobility (μ_n) of about 900 $cm^2/V{\cdot}s$, and a hole mobility (μ_p) of about 50 $cm^2/V{\cdot}s$, making it much less conductive at room temperature than other semiconductors such as silicon, germanium, and gallium arsenide, which is another III-V semiconductor [24].

Table 2 – Electronic properties for selected semiconductors [24]

Material	E_g eV	ε_r	μ_n $cm^2/V.s$	μ_p $cm^2/V.s$	E_c 10^6 V/cm	v_{sat} 10^7 V/cm	λ W/cm	n_i cm^{-3}
Si	1.1	11.8	1350	450	0.3	1.0	1.5	1.5×10^{10}
Ge	0.66	16.0	3900	1900	0.1	0.5	0.6	2.4×10^{13}
GaAs	1.4	12.8	8500	400	0.4	2.0	0.5	1.8×10^{6}
GaN	3.39	9.0	900	50	3.3	2.5	1.3	1.9×10^{-10}
3C-SiC	2.2	9.6	100	50	1.2	2.0	4.5	6.9
4H-SiC	3.26	10	720^a 650^c	50	2.0	2.0	4.5	8.2×10^{-9}
6H-SiC	2.86	9.7	370^a 50^c	50	2.4	2.0	4.5	2.4×10^{-5}
diamond	5.45	5.5	1900	1500	5.6	2.7	20	2.4×10^{-27}

Note: *a* — mobility along a-axis, *c* — mobility along c axis

GaN-based materials are thoroughly studied for several reasons. They can be used for LEDs, UV detectors, x-ray detectors, laser diodes, surface acoustic wave devices, cold cathodes [23], power

amplifiers, HEMTs, MISFETs, HBTs [25], and more recently, photovoltaic devices [26]. GaN-based materials have many ideal properties for superior photovoltaic devices [26], such as high energy radiation resistance in optical and electronic devices for potential applications in space [27] and a direct, tunable band gap between 0.7 and 3.4 eV for $In_{1-x}Ga_xN$ that spans nearly the whole solar spectrum [26].

2.2. Crystal Structure

As aforementioned, GaN usually exists in wurtzite structure, but it can also exist in a metastable zinc-blende (cubic) structure under certain growth conditions [28]. The wurtzite structure is formed by two interpenetrating hexagonal close-packed lattices, and it lacks an inversion center [29], resulting in a spontaneous polarization and piezoelectric field [28]. Glasser has performed an in-depth study on the symmetry of wurtzite structures [29]. Figure 5 shows the crystal structure of a wurtzite crystal [1].

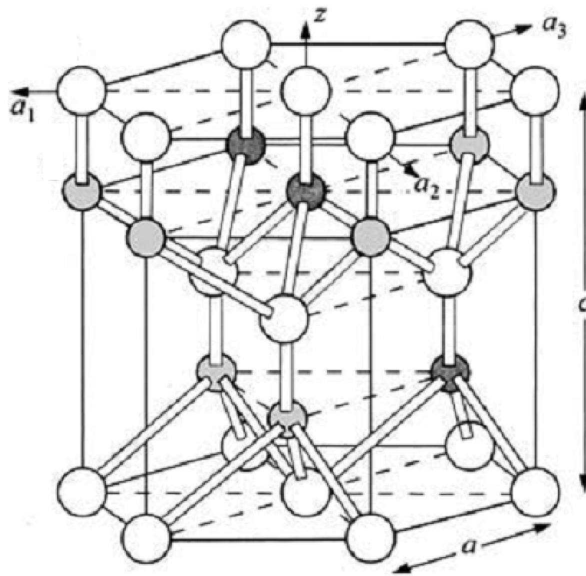

Figure 5 – The wurtzite (hexagonal) structure of GaN [1]

Since the inherent polarization and piezoelectricity in wurtzite GaN can inhibit the performance of certain optoelectronic devices [30], it is desirable to obtain a zinc-blende structure. Additionally, it would be possible to simply transfer the existing GaAs technology to GaN-based materials if viable cubic GaN layers could be easily fabricated [30]. In special growth conditions, the cubic GaN phase can be attained, and the cubic zinc-blende structure is seen in Figure 6. Mizuta, et. al., grew the first cubic GaN structure on (100) and (111) GaAs via MOCVD using hydrazine as the nitrogen source in 1986 [31]. Miyoshi, et. al., used dimethylhydrazine as the nitrogen source in 1992, and they achieved high-quality cubic GaN layers on (100) GaAs substrates with a growth temperature of 650°C and a V/III flow ratio of 160 [32]. In 1994, Hong, et. al., used Ammonia (NH_3), a much less dangerous chemical, as the nitrogen

source for MOCVD of GaN on GaAs substrates, and they found that the cubic phase dominates when the growth temperature is between 570°C and 650°C, but the wurtzite structure dominates at temperatures greater than 650°C [33]. Other growth methods have also been used to obtain cubic GaN, such as molecular beam epitaxy (MBE) [30] and pulsed laser deposition (PLD) [34]. Novikov, et. al., have taken MBE-grown cubic GaN growth a step further by using a chemical etch to remove the GaAs substrate, leaving a free-standing cubic GaN crystal [35] Still, most research is focused on the MOCVD processes and the much easier-to-produce wurtzite structure, which are grown on sapphire substrates.

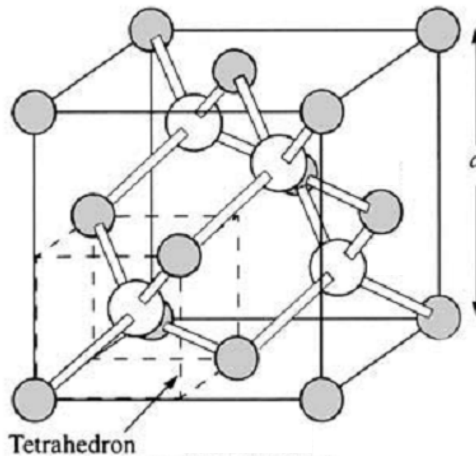

Figure 6 – The zinc blende (cubic) structure of GaN [1]

While cubic GaN might be important for the advancement of optoelectronic devices, my research will focus on the growth of wurtzite GaN.

2.3. History and Major Breakthroughs

Gallium nitride has an interesting history. While first synthesized by the German scientists Juza and Hahn in the 1930s and early 1940s [21, 36], there was little interest in GaN until the second half of the 20th century. In May 1968, the director of the Materials Research Division at the Radio Corporation of America (RCA), James Tietjen, asked Herb Maruska to create a single-crystal film of GaN, with the ultimate goal of creating a blue light-emitting diode [21]. Despite the previous work by Lorenz and Binkowski, which had indicated that GaN began to decompose in vacuum conditions at temperatures above 600°C [37], Maruska filled his hydride vapor phase epitaxy (HVPE) chamber with an ammonia environment and raised the deposition temperature to 850°C, and in 1969, he grew the first single-crystal GaN film [22].

Jacques Pankove became very interested in GaN in January 1970, and he formed a team with Maruska that conducted pioneering research on GaN until 1974, when RCA's revenues were plummeting

and funding for this project was revoked [21]. In addition to creating the world's first nitride-based LED in 1971 using Zn-doping and emitting faint blue light [38], Pankove published many other papers on GaN topics, including optical absorption [39], visible and UV electroluminescence [38, 40-42], and the creation of more intense, zinc-doped blue LEDs and unintentionally n-doped yellow LEDs [43-44]. Pankove used exclusively HVPE to create his GaN samples.

In 1974, Isamu Akasaki became the first person to use molecular beam epitaxy (MBE) to successfully grow a single crystal GaN layer [45]. While his GaN sample created by MBE had poor surface quality, this new technology ensured the continuation of GaN research. After realizing that neither MBE nor HVPE were ideal techniques for GaN film growth, Akasaki switched to using metal-organic vapor phase epitaxy (MOVPE, also known as metal-organic chemical vapor deposition, MOCVD) in 1979 [45]. He worked for several years to perfect MOCVD growth of GaN, but the lattice and thermal mismatch between the sapphire substrate caused the GaN film to have a high defect density, which inhibits device performance. In 1985, Akasaki and his research partner Amano used a low-temperature aluminum nitride (AlN) buffer layer to reduce the defect density, resulting in the best crystalline quality of a GaN sample to date [46], which was a breakthrough for GaN research. Six years later in 1991, Shuji Nakamura further improved the crystalline quality of MOCVD-grown GaN using a low-temperature (450-600°C) GaN buffer layer instead of AlN, and it was found that the optimal thickness for a GaN buffer layer was 20 nm [47].

A crucial problem for scientists studying GaN was that it seemed unable to be p-doped, essentially halting the further progress of a GaN LED. Even Maruska noted the difficulty of p-type doping when he created the first single-crystal GaN film using HVPE [22]. Many groups had experimented with zinc-doping, but electrical measurements had shown no evidence that the GaN was actually being doped when the attempt was made. Then came a huge breakthrough in 1988, when Akasaki realized that the blue luminescence intensity of his Zn-doped GaN permanently increased when it was exposed to electron beam irradiation [48]. Without knowing it, he created the first genuine p-type GaN sample. The following year, after realizing that Mg would be a shallower acceptor than Zn, Akasaki created not only a Mg-doped GaN sample using the electron beam irradiation technique, but more importantly the first GaN p-n junction [49]. In 1992, Nakamura reported even better success with making the GaN p-doped by using a thermal anneal of 700°C [50], and since this is a much easier method for a large sample than electron beam irradiation, the thermal anneal has become the standard process for achieving p-doping. Van Vechten proposed a theory of hydrogen compensation for explaining how the material becomes p-doped. He proposed that hydrogen was working its way into the GaN lattice, and H^+ was compensating the acceptors (A^-), thus inhibiting the electrical conductivity. However, with enough

energy, either from an electron beam or from a thermal anneal, the hydrogen would be removed, leaving a p-doped material [51]. This has become known as the activation step.

N-type doping was never as big a problem as p-type doping. Si and O are easily incorporated into GaN, often forming non-intentional n-type doping [52]. O has been shown by Korotkov and Wessels to act as a shallow donor in GaN and have a thermal ionization energy of 27 ± 2 meV [53]. However, Nakamura et. al. first created a very high quality GaN film, that was n-doped with Si up to 2 x 10^{19} cm^{-3} using a silane (SiH_4) flow in an MOCVD chamber [54]. The Si content is now able to be precisely controlled, and Si-doping using silane is now the most common n-type dopant in GaN [45].

The first MOCVD-grown $In_xGa_{1-x}N$ compounds were created in 1989, with In concentrations of up to 0.42 [55]. This was another huge step in creating p-n junctions emitting efficient blue light. Figure 7 shows how the band gap linearly decreases with an increasing indium composition to a level just above 2 eV at an In composition of 0.42.

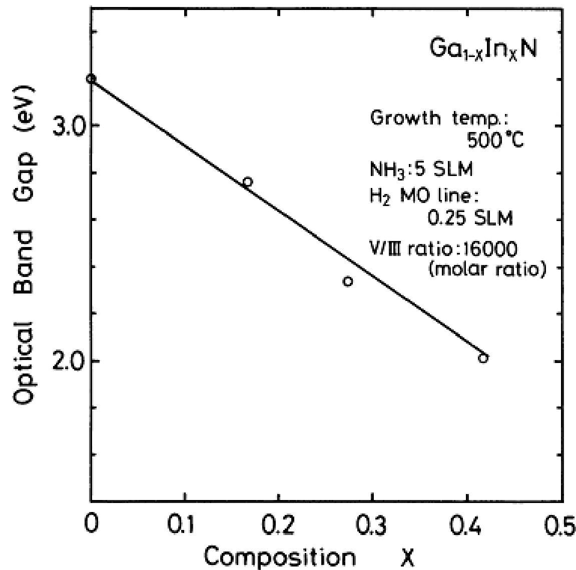

Figure 7- The effect of increasing In concentration in a GaInN compound on the optical band gap of the material [55]

It was previously experimentally determined that the room temperature band gap of InN was 1.89 eV [56], but the values in Figure 7 show that the band gap is approaching that value with an In concentration of only 0.42. What would happen if the indium content was further increased? In 1999, an MOVPE experiment that grew $Al_{1-x}In_xN$ first discovered that when the In concentration was 60%, the absorption edge decreased to 1.66 eV, well below the assumed band gap [57]. Further research has shown that high purity, single crystal hexagonal InN has a small band gap of around 0.7 eV, and the discrepancy between

this number and the previously determined band gap is explained by the improved quality of InN samples [58]. Now, it is possible to achieve band gaps that range all the way from 0.7 eV up to 6.2 eV using tertiary combinations of group III-nitrides, since the band gaps of InN, GaN, and AlN are 0.7 eV, 3.4 eV, and 6.2 eV respectively. These band gaps can result in luminescence or absorbance from the deep UV LEDs at 250 nm [59] all the way into the infrared range, making these materials attractive for many applications.

Table 3 shows a timeline for some of the major breakthroughs in the history of GaN. It is interesting to see that a lot of the names are repeated on the list, as they have been big contributors to the progress of GaN research.

Table 3 – Timeline of the breakthroughs in GaN history

Year	Discovery	People Responsible
1930s	First synthesis of GaN	Juza and Hahn [21]
1969	First single crystal GaN sample grown by HVPE	Maruska [22]
1970-1974	Pioneering research on optical absorption and photo- and electroluminescence; first nitride-based LED created in 1971	Pankove and Maruska [38-44]
1974	First successful single crystal GaN sample grown by MBE	Akasaki [45]
1985	First high-quality GaN sample grown by MOCVD, achieved by using AlN buffer layer	Amano and Akasaki [46]
1988	First notice of increase in luminescence in Zn-doped GaN after it had been exposed to an electron beam; first p-doped sample	Amano and Akasaki [48]
1989	Electron beam exposure is used on Mg-doped GaN, and first GaN p-n junction is created	Amano and Akasaki [49]
1991	High-quality GaN sample grown by MOCVD using GaN buffer layer for the first time	Nakamura [47]
1992	Thermal anneal was first used instead of electron beam irradiation to activate Mg-dopants	Nakamura [50]
1999	First report of an $Al_{1-x}In_xN$ compound with optical absorption below previously-accepted band gap of 1.89 eV for InN (not GaN, but still a III-N compound)	Yamaguchi, et. al. [57]

2.4. Fabrication Methods

2.4.1. Metalorganic Chemical Vapor Deposition

Currently, the most common technique for growing not only GaN, but other III-N semiconductors is metal-organic chemical vapor deposition (MOCVD) [60], which is also known as metal-organic vapor phase epitaxy (MOVPE). Although there is some dispute as to who invented MOCVD, Manasevit was

one of the pioneers of MOCVD-growing techniques in the late 1960s as he attempted to grow $GaAs_{1-x}P_x$ and $GaAs_{1-x}Sb_x$ films using triethyl- and trimethylgallium as precursor gases [61]. MOCVD essentially shoots various precursor gases, dopant sources, and carrier gases into a chamber with carefully controlled temperature, pressure, and other conditions. Inside the heated chamber, the pre-cursor gases undergo a pyrolysis reaction to decompose into the desired constituents. Later, these constituents bond with each other and the surface, and the desired material is deposited onto a well-positioned substrate. For MOCVD, at least one of the precursor gases must be a metal-organic compound, meaning it contains several polymers connected to a central metal atom. Inert carrier gases are added to propel the precursors so that they react and deposit in the proper section of the chamber. Figure 8 shows a brief summary of the main steps in a MOCVD system.

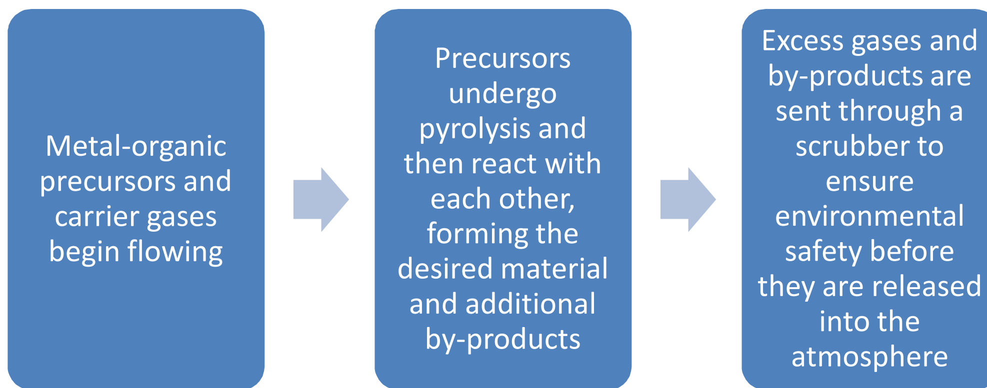

Figure 8 – Basic process flow for an MOCVD system

Although other nitrogen sources such as hydrazine have been experimented with [31], the most common precursor gases today for the MOCVD of GaN are trimethylgallium (TMGa), $Ga(CH_3)_3$, and ammonia, NH_3 [62]. GaN is usually grown on c-plane sapphire substrates in a two-step process: nucleation and bulk growth. As Amano and Akasaki first discovered using an AlN nucleation layer [46], and then later Nakamura with a GaN buffer layer [47], a nucleation (or buffer) layer should be grown at a low temperature (around 550°C) and a very high ammonia to TMGa ratio (on the order of 20,000) [63]. This nucleation layer is meant to compensate the 16 % lattice mismatch between GaN and sapphire, thus preventing threading dislocations in the sapphire substrate from penetrating into the bulk GaN film, which produces a much higher quality bulk GaN film [64]. However, through Huang and Yang's TEM study of MOCVD-grown GaN, it has been estimated that 7.5% of the surface dislocations on the substrate still coalesce into threading dislocations in the GaN [65]. The bulk growth step is usually grown at a much

higher temperature (1000°C to 1100°C) [63]. Since the ammonia decomposes at a slightly higher rate at these elevated temperatures, a lower NH_3 to TMGa ratio is required, which is usually around 6,000 [63].

MOCVD is heavily dependent upon thermodynamics, kinetics, mass transport, and surface characteristics. Thermodynamics determines what materials are formed through the reaction of the precursor gases based on a driving force of lowering the free energy. Kinetics determines how fast the pyrolysis reactions between the source gases will occur. Mass transport properties will determine the rate at which the vapor molecules reach the substrate. Surface processes determine how the desired material will adhere and grow on the substrate. An MOCVD process can either be characterized as mass transport limited, meaning that there are not enough molecules reaching the substrate, or kinetically limited, meaning that there is an abundance of molecules reaching the substrate, but the substrate can only accept a limited amount. Typically, GaN deposition is mass transport limited, as there is rarely enough nitrogen reaching the surface due to the low decomposition rate of ammonia.

There are several problems with MOCVD growth that need to be addressed. First, adduct formation often occurs when the precursors come into contact with each other, and each MOCVD system must be optimized to avoid this issue. Keuch, et al., have used the following chain of adduct reactions to describe MOCVD growth of GaN [62]:

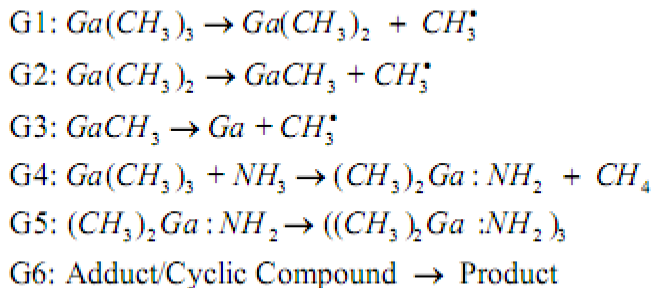

Next, the sapphire substrates often have high defect densities and are fairly expensive. Silicon substrates have been suggested to reduce cost and lower the defect density, however there is a huge lattice mismatch and a thermal expansion coefficient mismatch of 56% that hinders GaN deposition on silicon [66]. Finally, the temperature required for MOCVD of GaN (>1000°C) provides another obstacle when creating devices, since other materials used in these devices could become unstable at those high temperatures. Still, MOCVD growth of GaN yields the most pristine samples and is currently the most used method of growth.

2.4.2. Sputter Deposition

The process of sputtering is used for many applications, such as surface cleaning, Rutherford Backscattering Spectroscopy (RBS), Low Energy Ion Scattering (LEIS), and Secondary Ion Mass Spectroscopy (SIMS) [67]. Sputtering involves shooting accelerated ions at a target material with the purpose of ejecting electrons, ions, or atoms. My work concerns sputter deposition, which is the process of ejecting atoms from a target material and depositing them onto a substrate. This is a physical vapor deposition process, as no chemical reactions occur to form a film. Although it does not produce the pristine single crystal GaN films that MOCVD can produce, sputter deposition can be implemented fairly cheaply and is suitable for manufacturing conditions.

There are two types of collisions that occur when a target is bombarded with ions: electronic and nuclear [67]. Electronic collisions occur when the incident ions interact with the electrons in the target material, producing a constant energy loss of the ion. These electronic interactions are inelastic in nature, usually occur at high ion energies (>1000 keV), and result in the emission of characteristic x-rays, secondary electrons, and photons [67]. While there are some important applications for this type of emission, they are not useful for sputter deposition. Nuclear collisions are desired for sputter deposition because there is an exchange of momentum between the ions and the target material. The incident ions collide elastically with the nuclei of the atoms in the target material, causing atoms and secondary ions to be ejected from the target [67]. These ejected atoms are directed to a well-positioned substrate, where they will deposit and form an epitaxial layer under the right conditions. A basic schematic of the sputter deposition process can be seen in Figure 9. While sputtering was first observed in 1852 by Grove [67], the first papers on depositing GaN via sputtering were reported in the late 1970s [68-69].

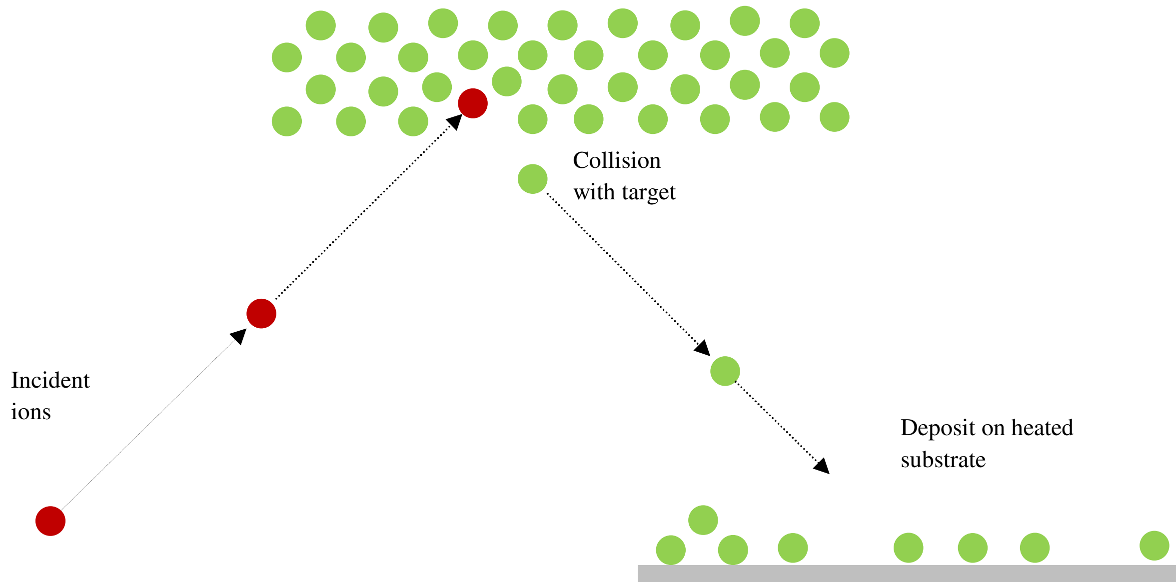

Figure 9 - Basic sputter deposition process

The most important property for sputter deposition is the sputter yield, Y, which is the ratio of ejected atoms to incident ions.

$$Y = \frac{number\ of\ ejected\ atoms}{number\ of\ incident\ ions} \tag{12}$$

Many factors affect the sputter yield, including target material, surface binding energy, energy and type of the incident ions, and the angle at which the ions are accelerated at the target [67]. In 1969, Peter Sigmund proposed a model to calculate the sputter yield that is often still used today, and it is shown below:

$$Y = 0.042\alpha \left(\frac{M_T}{M_I}\right) \frac{S_n(E)}{U} \tag{13}$$

where S_n is the nuclear stopping power of the target material, M_T is the average mass of an atom in the target material, M_I is the mass of the incident ion, E is the energy of the incident ion, U is the surface binding energy of the target material, and $\alpha(M_T/M_I)$ is a correction function that obviously depends on the masses of the atoms of the target and of the incident ions [8, 70].

Typically, the sputter yield begins when the energy of the incident ions is larger than the surface binding energy of the target atoms. The sputter yield then increases to a maximum value with increasing incident ion energy, and then begins to decrease as the higher ion energy results in the implantation of the ions in the target lattice rather than the ejection of target atoms. For most target materials, ion energy of

0.5 keV to 20 keV is used to achieve optimal sputter yield. The noble gas ions typically have the highest sputter yields, and argon is the most commonly used projectile ion [67].

There are many variations of normal sputter deposition, including reactive sputtering, DC sputtering, RF-sputtering, and magnetron sputtering [71]. Reactive sputtering introduces reactive oxygen or nitrogen species into the chamber during the sputtering of a metal target to deposit metal-oxides onto the substrate. DC sputtering places a bias between the target and the substrate to control deposition. RF sputtering is similar to DC sputtering, but it uses an alternating potential to reduce build up of charge on the substrate. Therefore, it is often used in the sputter deposition of insulating materials since the material cannot get rid of the surface charge when the ion beam strikes the surface. Magnetron sputtering is used to significantly increase the sputtering rate at the target material [71]. RF sputtering was used in this project since GaN exhibits insulating properties at room temperature.

2.4.3. Hydride Vapor Phase Epitaxy

At the beginning of modern gallium nitride research in the late 1960s, Herb Maruska created the first single-crystal gallium nitride sample using hydride vapor phase epitaxy (HVPE), based on his previous work with GaAs [21]. The first HVPE reactor used for GaN can be seen in Figure 10 [21]. In fact, HVPE was the most popular GaN deposition method until the early 1980s, when MOCVD gained widespread use [60].

Figure 10 – Herb Maruska's HPVE reactor where the first single crystal GaN sample was created [21].

HVPE systems flow hydrogen chloride gas over a liquid gallium source, causing $GaCl_{(g)}$ to be formed. Along with NH_3, the GaCl is transported into the deposition chamber with the aid of an inert carrier gas. The GaCl and NH_3 react, and GaN is deposited onto a substrate [60]. There are two possible thermodynamic reaction pathways that could occur, and they are seen below [72].

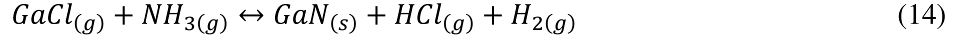

$$GaCl_{(g)} + NH_{3(g)} \leftrightarrow GaN_{(s)} + HCl_{(g)} + H_{2(g)} \quad (14)$$

$$3GaCl_{(g)} + 2NH_{3(g)} \leftrightarrow 2GaN_{(s)}\text{Error! Bookmark not defined.} + GaCl_{3(g)} + 3H_{2(g)} \quad (15)$$

An HVPE reactor is made of a high quality quartz tube that has a multiple zone furnace. The system operates at atmospheric pressure using electronic quality gases [60]

There are several problems associated with HVPE of GaN. Since the GaN has a thermodynamic inclination to form, it often deposits along the walls and other surfaces of the reactor [60], which is why sometimes a removable tungsten or graphite liner is placed in the reactor tube [72]. Other problems with this type of reactor are high impurity content in the GaN films and the difficulty to grow compounds containing magnesium or aluminum, which are necessary to grow p-type films or AlGaN tertiary alloys [60]. Additionally, there is often a formation of volatile chlorosilanes, which can lead to substantial oxygen and silicon inclusions in the film [62].

The major advantage of HVPE is a high and controllable growth rate of GaN, which can be tuned anywhere from 1 µm/h to greater than 100 µm/h [60]. These high growth rates are much higher than sputter deposited or MOCVD-grown GaN samples.

2.4.4. Other Deposition Methods

There have been experiments with other deposition methods for GaN, however they have little potential to be expanded beyond a laboratory scale. Shin, et. al., used vapor phase transport to grow seed GaN crystals and then bulk GaN using the seed crystals [73]. They heated a gallium source to 1260°C in nitrogen, and then switched to an ammonia environment from the hydrogen to achieve deposition [73]. However, prolonged exposure to the high temperatures required for bulk growth with this method (>10 hours) led to the degradation of the GaN, as it turned white [73].

Recently, Otha, et. al., grew GaN films with pulsed electron deposition (PED) [74]. This method pulses a polycrystalline GaN crystal with a high energy electron beam, causing GaN species to be ejected, which then deposit onto the heated substrate [74]. While epitaxial GaN films have been grown by this method at very low temperatures (~400°C), it has shown slow deposition rates (~0.5 µm/h) and this deposition method can only be used for very specific applications [74].

3. Experimental Details

As aforementioned, the long-term intention is to incorporate a GaN film into CdTe solar cells to improve solar cell performance. Before this can happen, the GaN films need to be further studied. Therefore, the goals of this project are to examine the effect of different GaN deposition processes on structural conditions and to understand the interfaces of GaN with CdTe and CdS. RF sputter deposition and MOCVD were both used to grow GaN films. Additionally, an InGaN film was grown by sputter deposition with the purpose of slightly lowering the band gap. These films were characterized by x-ray diffraction (XRD) and atomic force microscopy (AFM) to view structural differences. Afterward, each GaN/InGaN sample underwent interface studies with CdTe and CdS, which are described in Chapter 4.

3.1. Sample Creation

Two methods of sample creation were employed for this project: MOCVD and sputter deposition. For the interface studies, all CdTe and CdS deposition as well as XPS characterization was performed inside an integrated ultra-high vacuum system in the materials science department at TU-Darmstadt. This integrated system is known as the Darmstadt Integrated SYstem for SOLar cell research, or DAISY-SOL. While the sputtered samples were also grown inside the DAISY-SOL, the MOCVD samples were grown in the electrical engineering department, causing a transfer through air to be required.

3.1.1 Sputter Deposition

The sputtered GaN and InGaN samples were grown on glass substrates covered with a thin transparent conducting oxide (TCO) layer inside the DAISY-SOL at TU-Darmstadt. RF sputtering conditions included a nitrogen flow of 13 sccm, sputter power of 30W, substrate temperature of 450°C, and a deposition time of 1 hour to ensure a bulk GaN or InGaN growth.

As aforementioned, the DAISY-SOL system is a marvelous tool used for the fabrication and characterization of thin film solar cells in the materials science department at TU-Darmstadt. This elaborate system houses many deposition chambers for various layers required for the solar cells as well as an ESCALab 250 photoelectron spectroscopy tool. The DAISY-SOL can be seen in Figure 11.

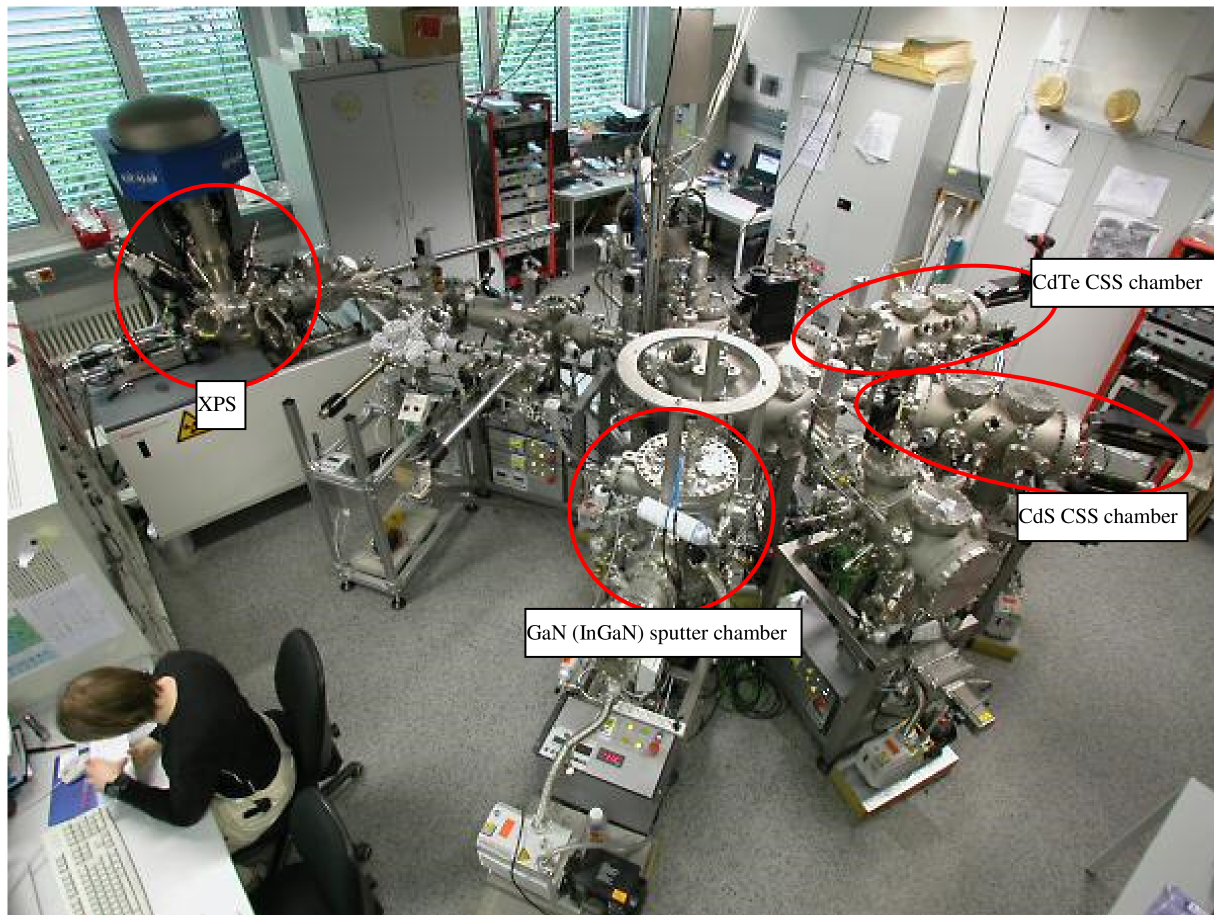

Figure 11 – The DAISY-SOL in the materials science department at TU-Darmstadt, which houses the sputter chamber for the GaN and InGaN, the CSS system for both CdTe and CdS, and the XPS system.

3.1.2 MOCVD

All MOCVD processes were performed in a standard Thomas Swann 3x2 close coupled showerhead reactor on top of 2 inch c-plane sapphire substrates. This MOCVD reactor is located in the electrical engineering department at TU-Darmstadt and can be seen in Figure 12. All temperatures were calibrated against an external blackbody to ensure accuracy.

Figure 12 – Thomas Swann MOCVD reactor in the electrical engineering department at TU-Darmstadt

For the standard GaN growth in this reactor, there were five main steps. The first step was an anneal in H_2 to eliminate any moisture or other contaminants on the wafer surface. Second, a low-temperature nucleation layer was grown to reduce defects in the bulk layer that resulted from the lattice mismatch between GaN and the sapphire substrate. After the third step of brief recrystallization, the bulk GaN layer was grown at high temperatures for the fourth step. Finally, the samples were cooled in an ammonia atmosphere before being removed from the reactor. Standard precursor gases are used for the deposition: trimethyl gallium (TMGa) for the gallium and ammonia (NH_3) for the nitrogen.

The initial anneal step was performed at 1050°C in an atmosphere of about 1000 torr of H_2, and it lasted for five minutes.

The nucleation layer was grown at 530°C. The TMGa flowed into the reactor at about 25 µm/min while the NH_3 flowed at 1.3 standard liters per minute (slm). To ensure deposition on the wafers, an H_2 carrier gas flowed at 7.5 slm. The total pressure in the system was held at 500 torr, and the deposition lasted for 120 seconds, resulting in a GaN nominal thickness of about 25 nm.

For the bulk GaN layer, the temperature was ramped up to 1030°C. The TMGa flow was about 100 µmol/min, the NH_3 flow was about 2.3 slm, and the H_2 carrier gas flow was 7.5 slm. The total

pressure in the chamber was held at about 200 torr. With deposition times between 20 and 60 minutes, nominal thicknesses of between 0.5 µm and 2.5 µm can be achieved.

At this point, the normal MOCVD samples were cooled to room temperature in an ammonia environment and then removed. However, in an attempt to prevent surface contamination as the sample was transferred from the electrical engineering building to the materials science building for characterization, a sacrificial SiN capping layer was grown directly on top of the GaN on one sample. 50 ppm silane (SiH_4) was used as the silicon source, and it was flowed at about 200 nmol/min. NH_3 was flowed at 0.8 slm for the nitrogen source while H_2 was flowed at 7 slm for the carrier gas. Deposition took place at a temperature of 850^oC, and the pressure was held at 50 torr. Cooling to room temperature followed the SiN deposition for this sample. The hope was that this SiN layer could be removed later by a focused ion beam inside vacuum to expose an uncontaminated GaN surface underneath.

3.2. Characterization

In order to compare the structural properties of MOCVD-grown GaN to sputter deposited GaN and InGaN, several characterization methods were employed. X-ray diffraction (XRD) was used to examine the crystal structure of both sets of samples and to check if wurtzite or cubic growth was achieved. It is also possible to see preferential growth directions and see if a crystal is polycrystalline or monocrystalline. Atomic force microscopy (AFM) was used to view the condition of the surfaces of the various samples and to compare the surface roughnesses.

3.2.1 X-Ray Diffraction (XRD)

3.2.1.1 Method

XRD is a non-destructive characterization technique that involves irradiating the sample with x-rays in order to determine information about crystalline phases. The incident x-rays diffract off of the various planes of atoms inside the crystalline structures. The diffraction angle yields information about the d-spacing between the planes of atoms, which are unique for different planes inside a material. As the x-ray source and detector are scanned through a wide range of angles, all of the present crystal orientations can be determined [75].

Clear XRD measurements have already been taken for the sputtered GaN material by Dr. Ganhua Fu of the surface science group in 2008. As this data was reliable and there were no process changes, it was used in this comparison. On the other hand, the sputter deposited InGaN material and the MOCVD GaN were examined using XRD. The XRD measurements of the sputtered InGaN were performed in a Brucker D8 powder diffraction machine since a polycrystalline material was expected. On the other hand, the MOCVD GaN was expected to be a single crystal film, so the XRD measurements of the

MOCVD GaN were performed in a Seifert XRD 30003 PTS-3 system. Both XRD measurements were performed by the Structural Research group in the materials science department at TU-Darmstadt.

3.2.1.2 Sputter Deposition Results

Here, the prior XRD results for the sputtered GaN and the current XRD measurements for the sputtered InGaN are presented. Figure 13 shows the theta-2-theta XRD measurements for the sputtered GaN. As the GaN is a fairly thin layer (~100-150 nm), the peaks are compared to the underlying fluorine-doped tin oxide (FTO) layer. The samples used in this project were grown at 450°C, so the data most relevant to this project is the blue data on top. Since there are several visible GaN XRD peaks at about 34°, 37°, 48°, and 63°, it is clear that this sample is polycrystalline. From this data and the data in the hexagonal GaN powder diffraction file (PDF) found in Appendix A, it is seen that the sputtered GaN grows primarily in the (002), (101), (102), and (103) directions at high temperatures (450°C). Furthermore, since the peaks line up with the hexagonal GaN PDF and not the cubic GaN PDF, it is concluded that the sputtered GaN has a wurtzite structure as opposed to cubic zinc-blende.

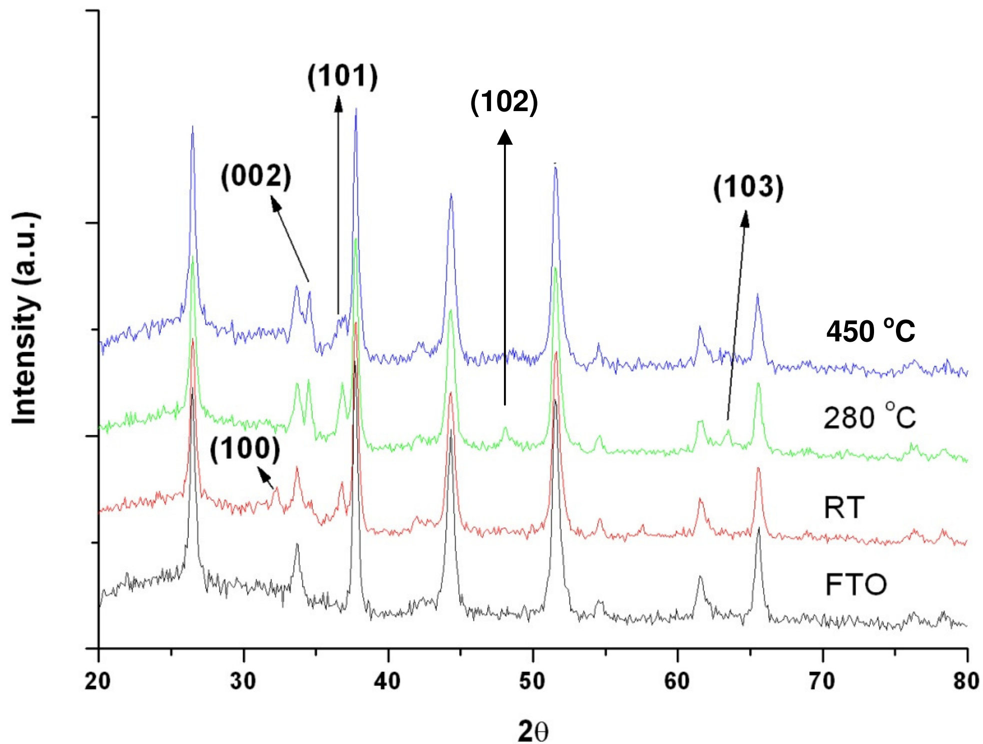

Figure 13 - Theta 2-theta XRD measurements for sputter deposited GaN

The sputter deposited InGaN was grown only at 450°C, and the theta-2-theta XRD data compared to the underlying substrate is seen in Figure 14. For this data, in contrast to Figure 13, the substrate is on top and the InGaN is on the bottom. Additionally, the blue lines show where peaks of a pure, polycrystalline, wurtzite GaN sample would appear. Since the indium concentration was relatively low (about 1.5 at%, as measured by XPS quantification), the hexagonal GaN PDF was used again to compare to the observed peaks, which is found in Appendix A. Again, the most prominent InGaN peaks appear at roughly 34°, 37°, 48°, and 63°, which indicate growth directions of (002), (101), (102), and (103). Similarly to the sputtered GaN, this XRD data shows polycrystalline InGaN in the wurtzite structure.

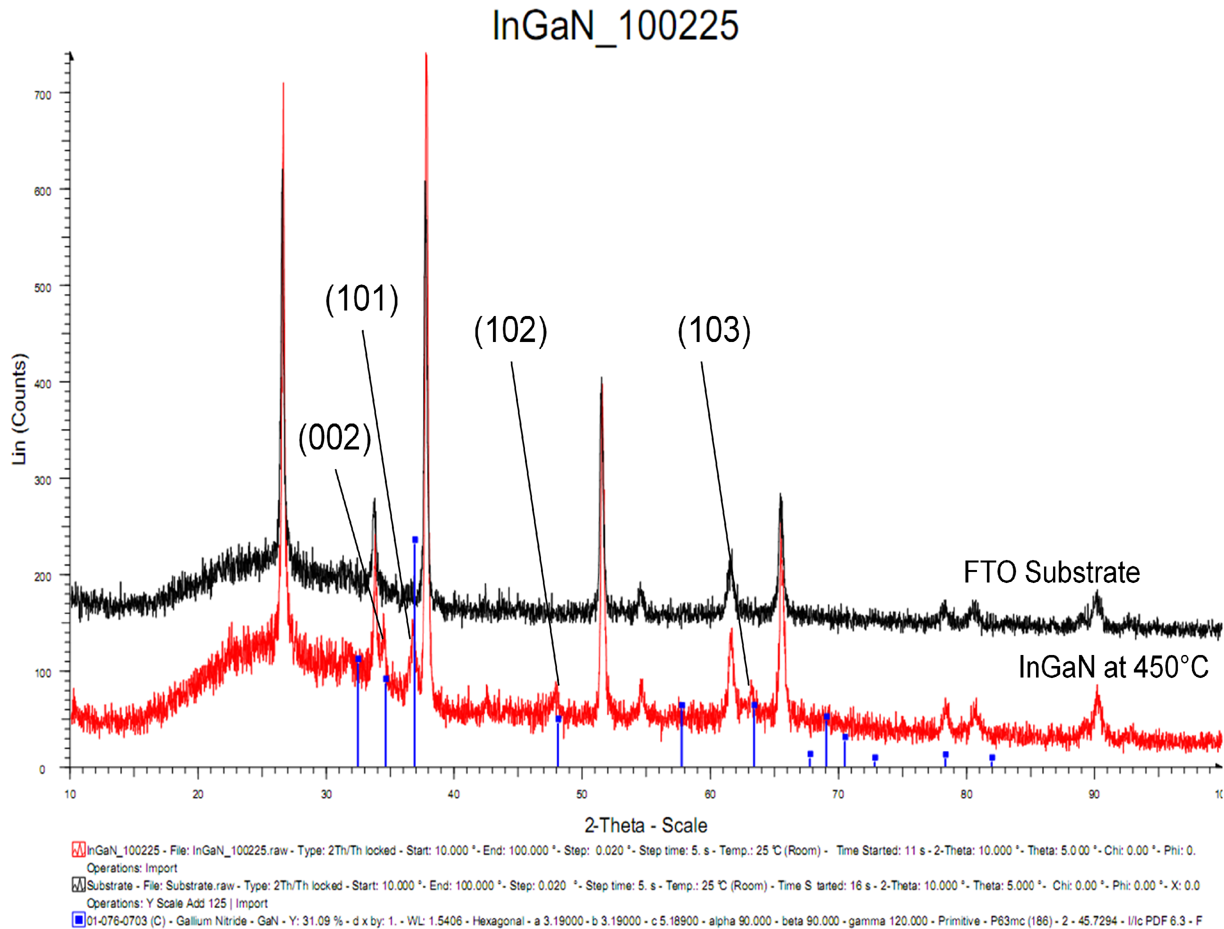

Figure 14 - Theta 2-theta XRD measurements for sputter deposited InGaN

3.2.1.3 MOCVD Results

The XRD for the MOCVD GaN samples can be seen in Figure 15. In contrast to the sputter deposited GaN and InGaN samples, the XRD data for the MOCVD GaN shows a single crystal of wurtzite GaN growing in the (002) direction.

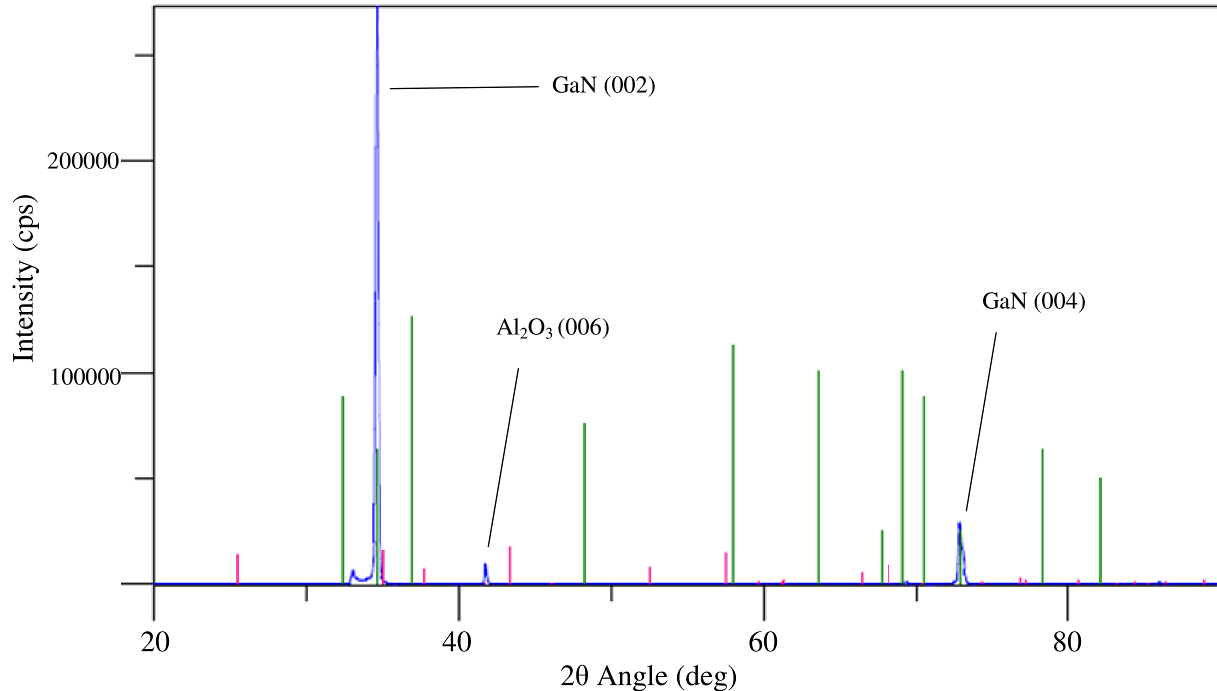

Figure 15 - Theta 2-theta XRD measurements for MOCVD GaN. While the blue lines are the actual XRD data, the green lines represent the wurtzite GaN peaks from the PDF, and the magenta lines represent the sapphire peaks from the PDF.

There are three visible peaks in the XRD data (the small peak at about 33° is a residual peak from the Mo x-ray source). The largest peak, which is at about 34.61^o, is the GaN (002) peak, and its second-order (004) peak is located at 72.90^o. As the MOCVD GaN was grown to be about 1.5 μm thick, and the x-ray penetration depth should be around 15-20 μm, a large peak from the sapphire substrate was expected. However, the sapphire substrates were single crystal c-plane sapphire, meaning that they were oriented in the (006) direction, and this orientation only yields a very low intensity diffraction at 41.80^o.

3.2.2 Atomic Force Microscopy (AFM)

3.2.2.1 Method

AFM was performed in an Asylum Research machine in non-contact mode in the Surface Science research group of the materials science department at TU-Darmstadt. AFM scans a microfabricated needle made of silicon or silicon nitride across the surface in contact mode or just above the surface of the sample in non-contact mode. The atomic forces between the sample and the needle (mechanical contact, Van der Waals, and electrostatic forces to name a few) cause the needle to deflect in the z-direction, perpendicular to the surface. This deflection is felt by a piezoelectric cantilever, which outputs a particular voltage dependent on the amount of deflection. By using these voltages, the relative height of the surface is determined at each point, and a 3-dimensional picture of the surface is obtained [76]. This

method was used to view the differences in the surface condition between the two sets of materials as well as check the surface roughnesses.

AFM measurements were taken on the sputter deposited GaN, sputter deposited InGaN, and the MOCVD GaN. Additionally, AFM was performed on the CdS and CdTe deposition on all sets of substrates to check for differences in the deposited materials. A 2 µm, 5 µm, and a 10 µm square picture of each material were taken. Only the 5 µm square pictures are presented in this section (along with the RMS roughness values), and the 2 and 10 µm pictures can be found in Appendix B.

3.2.2.2 Sputter deposition

AFM pictures of the surfaces of the sputter deposited GaN and sputter deposited InGaN can be seen in (a) (b)

Figure 16. The RMS roughness value of the sputter deposited GaN was 10.341 nm, while the RMS value of the InGaN was 14.898 nm. Therefore the InGaN was a little rougher than the GaN. Individual grains and grain boundaries are clearly visible in both samples, with the InGaN grains slightly elongated compared to the more circular GaN grains. As with the XRD measurements, this proves that sputter deposition of GaN and InGaN produced polycrystalline films.

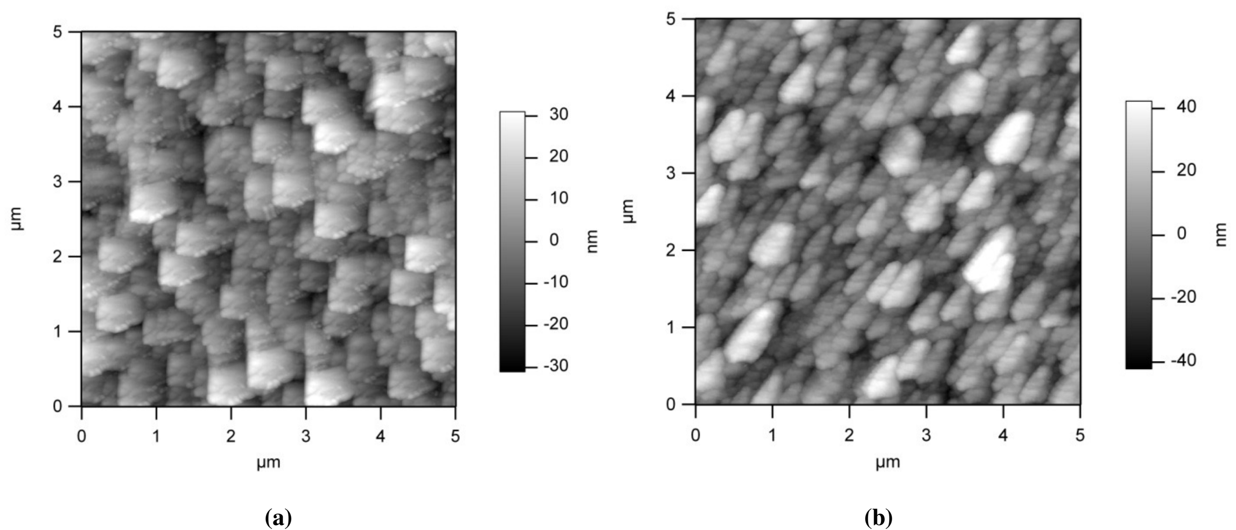

(a) **(b)**

Figure 16 - AFM pictures of a 5 µm x 5 µm square of sputter deposited GaN (a) and InGaN (b)

3.2.2.3 MOCVD GaN

The MOCVD GaN can be seen in Figure 17. The RMS roughness value is a tiny 0.294 nm, or 294 pm, which means the MOCVD surface is much smoother than the sputter deposited samples. Additionally, there are no visible grain boundaries, which indicates (but does not prove) the sample is

single crystal. There are some swirly vertical lines on the surface of the sample; however these are probably due to turbulent flow of the precursor gases from the MOCVD process.

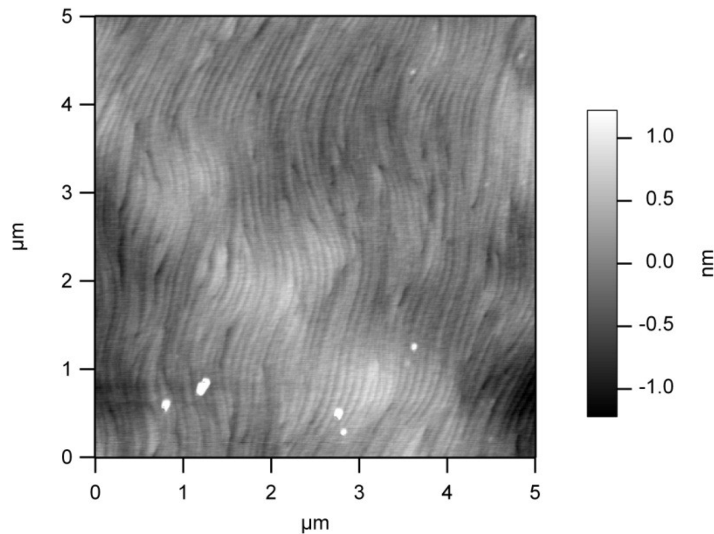

Figure 17 – AFM picture of a 5 µm x 5 µm square of MOCVD GaN

Since the surfaces of the sputtered samples and the MOCVD sample were so different, the CdTe and CdS did not deposit in the same fashion on the MOCVD and sputter deposited samples. It is believed that the smoothness of the MOCVD GaN samples led to a lower sticking coefficient for the CdTe and CdS deposition. Thus, many days were spent trying to find the correct deposition conditions for the interface studies with CdTe and CdS (see Section 4.1.2 Close Space Sublimation (CSS)).

3.2.2.4 CdTe Deposition

The underlying substrate had a strong affect on the deposited CdTe. Figure 18 shows CdTe on sputter deposited GaN and InGaN. Despite the difference in the sputtered GaN and InGaN texture, the roughnesses of these films are very similar. The RMS roughness value of the CdTe on sputtered GaN is 15.452 nm, and the RMS value of the CdTe on sputtered InGaN is 15.446 nm. Furthermore, they have similar grain sizes and overall appearance.

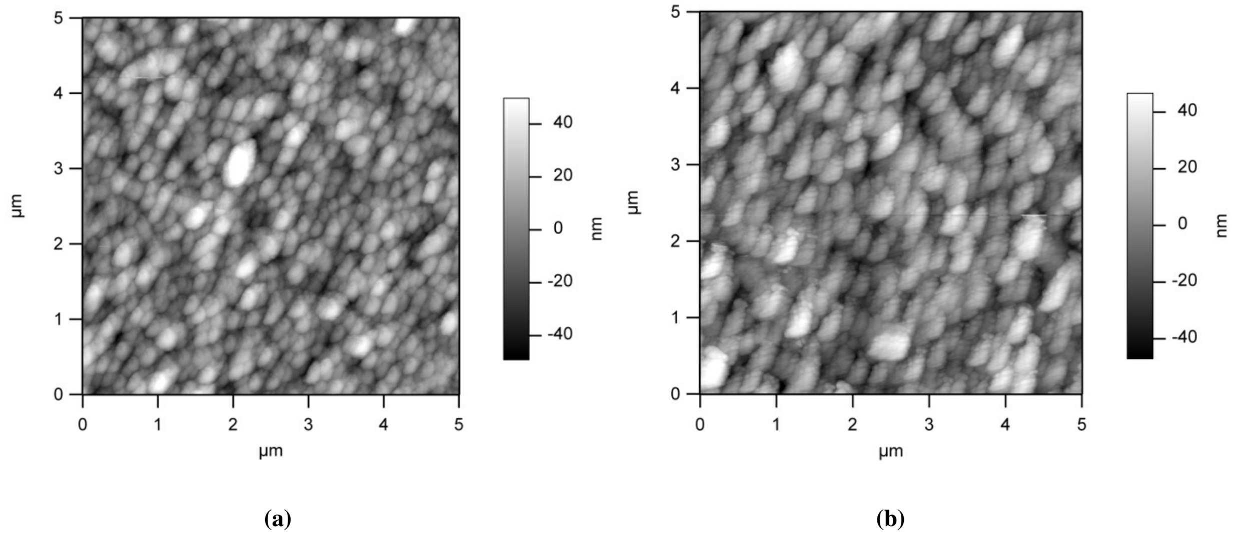

Figure 18 - AFM pictures for a 5 µm x 5 µm square of CdTe on sputtered GaN (a) and sputtered InGaN (b)

On the contrary to the CdTe deposited onto the sputtered samples, the CdTe deposited onto the MOCVD GaN was much smoother, with an RMS value of only 1.065 nm. Additionally, the CdTe grains were much smaller in the CdTe deposited onto the MOCVD GaN. Figure 19 shows an AFM picture of CdTe deposited onto MOCVD GaN. The question now is: is the profound change in the CdTe roughness and grain size due to the underlying substrate, or the change in deposition conditions? I believe it is due to the substrate.

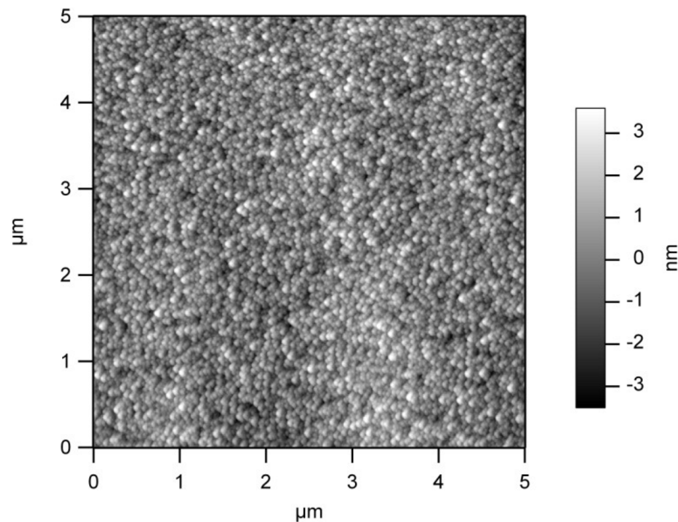

Figure 19 - AFM pictures for a 5 µm x 5 µm square of CdTe on MOCVD GaN

3.2.2.5 CdS Deposition

The structure of the CdS also was affected by the underlying substrate. Figure 20 shows AFM pictures of the CdS surfaces for a sputtered GaN substrate and a sputtered InGaN substrate, and again, the

surfaces are very similar despite the differences in the sputtered GaN and InGaN. The RMS roughness value of the CdS on the sputtered GaN was 11.158 nm, and the RMS value of the CdS onto the sputtered InGaN was 13.053 nm.

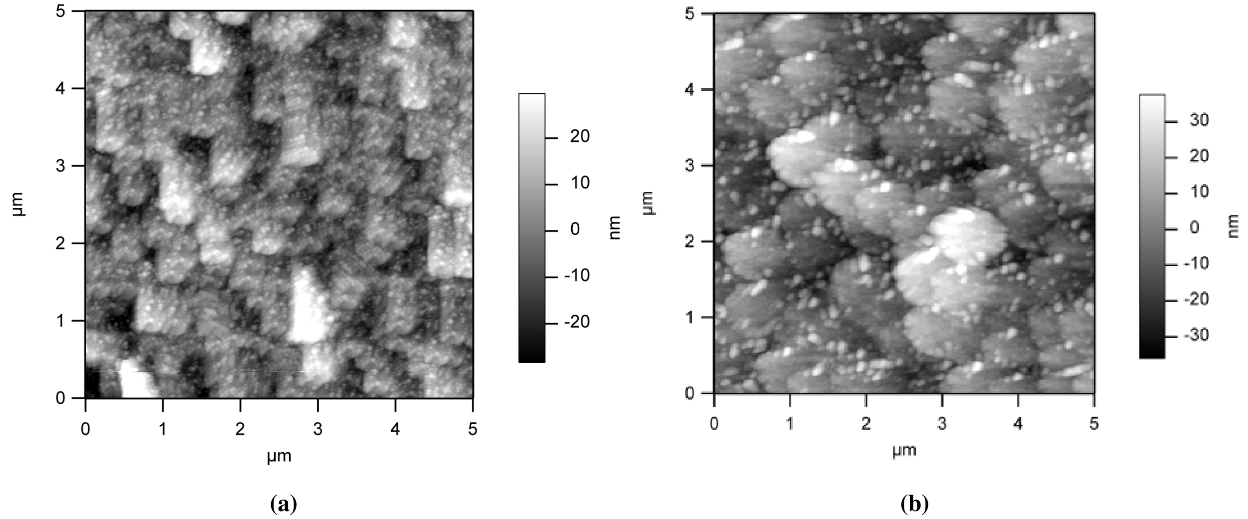

Figure 20 - AFM pictures for a 5 µm x 5 µm square of CdS on sputtered GaN (a) and sputtered InGaN (b)

Once again, as with the CdTe deposition, the CdS deposited onto the MOCVD GaN was much smoother. The RMS roughness value of the CdS on the MOCVD GaN was only 2.093 nm. Furthermore, the CdS grains are much smaller than the CdS grains grown on the sputtered samples. The surface can be seen in Figure 21.

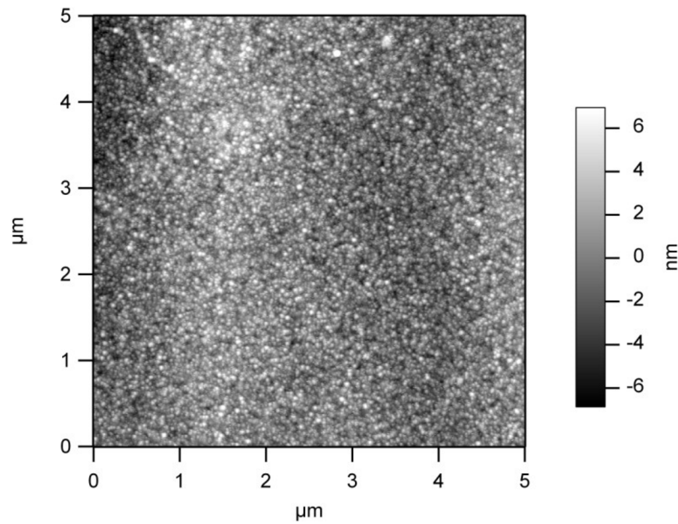

Figure 21 - AFM pictures for a 5 µm x 5 µm square of CdS on MOCVD GaN

3.2.2.6 AFM Summary

A summary of the AFM data can be found in Table 4. As can be seen, the MOCVD substrate has a much smoother surface, which produces much smoother CdTe and CdS layers when deposited on top. While the roughness of the sputtered GaN and sputtered InGaN are slightly different, they produce CdTe and CdS layers of almost exactly the same roughness. Additionally, the sputtered GaN and InGaN samples clearly consist of many grains, whereas the MOCVD GaN appears to be single crystal.

Table 4 - Summary of RMS roughness data acquired from AFM measurements

GaN	Deposition	RMS (nm)
Sputtered GaN		10.341
Sputtered InGaN		14.898
MOCVD GaN		0.294
Sputtered GaN	CdTe	15.452
Sputtered InGaN	CdTe	15.446
MOCVD GaN	CdTe	1.065
Sputtered GaN	CdS	11.158
Sputtered InGaN	CdS	13.053
MOCVD GaN	CdS	2.093

Further studies should be performed to examine whether these different roughness values have any effect on future processing or solar cell performance. Additionally, further studies should be carried out to confirm that the differences in the deposited CdTe and CdS layers between the sputtered GaN and MOCVD GaN substrates were indeed caused by the differences in substrate roughness and orientation. Other potential explanations for the difference in the AFM pictures could be the different CSS deposition conditions or different thicknesses of the CdTe and CdS between the different interfaces.

4. Interface Studies

4.1 *Methods for Performing Interface Studies*

4.1.1 X-Ray Photoelectron Spectroscopy (XPS)

It is necessary to very briefly discuss how the XPS and UPS measurements work in order to understand the interface studies. XPS, or x-ray photoelectron spectroscopy, is a non-destructive characterization technique that irradiates the surface of the sample with a high energy x-ray. The energy from these x-rays is known (we used an Al kα x-ray source with an energy of 1486.6 eV), and can be described by hν, where h is Planck's constant (4.136×10^{-34} eV·s) and ν is the frequency of the x-ray in s^{-1}, which can also be described as the speed of light, c (3×10^{8} m/s), divided by the wavelength of the x-ray, λ. Equation 16 below shows this relationship.

$$E_{x-ray} = hv = \frac{hc}{\lambda} \tag{16}$$

When this energy irradiates the sample, it causes electrons with binding energies of BE to be ejected from the surface with a kinetic energy of KE. The kinetic energy of the electrons is measured by a detector, and thus, the binding energy of each electron can be determined by equation 17.

$$BE = E_{x-ray} - KE = \frac{hc}{\lambda} - KE \tag{17}$$

After examining equation 17, if an electron has a low kinetic energy, it has a high binding energy, and vice versa. The binding energy of the electrons for each element is unique, thus, XPS allows us to determine the composition of the sample, the relative amount of each element present, and surface electron properties. UPS, or ultra-violet photoelectron spectroscopy, works in a similar fashion, except UPS uses ultra-violet light instead of x-rays as the excitation source. Since UV light has a much longer wavelength than x-rays, the excitation energy is much lower. We used a helium excitation source with an energy of 21.22 eV. UPS gives more accurate information about the valence electrons, and we used it to determine the work function of the material.

Both XPS and UPS are considered surface techniques, as the ejected electrons typically come from within the first 6 nm of the sample [75]. XPS can detect every element except for hydrogen and helium because they contain only valence levels and no core levels. XPS is not a great technique to determine trace amount of materials, as its detection limit is about 0.1-0.3 at% [75], but it is a very valuable tool for our interface experiments.

4.1.2 Close Space Sublimation (CSS)

For the interface studies, both the CdTe and the CdS were deposited via close space sublimation (CSS). This is a simple process where CdTe or CdS granules are placed in a carbon crucible and then heated to a point below the melting point. Sublimation occurs, and the sublimated material deposits congruently onto a closely-spaced, moving substrate. Since only relatively low vacuum conditions are required and the required temperatures are not extraordinarily high, this process can be implemented fairly cheaply [77]. CSS of both CdTe and CdS was performed in-situ inside the DAISY-SOL.

CSS of CdS onto sputtered GaN and InGaN was performed at a source temperature of 510°C and a substrate temperature of 250°C. CSS of CdTe onto sputtered GaN and InGaN was performed at a source temperature of 390°C and a substrate temperature of 250°C. The heating elements for each chamber had to be optimized for both the MOCVD-grown samples and sputter deposited samples because the CdTe and CdS deposited at different rates between the two GaN growth methods. The MOCVD surfaces had a lower sticking coefficient for the CSS. Thus, the deposition of CdTe and CdS onto MOCVD GaN samples required more aggressive heating. For CSS of CdS onto MOCVD-grown GaN, the source temperature was 545°C and the substrate temperature was nominally 200°C. It is difficult to know the exact temperature because a pyrometer was used to measure the temperature of the substrates. When the CdTe and CdS are deposited onto the sputter deposited GaN samples, the pyrometer measures the temperature of the glass substrate. However, for the MOCVD grown samples, a metallic sample holder is used and its temperature is controlled by the pyrometer. Since the pyrometer is calibrated for glass, the exact temperature is not known. For CSS of CdTe onto MOCVD-grown GaN, the substrate temperature was also set to 200°C and the source temperature was raised to 415°C.

4.1.3 Structure of Interface Studies

These interface studies consisted of a step-by-step deposition of CdTe or CdS with XPS and UPS measurements after each deposition step to understand how the materials behave at the interface. The XPS measurements and the CdTe/CdS deposition were both performed inside the ultrahigh vacuum DAISY-SOL, so the surfaces of the materials did not become contaminated between steps, resulting in a more accurate depiction of the interface.

The first step for our interface studies was to obtain a starting material, either GaN or InGaN. As aforementioned, the sputter deposited GaN and InGaN were grown inside the DAISY-SOL while the MOCVD GaN was grown in a separate building, which meant there was some surface contamination on the MOCVD GaN due to the transfer into the DAISY-SOL. In order to achieve maximum accuracy in our interface studies, many efforts were made to reduce the amount of surface contamination on the

MOCVD samples, as can be seen in section 4.2. Attempts for Contamination-Free MOCVD GaN In our interface studies, the MOCVD samples were annealed for 1 hour at $450^{o}C$ prior to characterization to remove some carbon and oxygen contamination. The starting material was then examined by XPS and UPS, prior to any deposition. After characterization, 1 minute of either CdTe or CdS was deposited onto the material by close space sublimation. Following this deposition step, the sample was then characterized by XPS and UPS once again. Then, another deposition step occurred and was followed by XPS and UPS characterization. After each deposition step, the Ga peaks should continue to decrease while the Cd and Te/S peaks should continue to increase, as the material transitions from bulk GaN/InGaN to bulk CdTe/CdS. This step-by-step deposition continues until the XPS peaks from the starting material (GaN or InGaN) completely disappear, leaving bulk CdTe or CdS. A basic flowchart describing the process can be found in Figure 22.

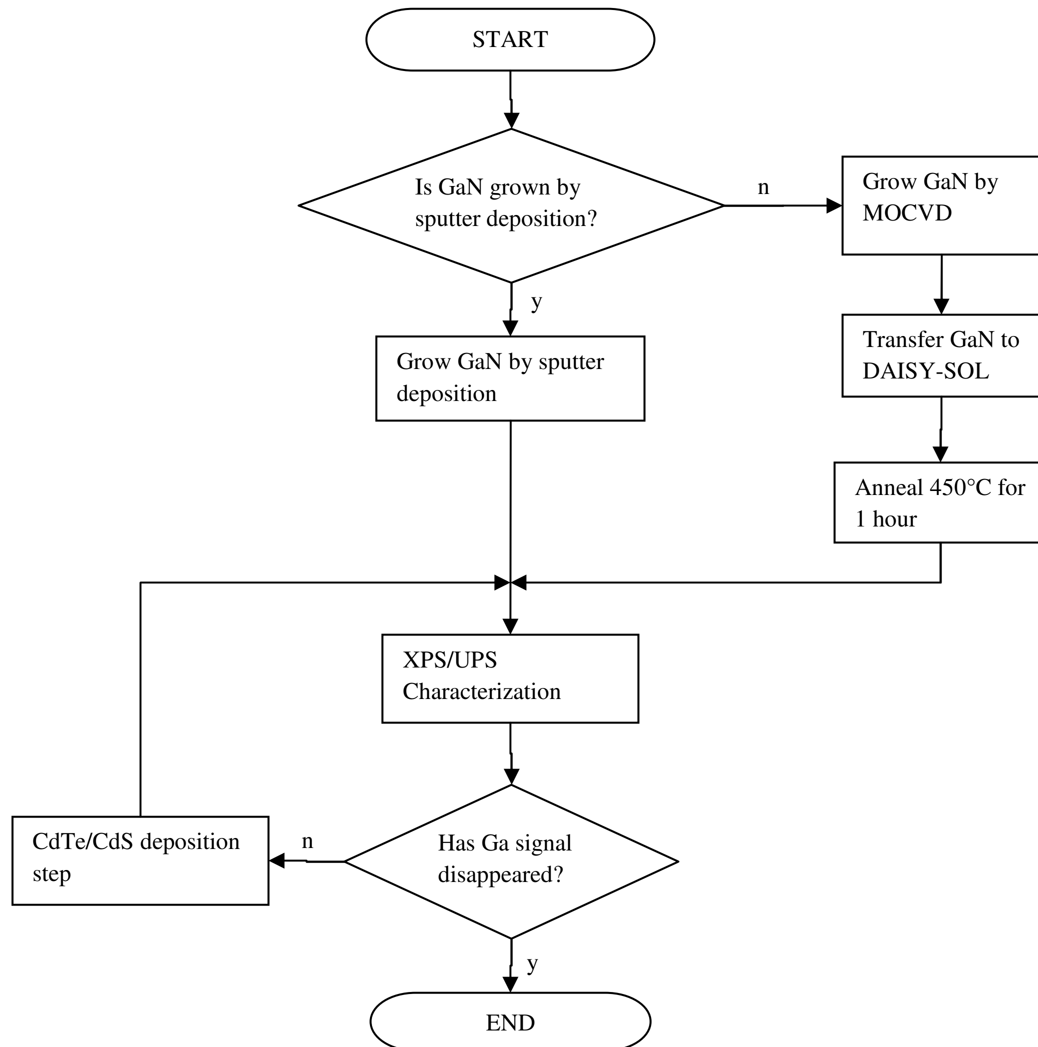

Figure 22 - Flowchart describing the structure of the interface studies between GaN (or InGaN) and CdS/CdTe

The samples were remeasured in the XPS after 1 minute, 2 minutes, 4 minutes, 8 minutes, 16 minutes, and 32 minutes of CdTe deposition. Some sputtered GaN substrates allowed for quicker deposition, so bulk CdS was reached after only 16 minutes of deposition instead of 32 minutes, but this was not a problem. The MOCVD interfaces proceeded even quicker and were finished after 8 minutes of deposition. Therefore, additional measurement steps were taken at intermediate times to understand the interface better. The investigated peaks from the XPS included gallium 2p at a binding energy of about 1118 eV, telluride 3d at 573 eV, cadmium 3d at 406 eV, and the valence band (measured from 14 eV to -2 eV) for a CdTe interface study. Additionally, the indium 3d peak at 444 eV was observed for the InGaN samples, and the sulfur 2s peak at 228 eV was monitored during the CdS interface studies.

4.1.4 What is Learned from Interface Studies

From the interface study, many crucial parameters can be determined to draw a proper band alignment when the two materials are put in contact with each other. The first step to drawing the band diagram is to align the Fermi levels of the bulk materials. The position of the Fermi level for the bulk materials is taken from the valence band measurements at 0 minutes of deposition for bulk GaN and at the last deposition for the bulk CdTe or CdS. The energy level where the XPS intensity falls to zero is the value $E_F - E_{VB}$. Thus, the position of the Fermi level relative to the valence band is known. Figure 23 shows how the Fermi level position was determined for both materials in the sputtered GaN and CdTe interface. As can be seen here, there is some room for human error as the lines are drawn by the researcher.

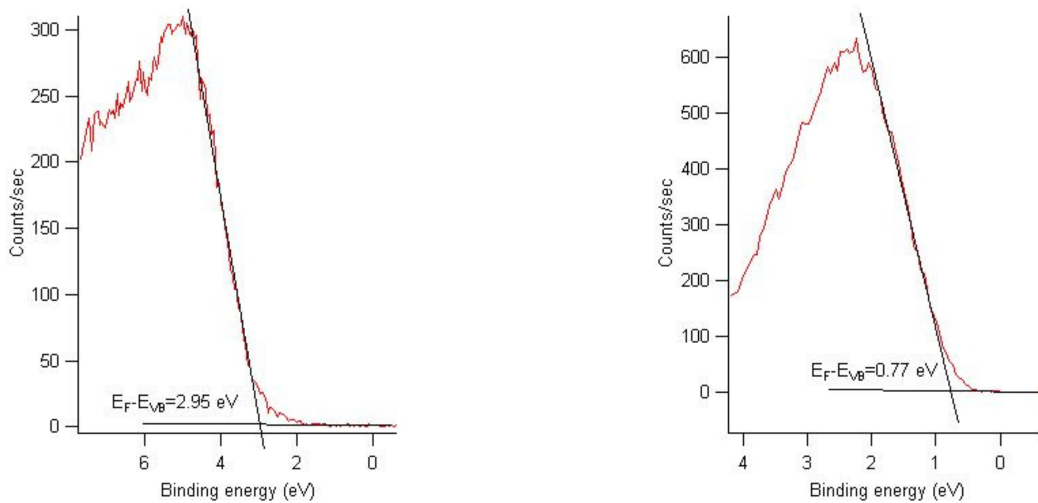

Figure 23 - XPS measurements of the valence band to determine the Fermi level position relative to the valence band. Sputtered GaN prior to any CdTe deposition is on the left and CdTe after 32 minutes of deposition is on the right.

The shifts in the core level peaks of the measured elements over the course of the interface study indicate the band bending at the interface due to the different Fermi levels in the two materials becoming equal at the interface [78]. Band bending was determined by monitoring the Ga2p peak for the GaN and InGaN and the Cd3d peak for CdTe and CdS since it is present in both materials. Figure 24 shows how the band bending was determined for the sputtered GaN and CdTe interface. Both sides show downward band bending as the binding energy of the peaks both increase as they approach the interface, meaning that the distance from the core level electrons to the valence band is increasing. The interface for the GaN is taken at the last visible Ga peak, while the interface for the CdTe is taken after 1 minute of CdTe deposition.

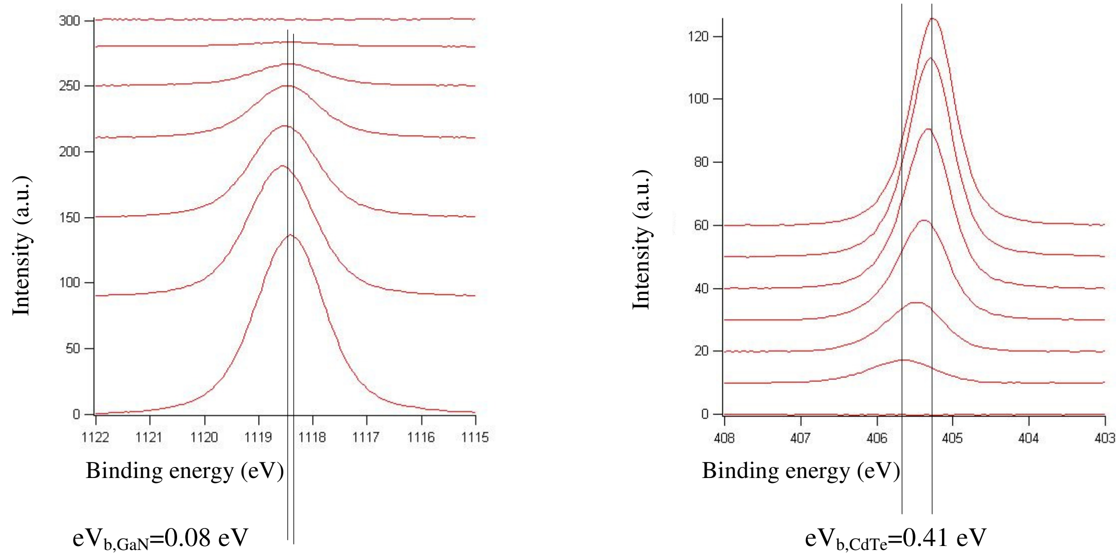

Figure 24 - Shifting of the XPS measurements for the Ga2p and Cd3d peaks over the course of the interface study to determine the band bending of each material

In addition to XPS measurements, UPS measurements were taken at each step of the interface study in order to determine the work function of the material. Although the work function was determined at each step, only the information from the bulk materials was used in creating the band diagrams. The electron affinity was determined in the bulk material from the work function and the position of the conduction band, and it was assumed that the electron affinity was constant throughout the material (see Figure 1 in section 1.1.4. Band Diagrams for a visual description of the relationship between work function and electron affinity). Helium gas was used as the excitation source for the UPS measurements, and its luminescence has an energy of 21.22 eV. Additionally, in order to ensure that the analyzer captures the emitted electrons, a positive bias of 6 eV was applied. Thus, the work function of the material was taken as:

$$\Phi = Excitation\ energy - Bias - UPS\ data = 21.22 - 6 - UPS\ data\ (eV) \qquad (18)$$

Much like the valence band measurements, the sharp cut-off where intensity falls to zero is used as the UPS data. Figure 25 shows the UPS measurements from the bulk GaN and the bulk CdTe for the sputter deposited GaN/CdTe interface.

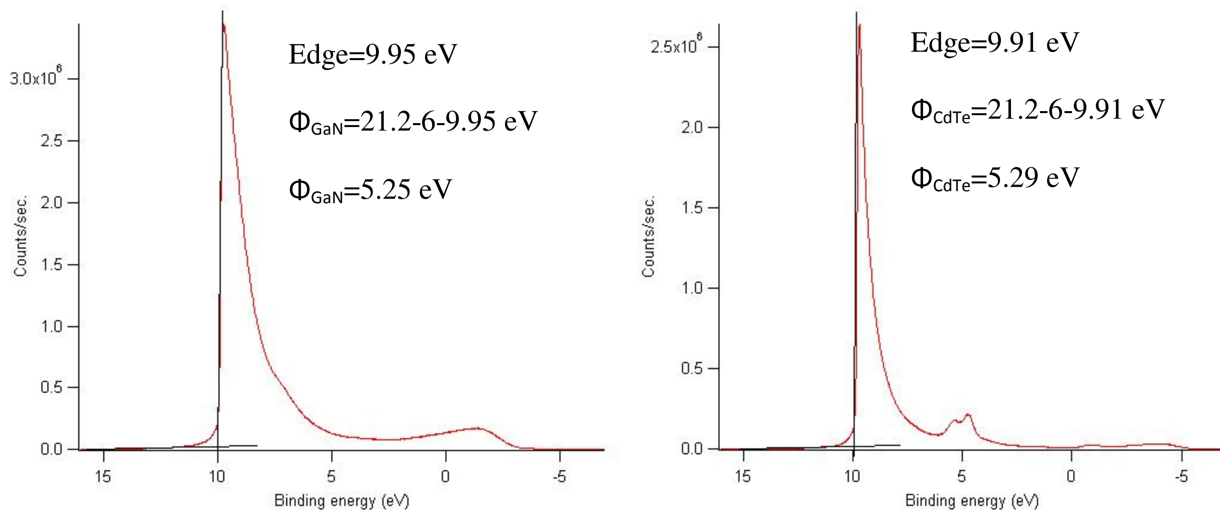

Figure 25 - UPS measurements for the bulk GaN (left) and bulk CdTe (right) and calculations to determine work function of each material

Now, the position of the Fermi level, the band bending for each material at the interface, and the distance from the valence band to the vacuum level is known. Additionally, the band gaps of most of the materials were determined by optical absorption, and they can be found in Table 5. Since we were not able to properly remove the background of the optical absorption data for the MOCVD-GaN, the band gap of the MOCVD GaN was taken as the commonly used value of 3.39 eV. After acquiring all of this data, an accurate band diagram can be created to describe the interface. For the intent of incorporating a GaN or InGaN film into the CdTe solar cell, an ideal interface would have no conduction band barrier when the Fermi levels are aligned, meaning that electrons can flow freely across the interface. Valence band discontinuities prohibit the movement of holes across the interface, but they are not as important as conduction band discontinuities in the desired positions for the GaN film in the CdTe solar cell.

Table 5 - Band gaps of materials used in interface studies determined by optical absorption

Material	Band Gap (eV) measured from optical absorption
Sputter deposited GaN	3.30
Sputter deposited InGaN	3.10
Close space sublimated CdTe	1.49
Close space sublimated CdS	2.40

Grant, et. al. in 1983 and Waldrop, et. al. in 1985 described a method of using XPS measurements to determine band offsets at an interface [79-80]. Their method involved taking the difference between

the distance from the core level to the valence band of the two materials at the interface and then subtracting the difference in core levels between the two materials, as can be seen in:

$$\Delta E_{VB} = \left(E_{CL}^{A} - E_{VB}^{A}\right) - \left(E_{CL}^{B} - E_{VB}^{B}\right) - \Delta E_{CL} \quad (19)$$

Once the valence band offset is known, the conduction band offset can be determined by:

$$\Delta E_{CB} = \Delta E_{g} - \Delta E_{VB} \quad (20)$$

When they create their band diagrams of an interface, they start with the band offsets and then use the band gaps and band bending to finish the diagram. However, since the core levels of the CdS and CdTe were dependent upon which type of material they were deposited on, we drew the band diagrams a slightly different way. We started by aligning the Fermi levels of each material, then drawing the position of the conduction and valence bands relative to the Fermi level. After taking the band bending into account, the conduction and valence band offsets were determined by simply taking the difference in energy between the bands of each material.

4.1.5 Different Interface Studies

Between four different materials (CdTe, CdS, GaN, and InGaN) and two different deposition methods for GaN (sputter deposition and MOCVD), many interface studies needed to be completed. There were six main interfaces that were studied: sputtered GaN/CdTe, MOCVD GaN/CdTe, sputtered GaN/CdS, MOCVD GaN/CdS, sputtered InGaN/CdTe, and sputtered InGaN/CdS. For various reasons, some of the interface studies needed to be repeated until accurate data was acquired.

It would have been nice to examine an MOCVD-InGaN sample at these interfaces, however a pure InGaN MOCVD sample could not be obtained.

4.2. Attempts for Contamination-Free MOCVD GaN

4.2.1 Attempts at removing surface contamination

The GaN samples that were grown via the MOCVD process described in the experiment section and then transported through air to DAISY-SOL were the first ones to be characterized by XPS. The purpose of this portion of the experiment was to get a baseline for what a normal MOCVD-grown GaN film consists of. As oxygen and carbon contaminants were expected, a significant portion of the measurement times were spent attempting to clean the surface to get rid of these contaminants. The surface contamination can skew the band alignment measurements, so it is desirable to eliminate it. Figure 26 shows the entire spectrum of the XPS data for the sample without any cleaning. At about 285

eV, there is clearly a small peak that represents carbon. Also, around 530 eV, there is a small oxygen peak, but it is difficult to see in this figure because it lies in the same region as the Ga Auger peaks.

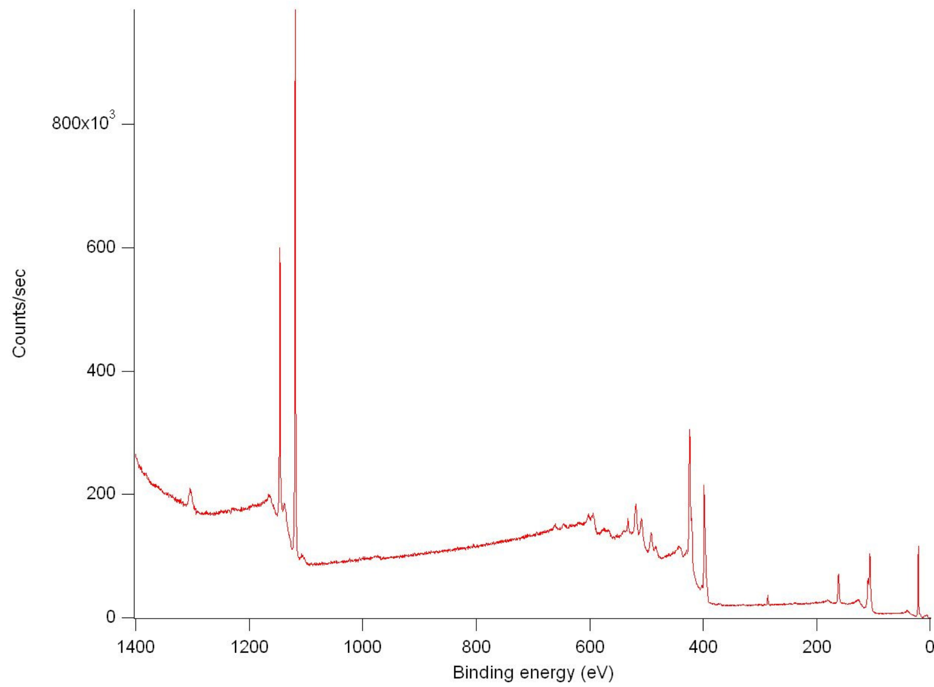

Figure 26 – XPS data from MOCVD-grown GaN sample exposed to air

The first attempt to eliminate the surface contamination involved a one hour anneal at 450°C inside the DAISY-SOL. After contamination was still present, the sample was annealed again for another hour, for a total anneal of two hours. The sample was then exposed to a nitrogen plasma treatment and then later to the same plasma treatment at an elevated temperature. While it appears in Figure 27 that the carbon peak has disappeared for the plasma treatment, it has actually just shifted about 10-15 eV to the left due to charging of the sample. Still, it should be noted that the plasma treatment removed a significant amount of carbon.

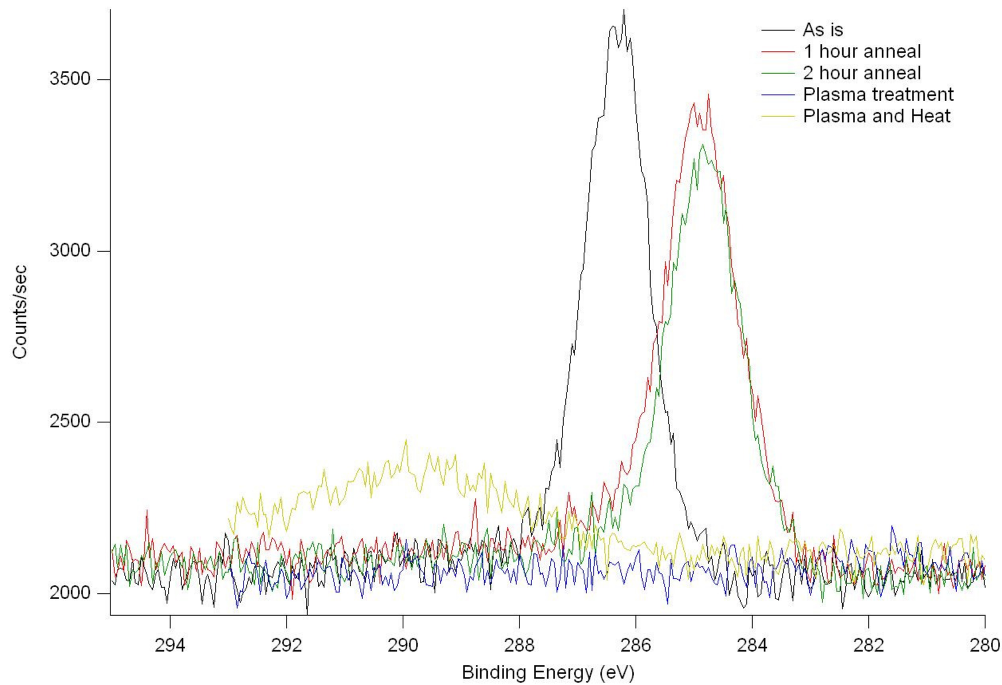

Figure 27 – XPS data for the C1s peak of MOCVD-grown GaN, averaged over 20 scans

The oxygen peaks can be seen in Figure 28. The oxygen was still present in all the samples. Again, however, the oxygen peak of the plasma treated sample was shifted to the left about 10-15 eV. In fact, in Figure 28, the shift caused a Ga Auger peak to appear where the O should be. The oxygen peaks in the annealing processes were actually the smallest, but once again, it is clear that still some contamination exists.

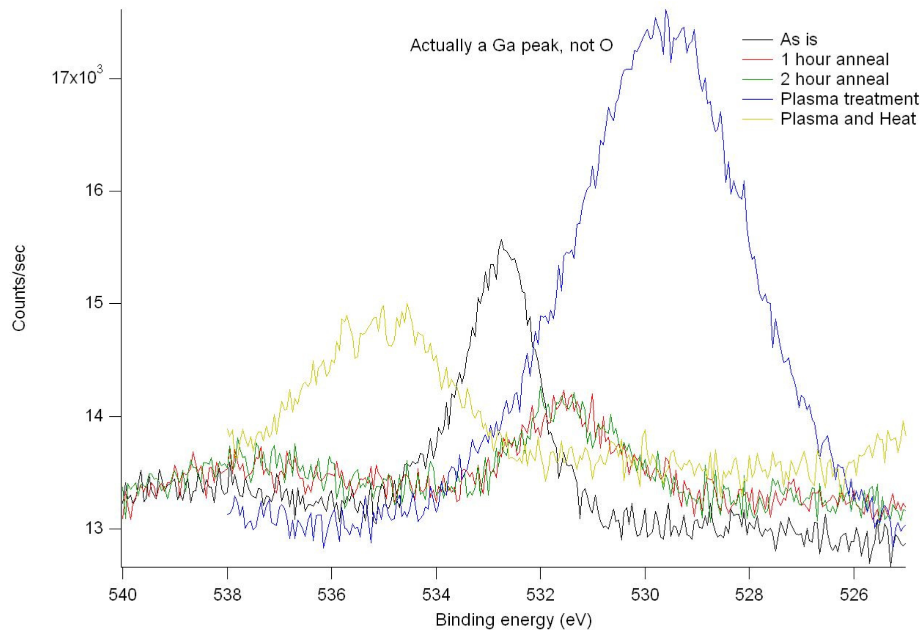

Figure 28 - XPS data for O peaks of MOCVD-grown GaN, averaged over 20 scans

This surface charging problem was eventually fixed by using a sample holder with longer screws, so that the sample sat slightly above the measurement platform.

4.2.2 MOCVD GaN with SiN cap

In an attempt to prevent surface contamination of MOCVD-GaN during the transport between the MOCVD tool and the DAISY-SOL, the GaN layer was given an MOCVD-grown SiN capping layer. Before the properties of the GaN could be tested on this sample, the SiN protective capping layer had to be removed without damaging the GaN layer underneath, which was attempted by using an ion sputter. The hope was that the sputter time could be precisely controlled as to sputter through the SiN layer, and then immediately shut off the ion beam, leaving an uncontaminated MOCVD-grown GaN layer. Unfortunately, the results did not turn out as hoped.

The attempted sputter removal of SiN was performed inside the ESCAlab 250 of the DAISY-SOL. First, the sample was examined by XPS after it had been grown in the electrical engineering department and then transferred to the materials science department. The Ga2p, N1s, O1s, C1s, Si2s, Si2p, and the valence band lines were specifically examined. Two silicon peaks were examined because the Si2p peak overlaps with a Ga peak at about 100 eV. Next, a one hour anneal at 450°C was performed to remove some of the surface contaminants. Following, Ar sputtering was performed for up to 50 seconds, with XPS characterization taking place after 5s, 10s, 20s, and 30 s for all the peaks, and then 40s and 50s for just the Si2s peak.

The survey results of the spectrum from 1400 eV to -2 eV can be seen in Figure 29. As a survey, they all look very similar, except for the appearance of a small carbon peak at 285 eV in the as received sample.

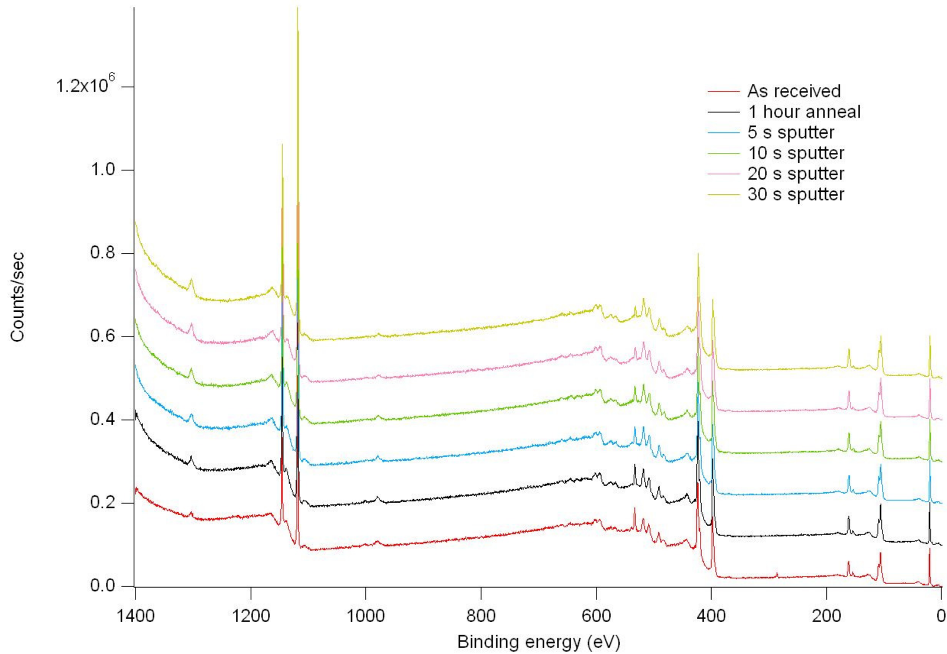

Figure 29 – XPS surveys of samples before and after sputtering

First the Si2s peak is examined more closely. As can be seen in Figure 30, the silicon peak decreases in magnitude and shifts slightly toward lower binding energy with increased sputtering time. The shift is assumed to be a tool drift, as a similar shift appears in the Ga2p peaks and the O1s peaks. Although the silicon signal decreases, it never completely disappears. It is possible that the ion beam is actually driving some of the silicon atoms into the gallium nitride lattice instead of removing them from the system.

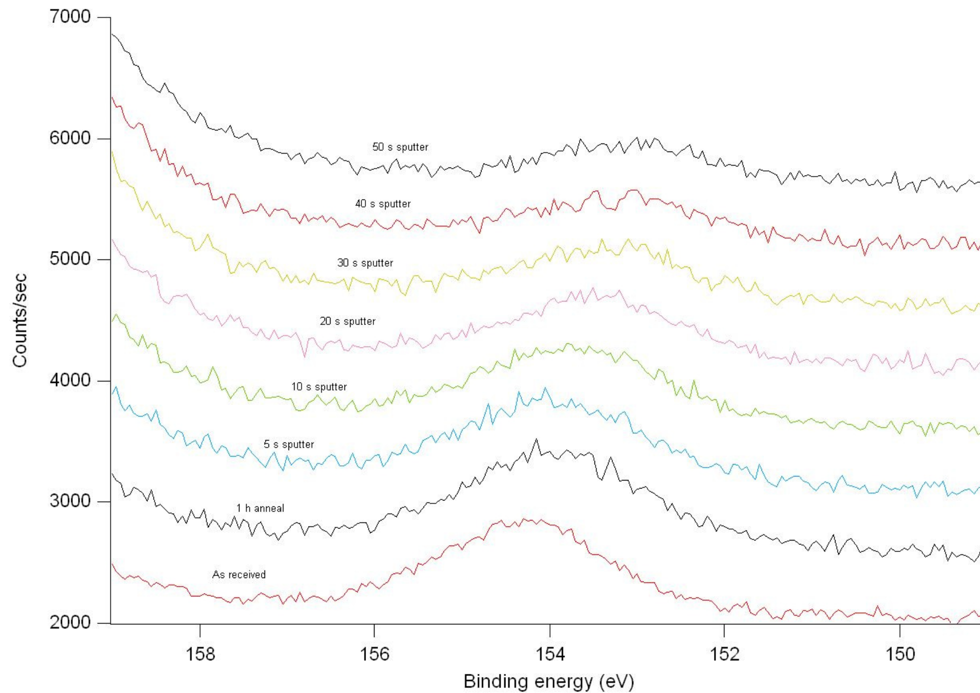

Figure 30 - XPS measurements of the Si2s peak for GaN with a SiN cap

More sputtering would have been performed to check if the silicon could be fully removed, however the valence band measurements indicated that the sputter was damaging the GaN layer underneath the SiN. In the valence band measurements, there should be a sharp cut off where the signal simply drops to zero. However, as can be seen in Figure 31, as the sputter is increased, the drop off becomes increasingly gradual. When the GaN layer is damaged, its properties can change, as surface states are present. Additionally, without the sharp cutoff of the valence band, the interface study with CdTe cannot be performed accurately.

One interesting item of note is that the distance from the cutoff to zero represents the difference between the Fermi level and the valence band. As GaN is usually intrinsically n-doped, it was expected that the Fermi level lie closer to the conduction band. However, in these samples, for the as-received and annealed samples, the Fermi level lies above the conduction band, indicating that this sample is very highly n-doped. As silicon is a known n-type dopant for GaN, the silicon might have actually diffused into the gallium nitride layer instead of staying in the SiN layer on top. This could also explain why there is still a residual Si2s peak even after 50 seconds of sputtering.

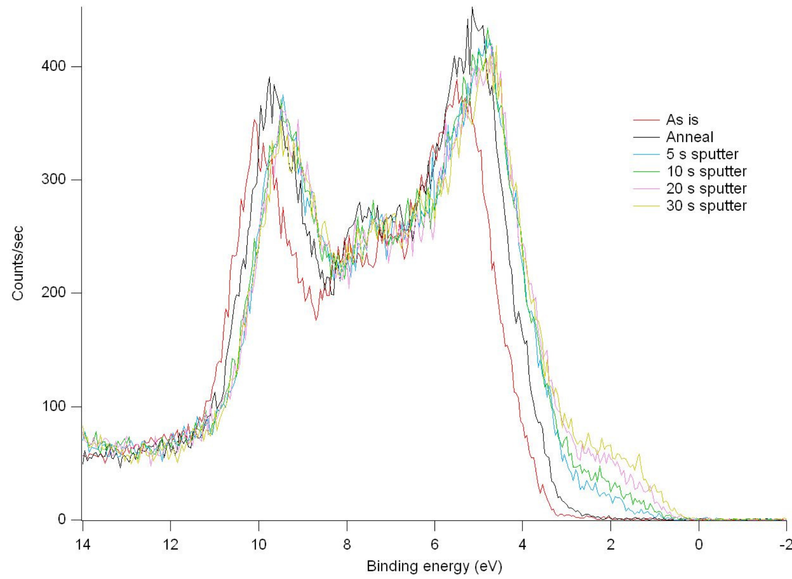

Figure 31 - XPS measurements of the valence band of GaN with a SiN cap

Another n-type dopant for GaN is oxygen. Interestingly, the oxygen 1s peak did not decrease at all with the annealing step. It did decrease as the sputter continued, but like the silicon, it never totally disappeared, still leaving a fairly strong signal after 30 s of sputtering. Again, it is possible that oxygen has worked its way into the GaN lattice, causing an increase in the n-doping and thus the Fermi level.

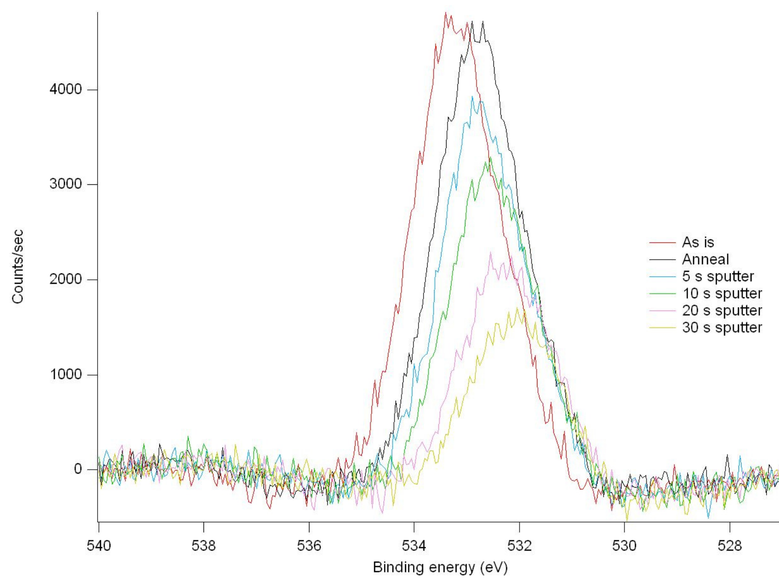

Figure 32 - XPS data of O1s peaks for GaN with SiN cap

Since none of the methods to reduce the surface contamination worked particularly well, a simple one hour anneal at 450°C was used to remove some of the O and C contamination on the MOCVD GaN samples without the SiN cap.

4.3. GaN and CdTe Interfaces

These interface studies were time consuming and produced copious amounts of data. Therefore, all of the data will be presented for the first interface, and then only the relevant data will be shown for the rest of the interfaces. The entirety of the data can be found in Appendix C.

To prevent human error, the core peaks and peak shifts were determined by removing the background and using a Gaussian fit in a program known as Igor Pro. The maximum of the Gaussian peak was taken as the correct value of the peak. The XPS was calibrated against a silver sample to ensure the accuracy of the data. However, human error was still possible for the valence band measurements and the UPS measurements.

4.3.1. CdTe onto Sputtered GaN

The first interface study performed was CdTe on top of sputter deposited GaN. All deposition and characterization was performed inside of the DAISY-SOL, preventing any exposure to atmospheric conditions. Figure 33 shows the important XPS peaks required to draw the band structures. The Ga peak shifts from 1118.31 eV at 0 minutes of CdTe deposition to 1118.39 eV at the interface (16 minutes). This shift corresponds to a downward GaN band bending at the interface of 0.08 eV. Furthermore, the Ga peak completely disappears after 32 minutes of CdTe deposition, indicating that bulk CdTe has been grown.

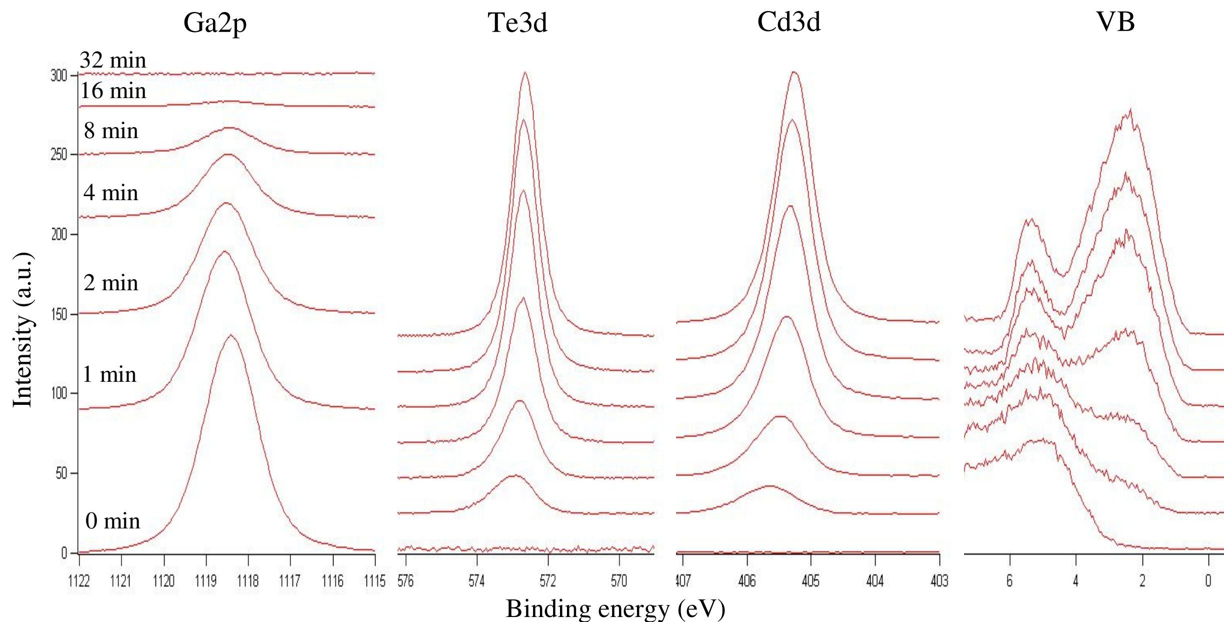

Figure 33 - The XPS peaks of Ga, Te, Cd, and the valence band as the material shifts from bulk GaN (0 minutes CdTe deposition) to bulk CdTe (32 minutes CdTe deposition)

Also in Figure 33, the Te peak shifts from 571.76 eV in the bulk CdTe (32 minutes) to 572.13eV at the interface (1 minute). The Cd peak shifts a similar amount (0.41 eV) to confirm the downward band bending of the CdTe. The valence band spectra give us information about the Fermi level location in the material. For a metal, the sharp decrease to 0 counts will occur at 0 eV. For semiconductor materials, the distance from the sharp decrease to 0 eV indicates the distance E_F-E_{VB} in the material. In Figure 33, it can be observed that this distance shifts from about 2.94 eV in the bulk GaN (0 minutes) to 0.77 eV in the bulk CdTe after a total of 32 minutes of deposition.

The full survey XPS measurements are shown in Figure 34. It can be seen that the intensity of the Ga and N peaks decrease with each deposition step until they disappear completely after 32 minutes of CdTe deposition. Meanwhile, the Cd and Te peaks increase with each deposition step

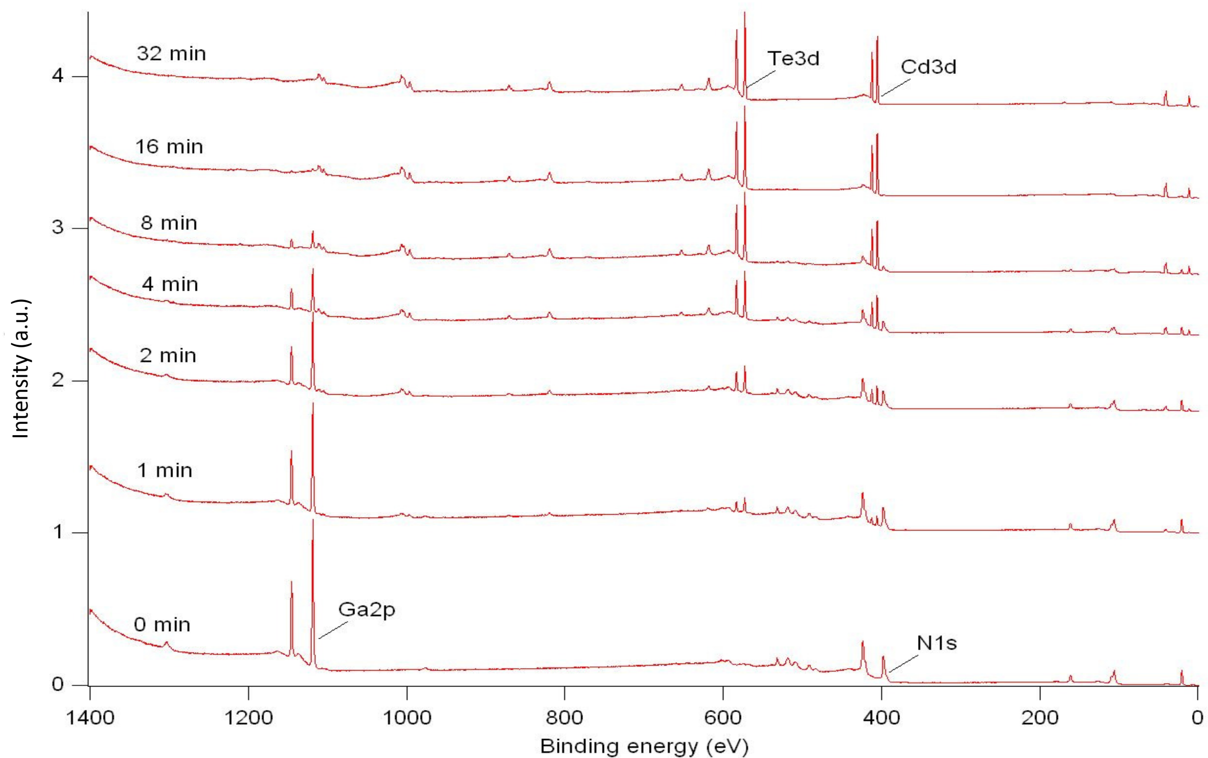

Figure 34 - Survey XPS measurements for the entire interface study of sputter deposited GaN and CdTe. Note the simultaneous decrease of the Ga and N peaks while the Te and Cd peaks gradually increase.

UPS measurements were carried out to learn the position of the vacuum level of the material. The sample was excited with a He UV lamp of energy 21.2 eV after each deposition step. Figure 35 shows the UPS measurements from this interface. A 6V bias was applied to the sample to help the analyzer detect the signal, so the peak should be increased by 6eV to about 16eV. The distance from the

UV energy to the beginning of the peak around 16 V represents the work function Φ, which is the distance from the Fermi level to the vacuum level.

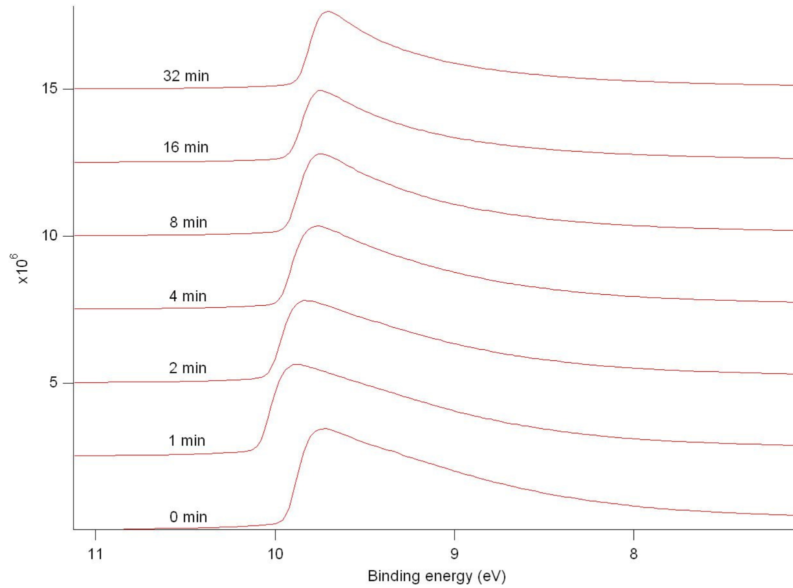

Figure 35 - UPS measurements for CdTe deposited on top of sputter deposited GaN

Information about the energy levels in the bulk materials as well as at the interface and the band bending at the interface has been acquired. Between this information and the previously known band gaps of the materials (3.30 eV for sputtered GaN, 1.49 eV for CdTe), it is possible to draw a full band diagram showing the interface between the two materials with the Fermi levels aligned, and this can be seen in Figure 36. On this band diagram, χ represents the electron affinity of the semiconductor, which is the distance from the conduction band to the vacuum level. Additionally, ΔE_{VB}, ΔE_{CB}, and ΔE_{Vac} represent the valence band offset, conduction band offset, and the vacuum level offset respectively. eV_b is the bend bending determined from the shift in the XPS peaks, and it shows the built-in potentials of each material at the interface.

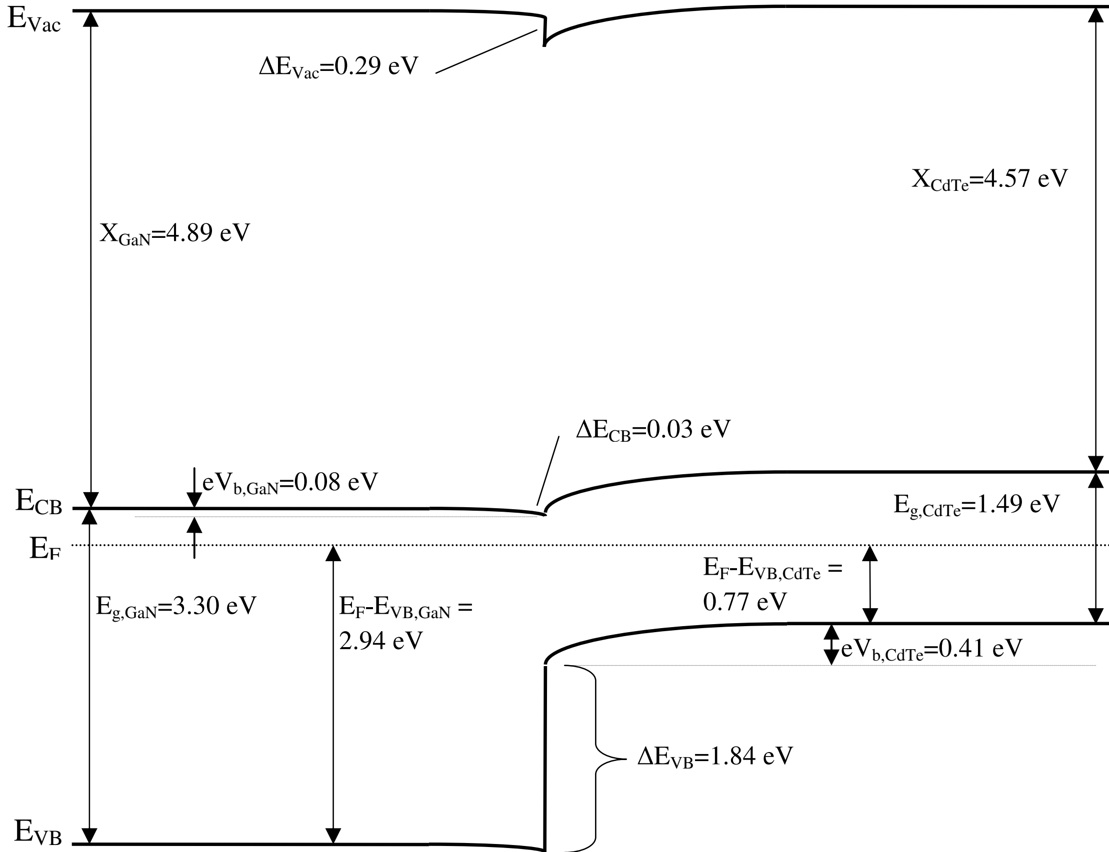

Figure 36 - Band diagram for CdTe deposited onto sputter deposited GaN. The GaN is on the left and the CdTe is on the right.

It is observed that a very small conduction band offset (ΔE_{CB}) exists, which indicates that electrons can flow freely across the interface. However, since both materials exhibit downward band bending, both materials draw electrons to the interface, but not across it. The 0.29 eV discontinuity in the vacuum levels indicates an interface dipole. The valence band discontinuity is much higher at 1.84 eV, which means that there is a large barrier for holes to move across the interface.

4.3.2. CdTe onto MOCVD-GaN

Several attempts at this interface study were required before reliable data was acquired. To acquire more measurements despite the rapid deposition, XPS and UPS measurements were taken at every minute, except for a two minute deposition from 5 to 7 minutes of total deposition. From Figure 37, it can be seen that the Ga peak shifts about 0.04 eV toward a higher energy, indicating a small downward band bending for the GaN. The cadmium peak also shifts to a higher energy as it approaches the interface, indicating a downward band bending of about 0.14 eV. The Fermi level of the pure GaN was about 2.97 eV above the valence band, while the Fermi level of the CdTe was about 0.83 eV above the valence band.

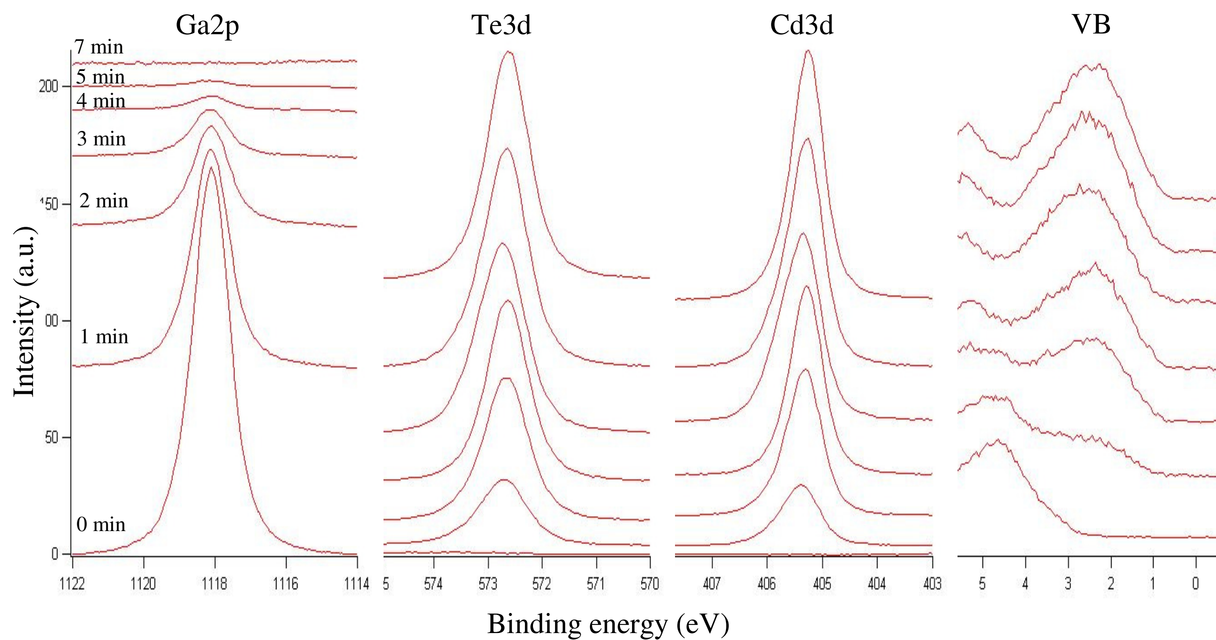

Figure 37 - XPS peaks for Ga, Te, Cd, and the valence band as the material shifts from bulk GaN (0 minutes) to bulk CdTe (7 minutes)

After examining the XPS and UPS data, the completed band diagram for the interface was created by aligning the Fermi levels of each material, which can be seen in Figure 38. While in the previous interface study, the conduction band offset was negligible at about 0.04 eV, the conduction band offset in this interface study was a little bit more significant at 0.13 eV. Due to the difference in band gaps between the materials, there was a large valence band offset of about 2.03 eV. Additionally, there was a vacuum level offset of about 0.76 eV, indicating an interface dipole. The XPS survey measurements, the UPS measurements, and graphs describing the shifts in the Fermi levels and the valence band offsets can be found in Appendix C.

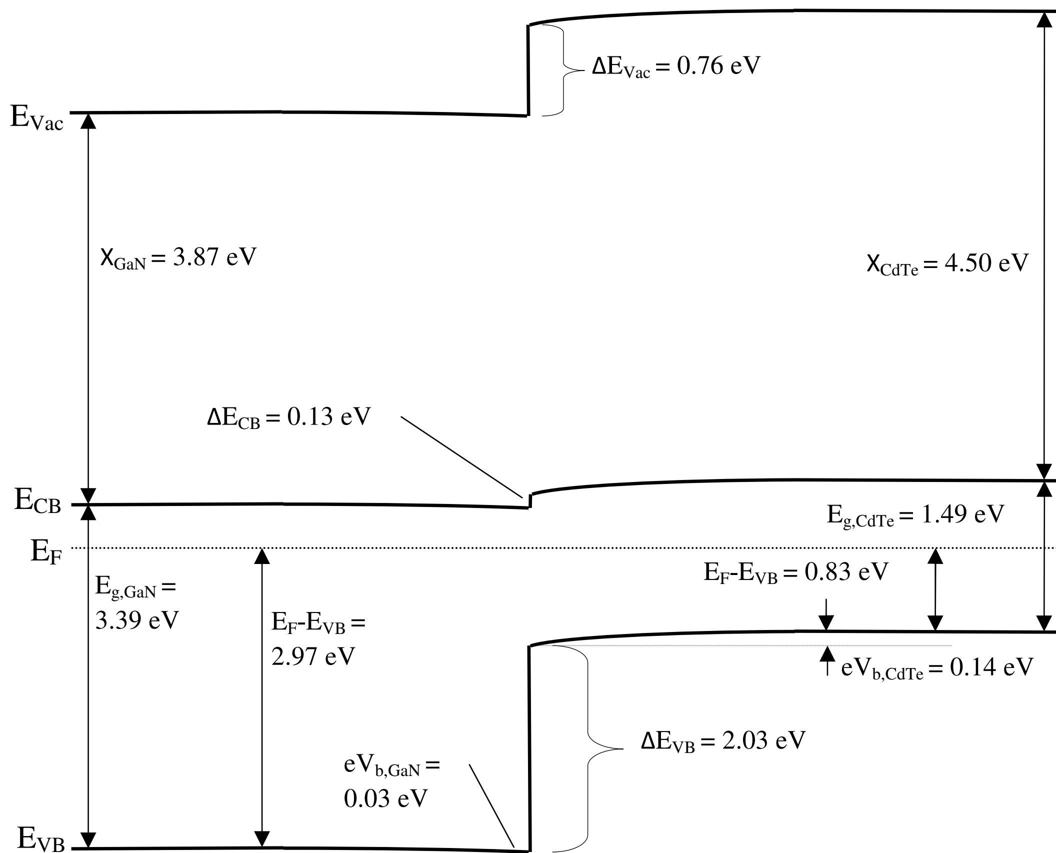

Figure 38 - Band diagram for CdTe deposited onto MOCVD GaN. The GaN is on the left and the CdTe is on the right.

4.3.3. Sputter Deposited InGaN and CdTe Interface

Again, all deposition and characterization steps were performed inside of the DAISY-SOL. Through XPS quantification, it was determined that the InGaN film contained only about 1.5 at% In, which was much lower than expected. However, that little amount of In provided several differences from the pure GaN. An interesting observation is that while the Ga peak completely disappeared after 32 minutes of CdTe deposition, an In peak was still visible, as can be seen in Figure 39. As In is known as a substitutional n-type dopant in CdTe at low concentrations [81], it is expected to cause the CdTe material to become n-doped through diffusion. This was observed as the Fermi level of the bulk CdTe in this study was about 0.12 eV higher than the Fermi level of the bulk CdTe deposited on GaN.

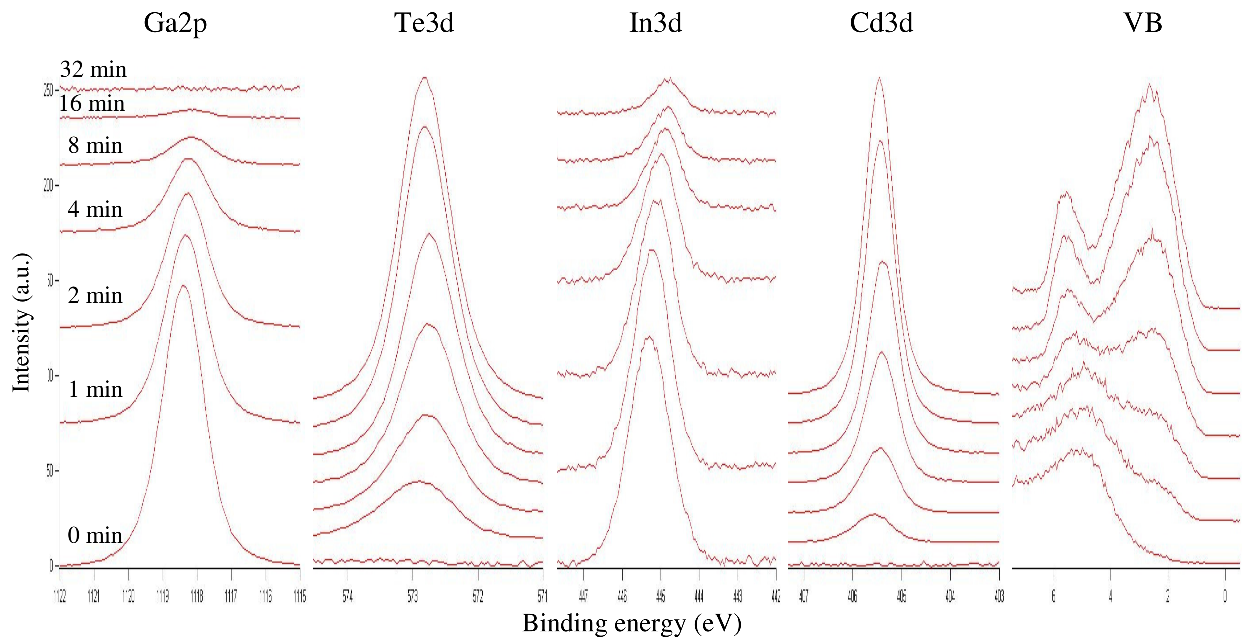

Figure 39 - XPS peaks for Ga, Te, In, Cd, and the valence band as the material shifts from bulk InGaN (0 minutes) to bulk CdTe (32 minutes)

It was suggested that the appearance of an In peak after 32 minutes of deposition was caused by a different attenuation length between the In signal and the Ga signal. Thus, it would be possible to see a In peak without seeing a Ga peak, and there would be no evidence of actual In diffusion. In order to strengthen the argument for In diffusion, Figure 40 shows how the nitrogen peak disappears but an In peak is still present after 32 minutes of deposition. Since In and N have similar attenuation lengths, this indicates that there is In diffusion.

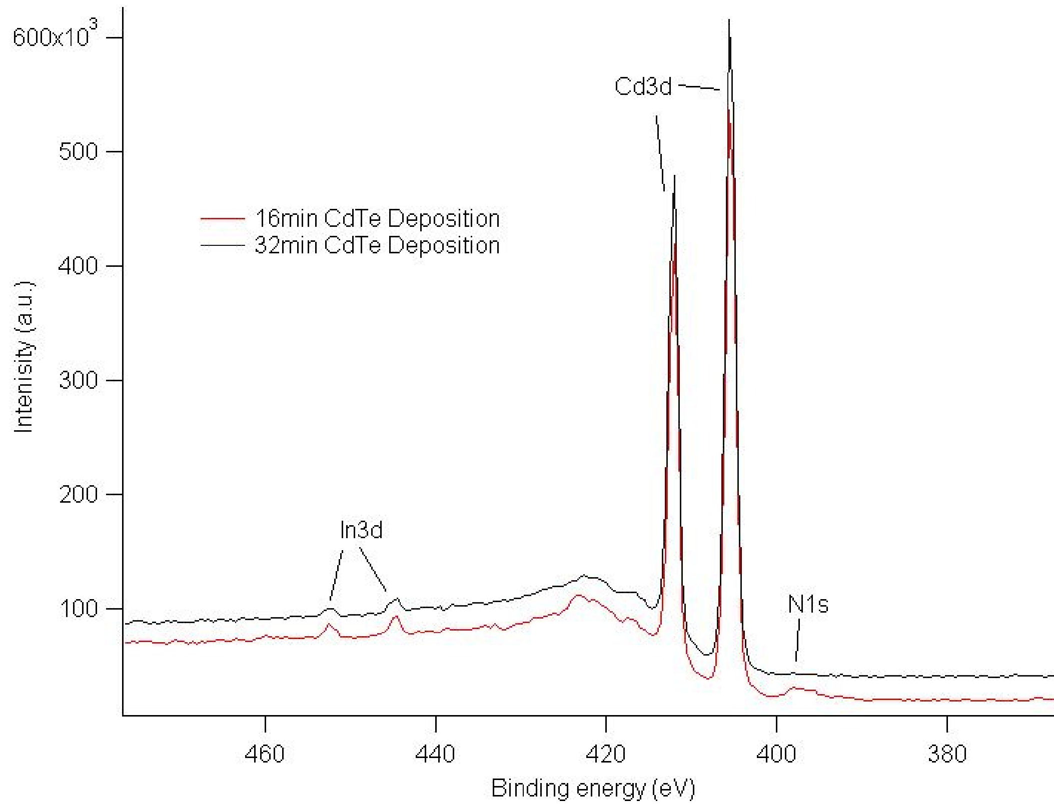

Figure 40 - XPS survey data showing the presence of In after the N peak has disappeared

The completed band diagram for the sputter deposited InGaN and CdTe interface appears in Figure 41. In this band diagram, it is seen that the InGaN has an upward band bending of about 0.18 eV while the CdTe exhibits a downward band bending of about 0.13 eV, which is significantly smaller than the CdTe band bending at the sputtered GaN interface. Due to this structure of the band bending, the electrons are drawn across the interface from the CdTe to the InGaN in order to reduce their energy. Still, the band bending is fairly modest, and only a small electric field exists. This band diagram also exhibits a small ΔE_{CB} of 0.04 eV, which does not inhibit the electron flow over the interface. A large vacuum level discontinuity of about 0.69 eV exists at this interface, indicating that the work function for InGaN is smaller than GaN. There is again a significant valence band discontinuity of about 1.65 eV. As previously mentioned, the Fermi level of the CdTe is higher in this situation due to the indium diffusing into the material and acting as an n-type dopant.

The entire XPS and UPS data can be found in Appendix C.

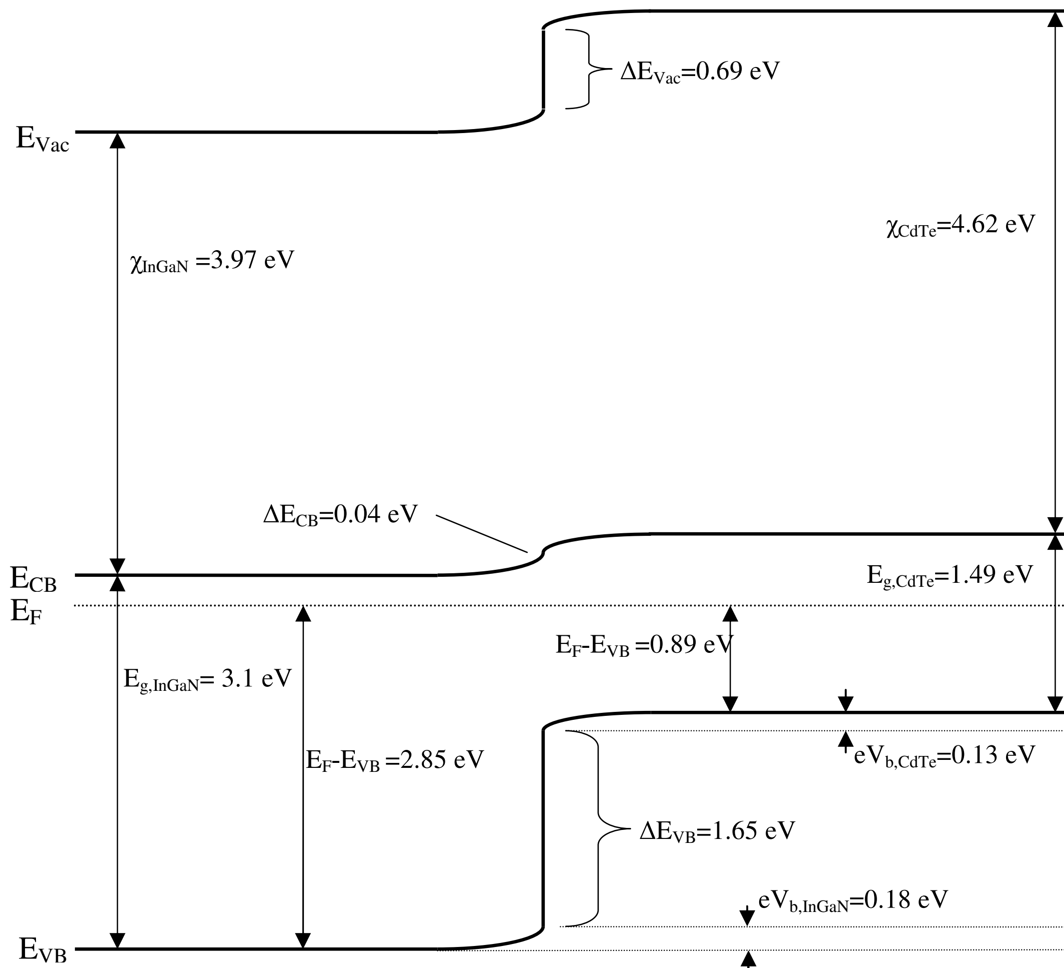

Figure 41 - Completed band diagram with Fermi level alignment for sputter deposited InGaN (left) and CdTe (right)

4.4. GaN and CdS Interfaces

4.5.1. CdS on Sputtered GaN

Figure 42 shows the XPS peaks measured at 0, 1, 2, 4, 8, and 16 minutes of cadmium sulfide deposition. Unlike the sputtered GaN and CdTe interface study which required 32 minutes of deposition, bulk CdS was achieved at 16 minutes deposition, meaning that the gallium peaks completely disappeared. This interface differed from the others because it showed flat band conditions on both sides, meaning with the doping levels in each material, there was no internal electric field at the interface. From bulk GaN at 0 minutes of deposition to the last deposition step where Ga was visible at 8 minutes of deposition, the Ga peak appeared consistently at the same position of about 1118.33 eV. Since there was no obvious shift present in the position of the Ga peaks, there is no band bending on the GaN side of the interface.

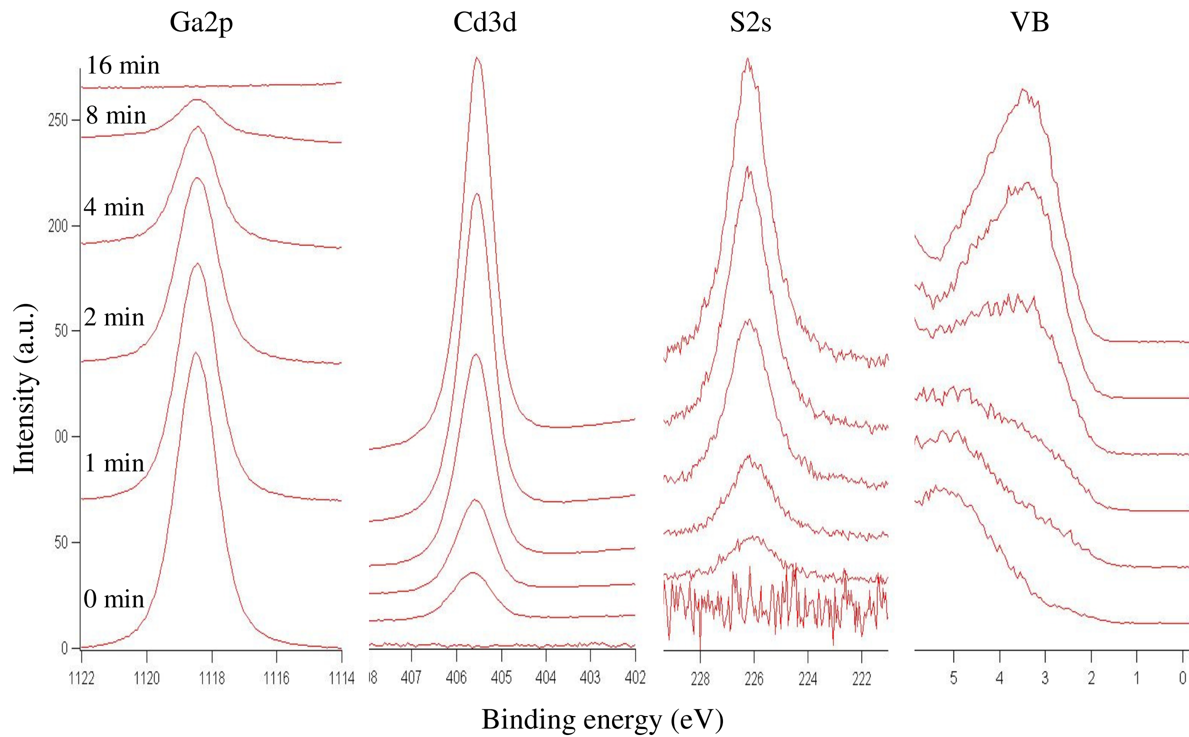

Figure 42 - XPS peaks for Ga, Cd, S, and the valence band as the material shifts from bulk GaN (0 min) to bulk CdS (16 min)

On the other hand, the cadmium peak shifted from 405.41eV in the bulk CdS to 405.52 eV at the interface (1 min CdS deposition), which would indicate a downward band bending of 0.11 eV. However, the sulfide peak showed a similar shift of about 0.09 eV in the opposite direction. It is believed that the conflicting XPS measurements in the CdS layer cancel each other out, and the overall band bending is negligible.

(a) (b)

Figure 43a shows the conflicting changes in the Fermi level position of the CdS taken from the Cd and the S peaks. Similarly,

(a) (b)

Figure 43b shows the valence band offset at the interface move in opposite directions as the deposition proceeds.

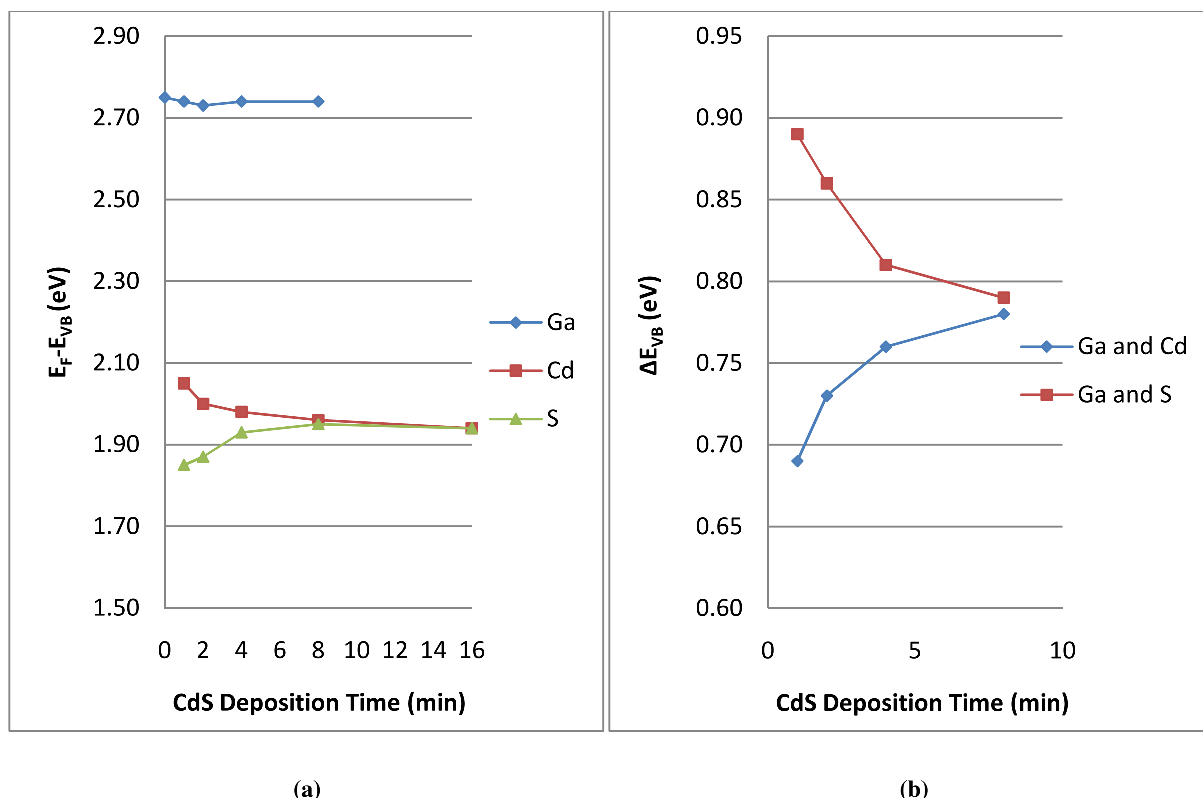

Figure 43 - Left: The change in Fermi level position for each element as the interface study proceeds. Right: The change in valence band offset between the two materials as the interface study proceeds.

In the bulk GaN, the valence band measurements indicated that the Fermi level lay about 2.75 eV above the valence band. Likewise, the Fermi level of the bulk CdS lay about 1.94 eV above the valence band. With the position of the Fermi levels and the amount of band bending (or lack thereof), the completed band diagram is presented in Figure 44. The conduction band offset is about 0.09 eV, and the valence band offset is about 0.81 eV. The conduction band offset is slightly higher than the conduction band offset for the sputtered GaN and CdTe interface. Additionally, the vacuum level offset indicates an interface dipole of 0.54 eV.

The Fermi level of this sputtered GaN sample was about 0.2 eV lower than the sample used for the sputtered GaN and CdTe sample. This is probably due to drift in the sputter target as the GaN/CdTe interface study was performed at the end of January and the GaN/CdS interface study was performed at the beginning of May. During these three months, the sputter target was also removed from the sputter chamber and replaced with the InGaN sputter target to perform the sputtered InGaN interface studies. Although the Fermi level affects the band bending of the materials, it does not affect the barrier heights (band offsets) at the interface. Thus, the band offsets are characteristic of the materials and do not depend on the doping levels. Since we are primarily concerned with the band offsets to determine if the carriers

are being prevented from moving across the interface, the exact location of the Fermi level is not crucial for our purposes.

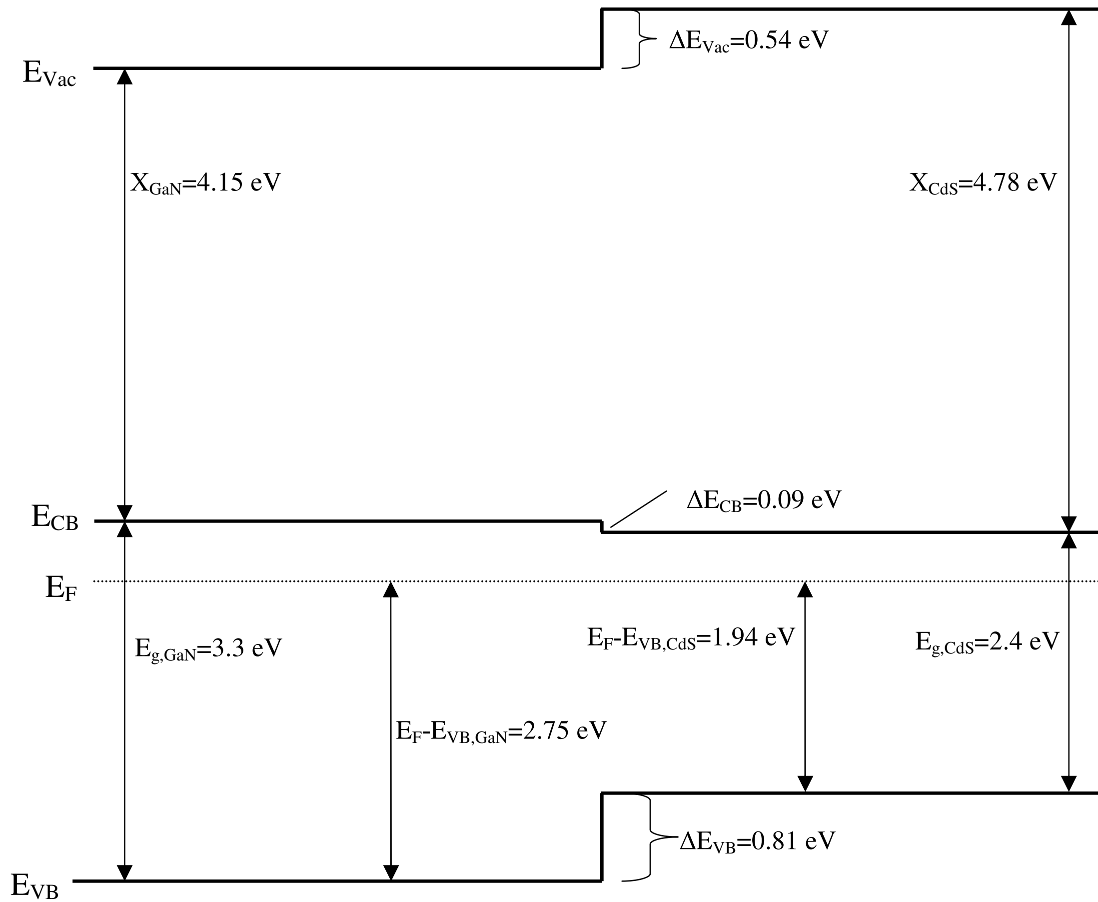

Figure 44 - Completed band diagram with Fermi level alignment for sputter deposited GaN (left) and CdS (right)

The entire XPS spectrums and the UPS measurements over the entire course of the interface study can be found in Appendix C.

4.5.2. CdS on MOCVD-GaN

As in the interface study between MOCVD grown GaN and CdTe, this interface study required several attempts before reliable data was attained. Figure 45 shows the XPS data for the Ga, Cd, S, and valence band peaks over the whole interface study. The Ga peak shifts about 0.25 eV to a higher binding energy as it approaches the interface, so this indicates a downward band bending for the GaN. The Cd peak shifts about 0.13 eV toward a higher binding energy, indicating a downward band bending for the CdS. The E_F-E_{VB} distance of the bulk GaN was about 2.94 eV while the E_F-E_{VB} distance for the bulk CdS was about 2.22 eV.

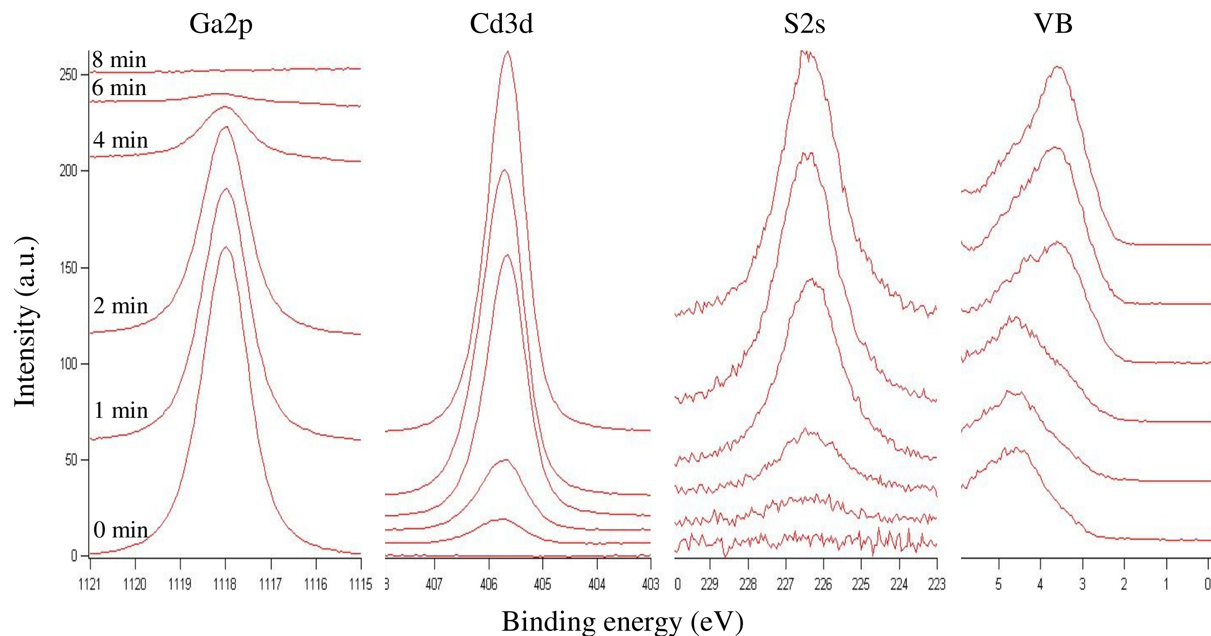

Figure 45 - XPS peaks for Ga, Cd, S, and the valence band as the material shifts from bulk GaN (0 min) to bulk CdS (8 min)

Figure 46 shows the completed band diagram for this interface study. The UPS was not functioning properly when this interface study was performed, so there is no data about the vacuum levels or electron affinity. Due to the extra measurement after 6 minutes of CdS deposition, a more pronounced downward band bending of the GaN was observed, which reduced the conduction band offset to 0.15 eV. This value was still higher than expected, but it is a reasonable value that does not prevent electron flow. It should be noted that if a band gap of 3.30 eV for the MOCVD-GaN is used (which is the measured band gap of the sputtered GaN samples), then the conduction band offset would drop to 0.06 eV. The valence band offset at this interface is 0.81 eV.

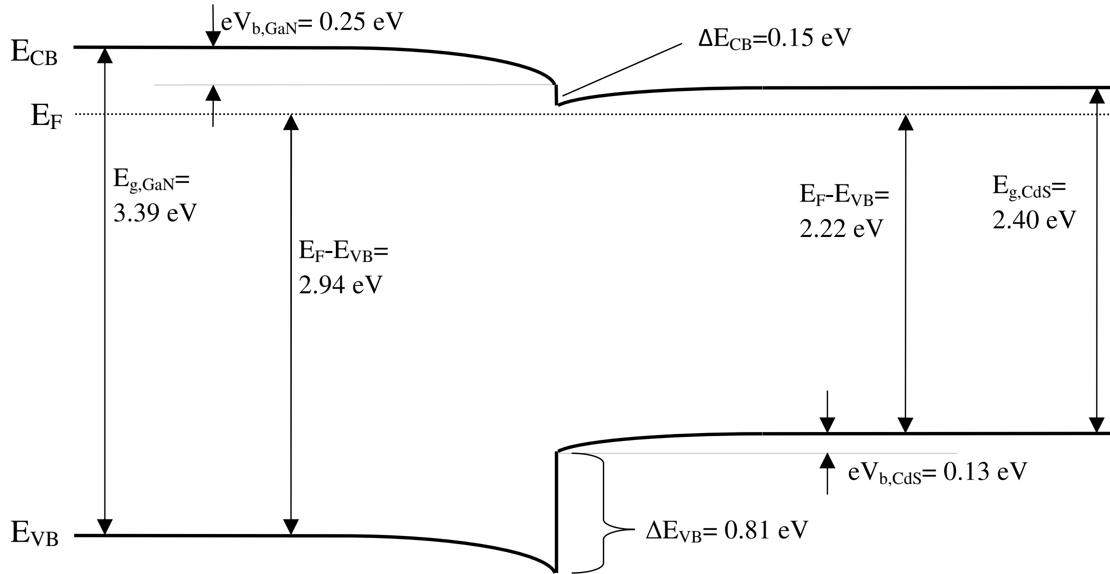

Figure 46 - Completed band diagram with Fermi level alignment for sputter deposited GaN (left) and CdS (right). The UPS was not functioning properly during this interface study, so there is no information about the electron affinity or the vacuum levels.

4.5.3. Sputter Deposited InGaN and CdS Interfaces

The XPS peaks of Ga, In, Cd, S, and the valence band gathered during the interface study can be seen in Figure 47. From this data, the gallium peak shifted about 0.10 eV to the right, which represents an upward band bending. The cadmium peak showed no overall shift from the interface to the bulk CdS. The distance E_F-E_{VB} shifts from about 2.88eV in the bulk InGaN to about 2.11 eV in the bulk CdS. Again, a small In peak appeared in the bulk CdS layer when the normally stronger Ga peak completely disappeared. As in the InGaN and CdTe interface, it is believed that the In is diffusing into the CdS and acting as an n-type dopant. The In peak is compared to the N peak after 8 minutes and 16 minutes of deposition in Figure 48. Once again, a very small In peak still exists whereas the N peak completely disappears, indicating In diffusion instead of a residual peak due to differences in attenuation length between the In and Ga.

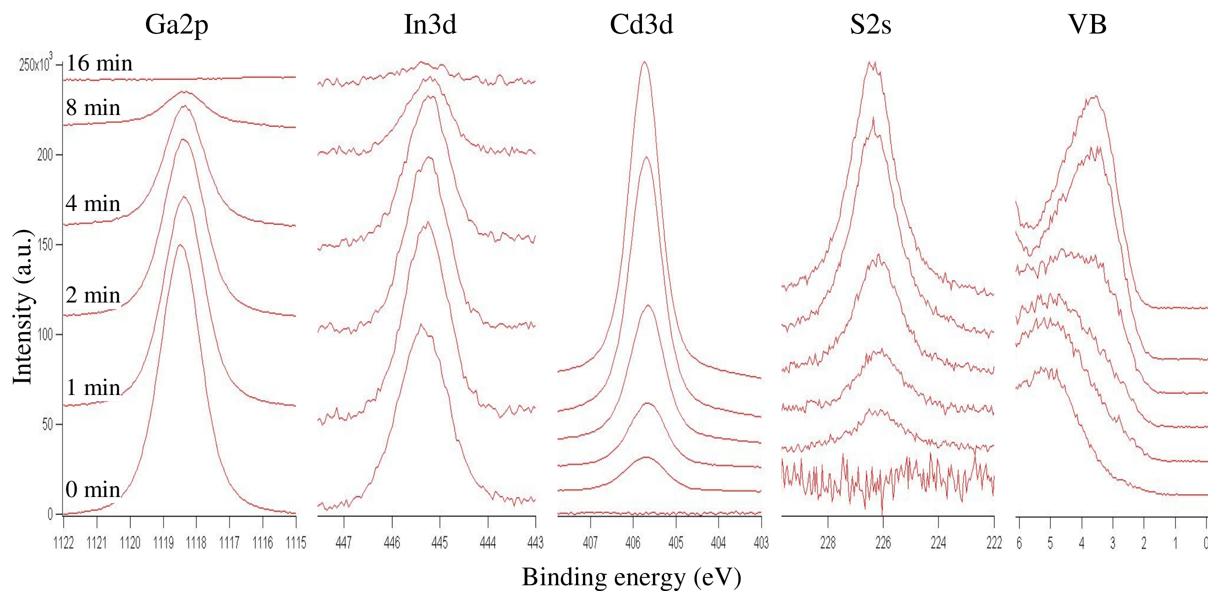

Figure 47 - XPS peaks for Ga, In, Cd, S, and the valence band as the material shifts from sputter deposited InGaN (0 min) to CdS (16 min)

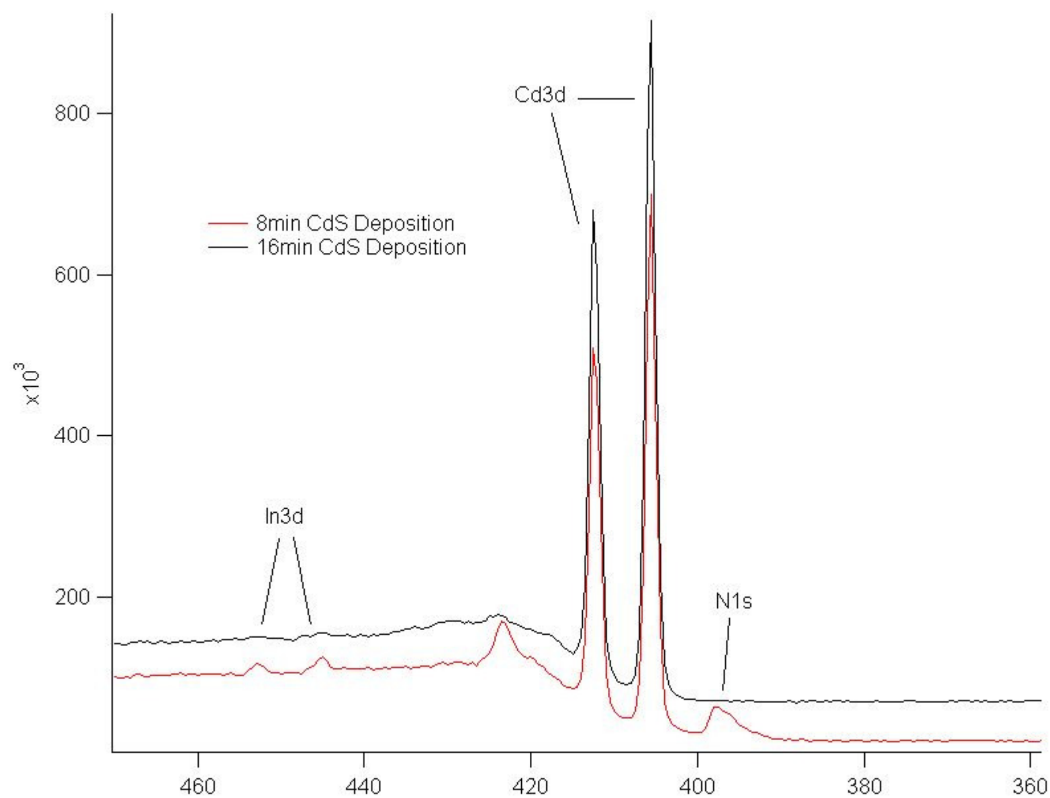

Figure 48 - XPS survey data showing the presence of In after the N peak has disappeared

Figure 49 shows the completed band diagram of the experiment. Since it has been shown in this paper that the sputtered InGaN forms a tiny conduction band offset with CdTe, and previous experiments have shown that there is no conduction band offset at the interface between CdTe and CdS [82-83], using the transitive property, there should be a tiny conduction band offset between sputtered InGaN and CdS. This is confirmed by this interface study since it has a conduction band offset of only 0.04 eV. Also from this data, it is seen that a valence band offset of 0.66 eV and an interface dipole (ΔE_{Vac}) of 0.68 eV exist. As the Cd peak did not shift at all in the XPS measurements, this indicates there is no band bending of the CdS at this particular interface.

The surveys of the XPS data and the UPS data to acquire the work function can be found in Appendix C.

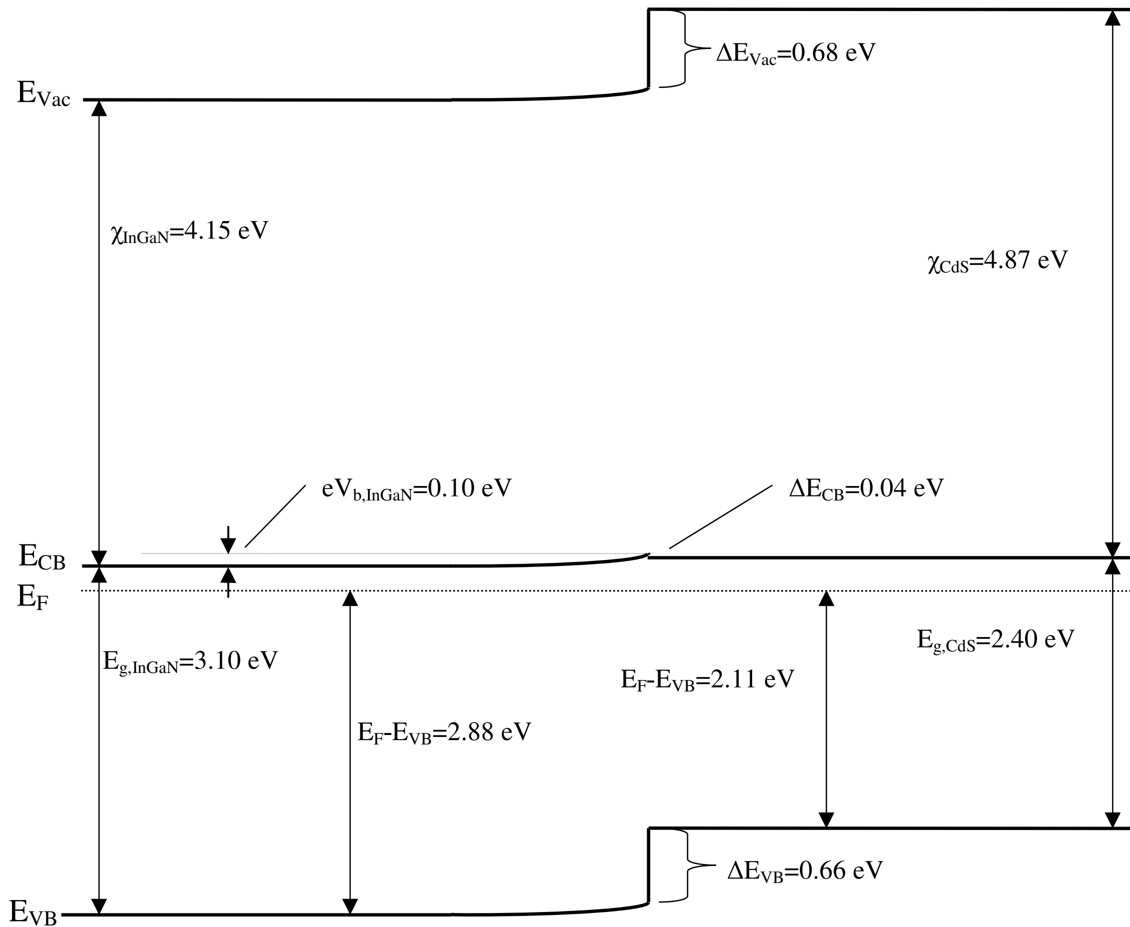

Figure 49 - Completed band diagram with Fermi level alignment for the sputter deposited InGaN (left) and the CdS (right)

4.7. *Interface Study Summary*

A summary of the important data from the interface studies is seen in Table 6. Most importantly for the purposes of incorporating a GaN or InGaN film into the CdTe solar cell, there are small conduction band offsets of less than or equal to 0.15 eV at every interface. These small conduction band offsets do not significantly restrict the flow of electrons across the interface. Interestingly, the interfaces with MOCVD GaN have slightly higher conduction band offsets than the interfaces with sputtered GaN, showing that deposition method truly does influence the interface properties. The interface studies performed in early June do not include information about the electron affinities (χ) or the vacuum levels due to UPS downtime.

Table 6 - Summary of interface studies

Date	Starting Material	Deposited Material	$eV_{b,\,GaN}$	$eV_{b,\,CdS\ or\ CdTe}$	E_F-$E_{VB,\,GaN}$	E_F-$E_{VB,\,CdS\ or\ CdTe}$	χ_{GaN}	$\chi_{CdS\ or\ CdTe}$	ΔE_{VB}	ΔE_{CB}	ΔE_{Vac}
Jan. 31, 2010	sputter deposited GaN	CdTe	-0.08	-0.41	2.94	0.77	4.89	4.57	1.84	0.03	0.29
Feb. 28, 2010	sputter deposited InGaN	CdTe	0.18	-0.13	2.85	0.89	3.97	4.62	1.65	0.04	0.69
Mar. 12, 2010	sputter deposited InGaN	CdS	0.10	-0.01	2.88	2.11	4.15	4.87	0.66	0.04	0.68
May 3, 2010	sputter deposited GaN	CdS	0.01	0.00	2.75	1.94	4.15	4.78	0.81	0.09	0.54
June 8, 2010	MOCVD-GaN	CdS	-0.25	-0.13	2.94	2.22	-	-	0.84	0.15	-
June 22, 2010	MOCVD-GaN	CdTe	-0.03	-0.14	2.97	0.83	3.87	4.50	2.03	0.13	0.76

Figure 50 gives a comparison for the E_F-E_{VB} distance for the various GaN and InGaN samples. The MOCVD samples consistently have the highest Fermi level, possibly due to absorbed oxygen, which acts as an n-type dopant. The InGaN samples tend to be the most consistent, as the Fermi level position is between 2.85 and 2.90 eV for all three samples. The sputtered GaN showed two different Fermi level positions, and this could be due to changes in the GaN target over time. The first sputtered GaN sample was created on January 31st, while the second was produced on May 3rd. In between, the GaN target was taken out of vacuum, as it was replaced with an InGaN target.

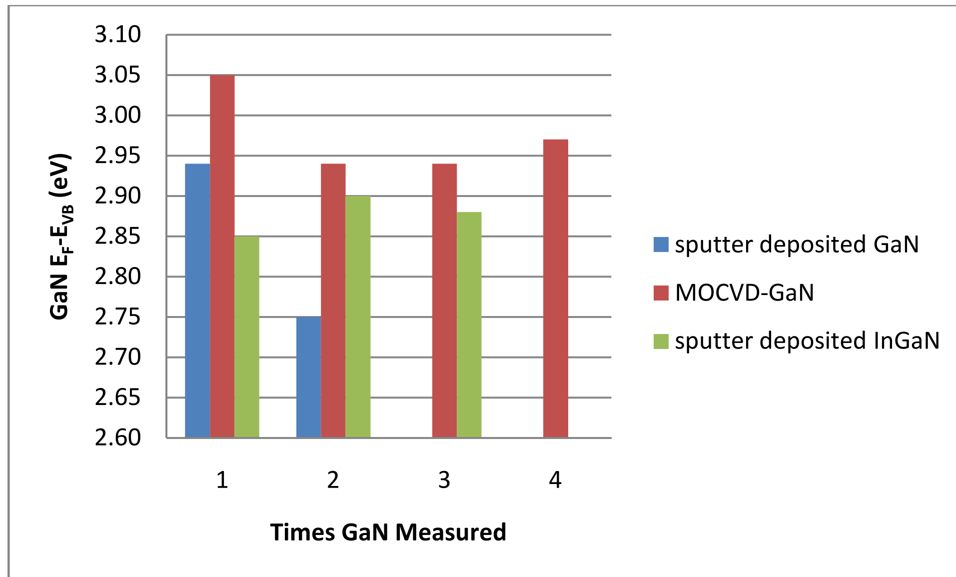

Figure 50 - Comparison between the values E_F-E_{VB} for GaN and InGaN. The MOCVD GaN films have the highest Fermi level position position.

Interestingly, as can be seen in Figure 51, the core Ga2p peak is dependent upon the growth method. The MOCVD GaN has consistently lower binding energy for the Ga2p peak than the sputtered GaN and InGaN samples, which are both relatively stable between 1118.3 and 1118.4 eV. This is slightly strange due to the fact that the lower binding energy should yield a lower Fermi level position. However, this variation in the binding energies of the Ga2p peaks is believed to be caused by the differences in growth direction between the MOCVD and sputtered samples. Since the MOCVD GaN is single crystal, the emitted electrons have a much clearer exit route than in the polycrystalline sputtered samples. Therefore, the sputtered samples require a slightly higher amount of energy to eject the electrons, especially from planes not immediately on the surface. It would have been nice to have also monitored another Ga peak for each sample in order to compare it to the values of the 2p peak, however this was not done.

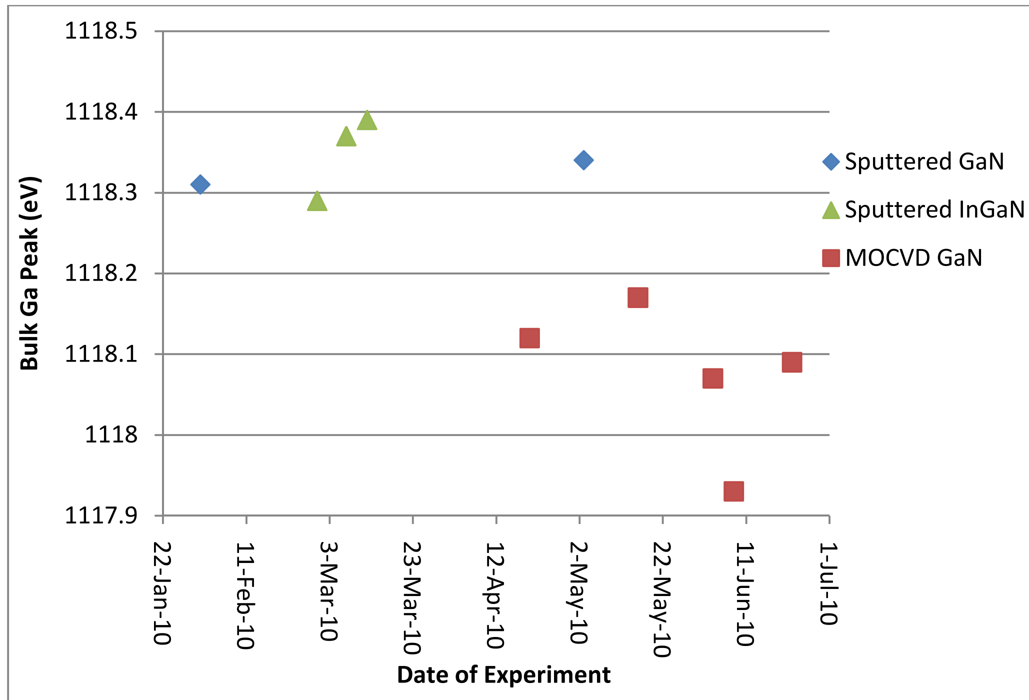

Figure 51 - Bulk Ga2p peak for sputtered GaN, sputtered InGaN, and MOCVD GaN

As there are significant differences in the different GaN substrates, there are also differences in the deposited CdTe and CdS. Figure 52 shows the E_F-E_{VB} values for CdTe deposited onto the various substrates. As aforementioned, the sputter deposited InGaN has a higher Fermi level position than the sputter deposited GaN, likely due to In diffusion into the CdTe film. The CdTe deposited onto MOCVD films also has higher Fermi levels than when deposited onto sputtered GaN. This occurs probably due to contamination on the MOCVD GaN surface or the elevated CdTe deposition temperature for this sample.

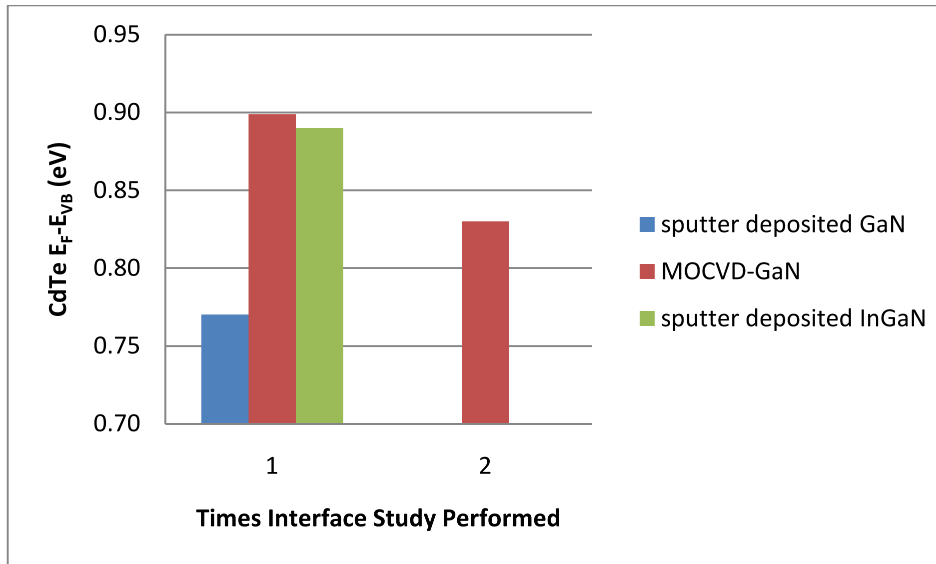

Figure 52 - E_F-E_{VB} values for CdTe films deposited onto sputter deposited GaN and InGaN as well as MOCVD GaN

The CdS films behave similarly to the CdTe films in terms of the substrate differences, as can be seen in Figure 53. The CdS films deposited onto MOCVD GaN have the highest Fermi level position. Again, the CdS deposited onto the InGaN has a higher Fermi level than the CdS deposited onto the sputtered GaN due to the indium diffusion into the CdS.

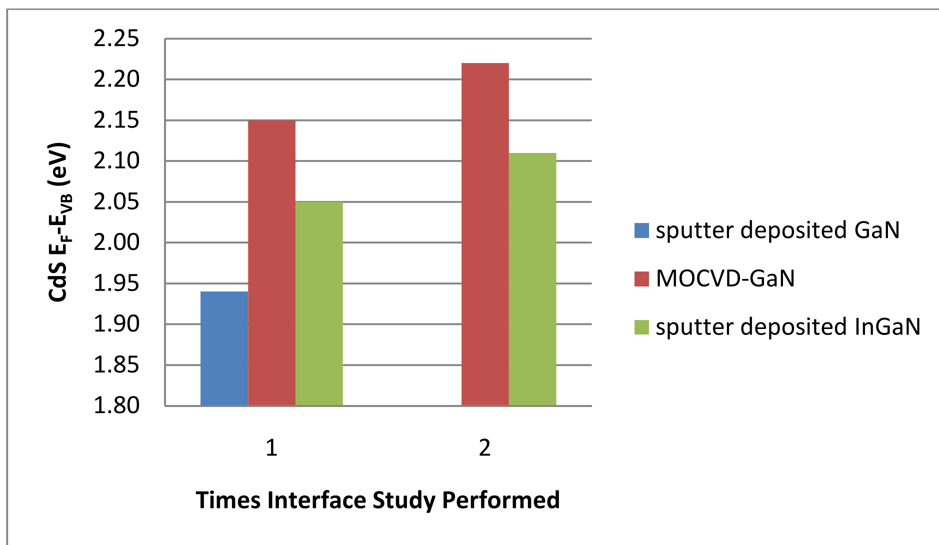

Figure 53 – E_F-E_{VB} values for CdS films deposited onto sputter deposited GaN and InGaN as well as MOCVD GaN

Another interesting phenomenon occurred while using the XPS to characterize the CdS and CdTe films on the MOCVD GaN. It is believed that the differences in substrate roughness caused differences in the XPS measurements. Since the sputter deposited GaN samples were relatively rough, a thicker layer of CdTe or CdS was required to ensure full coverage of the GaN so that the Ga XPS peaks would disappear.

The Ga peaks will not completely disappear until every peak and valley of the GaN is covered. However, the very smooth MOCVD grown samples allowed for a layer by layer coverage when the CdTe or CdS were deposited. Thus, the MOCVD grown GaN would be completely covered quicker than the sputter deposited GaN, and the Ga XPS peaks would disappear after a thinner layer of CdTe or CdS was deposited. This is why the interface studies with the MOCVD grown GaN were finished much faster than the interface studies with the sputter deposited GaN and InGaN. Figure 54 shows a simplified drawing of the CdTe coverage in order to visualize this concept

Figure 54 - CdTe coverage of MOCVD grown GaN (left) and sputter deposited GaN (right). Even though some parts of the CdTe on the sputter deposited GaN are fairly thick, the sputter deposited GaN is not fully covered, and Ga peaks will still be seen in the XPS measurements after longer deposition times when compared to the MOCVD grown GaN

5. Conclusions

Several important conclusions can be taken from this project. First, the method of deposition strongly influences the physical properties of GaN. As determined from AFM measurements, the sputter deposited GaN had a much rougher surface than the MOCVD-GaN, and this surface roughness resulted in a much higher sticking coefficient for the deposition of CdTe and CdS. On the other hand, MOCVD-GaN showed a single crystal from the XRD measurements, whereas the sputtered samples were polycrystalline.

A series of interface studies were performed between GaN/InGaN and CdTe/CdS to determine feasibility of implementation into an established CdTe solar cell process. Most importantly, the conduction band offsets at these interfaces were small enough (< 0.15 eV) so that they do not prevent electron flow across the interface at normal operating temperatures. Valence band offsets were much more significant as they ranged anywhere from about 0.4 eV to over 2 eV. Therefore, holes are significantly blocked from crossing the interface; however it is believed that this does not affect the solar cell performance.

The sputter deposited GaN/InGaN was much better suited for the interface studies because sputter deposition of GaN, close space sublimation of CdTe and CdS, and XPS measurements were all performed inside of the ultra-high vacuum DAISY-SOL. Therefore, there was no surface contamination of the GaN/InGaN samples. The MOCVD-GaN, on the other hand, was exposed to air as it had to be transported from the MOCVD tool to the DAISY-SOL. Surface contamination could not be fully removed, and it is believed that this surface contamination affected the peak positions of the GaN samples. Surface contamination, and the skewed initial peak positions, causes the interface study to be more inaccurate than an interface study all performed in situ.

In all of the interfaces using InGaN, it was observed that In migrated into the CdTe and CdS layers, as small In XPS peaks were observed in the bulk CdS and CdTe layers. Our data agreed with the literature in that the In acted as an n-type dopant in both the CdTe and CdS. This was observed as the Fermi level increased about 14% between the CdTe deposited on sputtered GaN and InGaN. Similarly, the Fermi level in the CdS deposited on the sputtered InGaN was about 6% higher than CdS deposited on sputtered GaN. While the Fermi levels of the materials affect the band bending at the interface, the band offsets are independent of the Fermi level position.

6. Future Work

Although this project lasted 10 months, there is still work that needs to be done. First off, it would be very interesting to actually create a CdTe solar cell that contains a GaN passivation layer. The performance of this cell could then be compared to the performance of the current CdTe solar cell.

It would also be quite interesting to perform the inverse of the interface studies, and use an ion beam to drill through the deposited CdS or CdTe until the GaN is reached. This would show if the interface is dependent upon which way the interface is reached.

Next, although extremely difficult due to the enormous size and complexity of an MOCVD system, it would be intriguing to incorporate an MOCVD system into the DAISY-SOL. This would allow for MOCVD-grown samples to be measured by the XPS and have CdTe and CdS to be deposited without any surface contamination. This would significantly increase the accuracy of the MOCVD-GaN and CdTe/CdS interface studies.

Finally, it would be wise to repeat all of these experiments and interface studies several times to ensure the accuracy of the data. While this data is believed to be accurate due to the historical accuracy of interface studies performed in the DAISY-SOL, many repeated trials would confirm this.

References:

1. Sze, S.M.a.K.K.N., *Physics of Semiconductor Devices*. 2007, John Wiley & Sons, Inc.: Hoboken.
2. Van Zeghbroeck, B. *Principles of Semiconductor Devices*. [Online Book] 2007 2007 [cited 2009 November 19]; Available from: http://ecee.colorado.edu/~bart/book/book/index.html.
3. Piprek, J., *Semiconductor Optoelectronic Devices*. Electronics & Electrical. 2003: Academic Press. 1-296.
4. Liaw, H.M., *Properties and Selection: Nonferrous Alloys and Special-Purpose Materials: Properties of Pure Metals: Silicon (Si)*, in *ASM Handbooks Online*. 2002, ASM International.
5. Thurmond, C.D., *Properties and Selection: Nonferrous Alloys and Special-Purpose Materials: Properties of Pure Metals: Germanium (Ge)*, in *ASM Handbooks Online*, J.H. Adams, Editor. 2002, ASM International.
6. Hunsicker, H.Y., Mondolfo, L.F. and P.A. Tomblin, *Properties and Selection: Nonferrous Alloys and Special-Purpose Materials: Aluminum (Al)*, in *ASM Handbooks Online*. 2002, ASM International.
7. Blackwood, A.W.a.J.E.C., *Properties and Selection: Nonferrous Alloys and Special-Purpose Materials: Properties of Pure Metals: Copper (Cu)*, in *ASM Handbooks Online*. 2002, ASM International.
8. Rockett, A., *The Materials Science of Semiconductors*. 2008, New York: Springer.
9. Goetzberger, A.a.V.U.H., *Photovoltaic Solar Energy Generation*. 2005, Heidelberg: Springer.
10. Krauter, S.C.W., *Solar Electric Power Generation - Photovoltaic Energy Systems*. 2006, New York: Springer.
11. USEIA. *Solar Photovoltaic Cell/Module Manufacturing Activities*. 2008 [cited 2009 December 21]; Available from: http://www.eia.doe.gov/cneaf/solar.renewables/page/solarphotv/solarpv.html.
12. USDOE. *The History of Solar*. January 2006 [cited 2010 January 11]; Available from: http://www1.eere.energy.gov/solar/pdfs/solar_timeline.pdf.
13. Ohl, R.S., *Light-sensitive electric device*. 1946: US Patent 2,402,662.
14. Sharp_Corp. *Sharp Develops Solar Cell with World's Highest Conversion Efficiency of 35.8%*. 2009 [cited 2009 December 21]; Available from: http://www.sharp-world.com/corporate/news/091022.html.
15. Ferekides, C.S., et al., *CdTe thin film solar cells: device and technology issues.* Solar Energy, 2004. **77**(6): p. 823-830.
16. Bosio, A., et al., *Polycrystalline CdTe thin films for photovoltaic applications.* Progress in Crystal Growth and Characterization of Materials, 2006. **52**(4): p. 247-279.
17. Wu, X., *High-efficiency polycrystalline CdTe thin-film solar cells.* Solar Energy, 2004. **77**(6): p. 803-814.
18. Jaegermann, W., Andreas Klein, Jochen Fritsche, Daniel Kraft and Bettina Späth, *Interfaces in CdTe Solar Cells: from Idealized Concepts to Technology.* Materials Research Society symposia proceedings, 2005. **865**: p. F6.1.
19. Vodakov, Y.A., *Fotoelement S p-n-perekhodom iz telluristogo kadmiya (P-n junction photocell made of cadmium telluride).* Physics of the solid state, 1960. **2**(1): p. 3.
20. Sunovia. *Solar PV Energy Materials*. 2009 2009 [cited 2009 December 4th]; Available from: http://sunoviaenergy.com/technologies/sunoviasolar/solar-pv-energy-materials/.
21. Maruska, H.P. *A Brief History of GaN Blue Light-Emitting Diodes*. 2006 March 15, 2006 [cited 2009 November 9, 2009]; Available from: http://www.onr.navy.mil/sci_tech/31/312/ncsr/materials/gan/maruskastory.asp.
22. Maruska, H.P.a.J.J.T., *The preparation and properties of vapour-deposited single- crystal-line GaN.* Applied Physics Letters, 1969. **15**(10): p. 327.
23. Pankove, J.I., *GaN: from fundamentals to applications.* Materials Science and Engineering B, 1999. **61-62**: p. 305-309.

24. Chow, T.P.a.M.G., *SiC Power Devices.* Materials Research Society symposia proceedings, 2000. **423**: p. 9.
25. Pavlidis, D., *Recent advances in III-V nitride electronic devices.* Technical digest - International Electron Devices Meeting, 2004: p. 795.
26. Neufeld, C.J., et al., *High quantum efficiency InGaN/GaN solar cells with 2.95 eV band gap.* Applied Physics Letters, 2008. **93**(14): p. 143502.
27. Wu, J., et al., *Superior radiation resistance of In[sub 1-x]Ga[sub x]N alloys: Full-solar-spectrum photovoltaic material system.* Journal of Applied Physics, 2003. **94**(10): p. 6477-6482.
28. Park, S.-H. and S.-L. Chuang, *Comparison of zinc-blende and wurtzite GaN semiconductors with spontaneous polarization and.* Journal of Applied Physics, 2000. **87**(1): p. 353.
29. Glasser, M.L., *Symmetry properties of Wurtzite structure.* Physics and Chemistry of Solids, 1959. **10**(2): p. 229.
30. As, D.J., *Cubic group-III nitride-based nanostructures--basics and applications in optoelectronics.* Microelectronics Journal, 2009. **40**(2): p. 204-209.
31. Mizuta, M., S. Fujieda, Y. Matsumoto and T. Kawamura, *Low Temperature Growth of GaN and AlN on GaAs Utilizing Metalorganics and Hydrazine.* Japanese Journal of Applied Physics, 1986. **25**(12): p. L945.
32. Miyoshi, S., et al., *MOVPE growth of cubic GaN on GaAs using dimethylhydrazine.* Journal of Crystal Growth, 1992. **124**(1-4): p. 439-442.
33. Hong, C.H., et al., *Phase-controlled metal-organic chemical vapor deposition epitaxial growth of GaN on GaAs(100) using NH3.* Materials Science and Engineering B, 1995. **32**(1-2): p. 69-74.
34. Wang, L.D. and H.S. Kwok, *Cubic aluminum nitride and gallium nitride thin films prepared by pulsed laser deposition.* Applied Surface Science, 2000. **154-155**: p. 439-443.
35. Novikov, S.V., et al., *Free-standing zinc-blende (cubic) GaN layers and substrates.* Journal of Crystal Growth, 2008. **310**(17): p. 3964-3967.
36. Juza, R.a.H.H., *Uber die Kristallstrukturen von Cu3N, GaN und InN.* Zeitschrift fur anorganische und allgemeine Chemie, 1938. **239**: p. 282-287.
37. Lorenz, M.R. and B.B. Binkowski, *Preparation, Stability, and Luminescence of Gallium Nitride.* Journal of The Electrochemical Society, 1962. **109**(1): p. 24-26.
38. Pankove, J.I., et al., *Electroluminescence in GaN.* Journal of Luminescence, 1971. **4**(1): p. 63-66.
39. Pankove, J.I., *Optical absorption of GaN.* Applied Physics Letters, 1970. **17**(5): p. 197.
40. Pankove, J.I., *UV dc electroluminescence from GaN.* Journal of Luminescence, 1972. **5**(6): p. 482-484.
41. Pankove, J.I., et al., *Luminescent properties of GaN.* Solid State Communications, 1970. **8**(13): p. 1051-1053.
42. Pankove, J.I. and M.A. Lampert, *Model for Electroluminescence in GaN.* Physical Review Letters, 1974. **33**(Copyright (C) 2009 The American Physical Society): p. 361.
43. Pankove, J.I., E.A. Miller, and J.E. Berkeyheiser, *GaN blue light-emitting diodes.* Journal of Luminescence, 1972. **5**(1): p. 84-86.
44. Pankove, J.I., E.A. Miller, and J.E. Berkeyheiser, *GaN yellow-light emitting diodes.* Journal of Luminescence, 1973. **6**(1): p. 54-60.
45. Akasaki, I., *Key inventions in the history of nitride-based blue LED and LD.* Journal of Crystal Growth, 2007. **300**(1): p. 2-10.
46. Amano, H., et al., *Metalorganic vapor phase epitaxial growth of a high quality GaN film using an AlN buffer layer.* Applied Physics Letters, 1986. **48**(5): p. 353.
47. Nakamura, S., *GaN Growth Using GaN Buffer Layer.* Japanese Journal of Applied Physics, 1991. **30**(10A): p. L1705.
48. Amano, H., et al., *Electron beam effects on blue luminescence of zinc-doped GaN.* Journal of Luminescence, 1988. **40-41**: p. 121-122.

49. Amano, H., M. Kito, K. Hiramatsu, and I. Akasaki, *P-Type Conduction in Mg-Doped GaN Treated with Low-Energy Electron Beam Irradiation (LEEBI).* Japanese Journal of Applied Physics, 1989. **28**(12): p. L2112-L2114.
50. Nakamura, S., T. Mukai, M. Senoh, and N. Iwasa, *Thermal Annealing Effects on P-Type Mg-Doped GaN Films.* Japanese Journal of Applied Physics, 1992. **31**: p. L139.
51. Van Vechten, J.A., J.D. Zook, R.D. Horning and B. Goldenberg, *Defeating Compensation in Wide Gap Semiconductors by Growing in H that is Removed by Low Temperatuer De-Ionizing Radiation.* Japanese Journal of Applied Physics, 1992. **31**(11): p. 3662.
52. Van de Walle, C.G., C. Stampfl, and J. Neugebauer, *Theory of doping and defects in III-V nitrides.* Journal of Crystal Growth, 1998. **189-190**: p. 505-510.
53. Korotkov, R.Y.a.B.W.W., *Electrical Properties of Oxygen Doped GaN Grown by Metalorganic Vapor Phase Epitaxy.* Materials Research Society symposia proceedings, 2000. **595**: p. F99W3.80.
54. Nakamura, S., T. Mukai and M. Senoh, *Si- and Ge-Doped GaN Films Grown with GaN Buffer Layers.* Japanese Journal of Applied Physics, 1992. **31**(9A): p. 2883.
55. Nagatomo, T., T. Kuboyama, H. Minamino, and O. Omoto, *Properties of Ga(1-x)In(x)N Films Prepared by MOVPE.* Japanese Journal of Applied Physics, 1989. **28**(8): p. L1334.
56. Tansley, T.L. and C.P. Foley, *Optical band gap of indium nitride.* Journal of Applied Physics, 1986. **59**(9): p. 3241.
57. Yamaguchi, S., et al., *Anomalous features in the optical properties of Al[sub 1-x]In[sub x]N on GaN grown by metal organic vapor phase epitaxy.* Applied Physics Letters, 2000. **76**(7).
58. Davydov, V.Y., et al., *Band Gap of InN and In-Rich In_{<FONT SIZE='-1'>x</FONT>}Ga_{<FONT SIZE='-1'>1 - x</FONT>}N alloys (0.36 < x < 1).* physica status solidi (b), 2002. **230**(2): p. R4-R6.
59. Razeghi, M. and R. McClintock, *A review of III-nitride research at the Center for Quantum Devices.* Journal of Crystal Growth, 2009. **311**(10): p. 3067-3074.
60. Ruterana, P., M. Albrecht, and J. Neugebauer, ed. *Nitride Semiconductors: Handbook on Materials and Devices*. 2003, Wiley-VCH GmbH & Co. KGaA: Darmstadt.
61. Manasevit, H.M. and W.I. Simpson, *The Use of Metal-Organics in the Preparation of Semiconductor Materials.* Journal of The Electrochemical Society, 1969. **116**(12): p. 1725-1732.
62. Keuch, T.F., Shulin Gu, Ramchandra Wate, Ling Zhang, Jingxi Sun, J.A. Dumesic, and J.M. Redwing, *The Chemistry of GaN Growth.* Materials Research Society symposia proceedings, 2001. **639**: p. G1.
63. Jang, J.H., A M Herrero, Seungyoung Son, B Gila, C Abernathy, and V Craciun, *Growth optimization for high quality GaN films grown by metal-organic chemical vapor deposition.* Materials Research Society symposia proceedings, 2008. **1068**: p. 123.
64. Stringfellow, G.B., *Organometallic Vapor-Phase Epitaxy: Theory and Practice*. Second Edition ed. 1999, New York: Academic Press.
65. Huang, S.-Y.a.J.-R.Y., *A Transmission Electron Microscopy Observation of Dislocations in GaN grown on (0001) Sapphire by Metal Oragnic Chemical Vapor Deposition.* Japanese Journal of Applied Physics, 2008. **47**(10): p. 7798-8002.
66. Zhang, B., et al., *High-performance III-nitride blue LEDs grown and fabricated on patterned Si substrates.* Journal of Crystal Growth, 2007. **298**: p. 725-730.
67. Sree Harsha, K.S., *Principles of Physical Vapor Deposition of Thin Films*. 2006, Amsterdam: Elsevier.
68. Puychevrier, N. and M. Menoret, *Synthesis of III-V semiconductor nitrides by reactive cathodic sputtering.* Thin Solid Films, 1976. **36**(1): p. 141-145.
69. Hariu, T., et al., *Reactive sputtering of gallium nitride thin films for GaAs MIS structures.* Applied Physics Letters, 1978. **32**(4): p. 252-253.
70. Sigmund, P., *Theory of Sputtering. I. Sputtering Yield of Amorphous and Polycrystalline Targets.* Physical Review, 1969. **184**(Copyright (C) 2010 The American Physical Society): p. 383.

71. Wasa, K., Kitabatake, M. and H. Adachi, *Thin Film Materials Technology: Sputtering of Compound Materials*. 2004, New York: William Andrew, Inc.
72. Ban, V.S., *Mass Spectrometric Studies of Vapor-Phase Crystal Growth.* Journal of The Electrochemical Society, 1972. **119**(6): p. 761-765.
73. Shin, H., D.B. Thomson, P.Q. Miraglia, S.D. Wolter, R. Schlesser, Z. Sitar, and R.F. Davis, *Growth and Characterization of GaN Bulk Crystals via Vapor Phase Transport.* Materials Research Society symposia proceedings, 2001. **639**: p. G3.54.1-G3.54.6.
74. Ohta, J., et al., *Growth of group III nitride films by pulsed electron beam deposition.* Journal of Solid State Chemistry, 2009. **182**(5): p. 1241-1244.
75. Brundle, R., Charles Evans, and Shaun Wilson, ed. *Encyclopedia of Materials Characterization: Surfaces, Interfaces, Thin Films*. Materials Characterization Series. 1992, Elsevier Butterworth-Heinemann: Boston.
76. Geisse, N. *AFM and Combined Optical Techniques*. Available from: http://www.asylumresearch.com/Applications/CombinedAFMOptical/CombinedAFMOptical.shtml.
77. Bonnet, D., *Manufacturing of CSS CdTe solar cells.* Thin Solid Films, 2000. **361-362**: p. 547-552.
78. G. Liu, T.S., A. Thissen, A. Klein and W. Jaegermann, *In Situ preparation and interface characterization of TiO2/Cu2S heterointerface.* Applied Physics Letters, 2003. **82**(14): p. 2269-2271.
79. Grant, R.W., et al., *Measurement of potential at semiconductor interfaces by electron spectroscopy.* Journal of Vacuum Science & Technology B: Microelectronics and Nanometer Structures, 1983. **1**(2): p. 320-327.
80. Waldrop, J.R., et al., *Measurement of semiconductor heterojunction band discontinuities by x-ray photoemission spectroscopy.* Journal of Vacuum Science & Technology A: Vacuum, Surfaces, and Films, 1985. **3**(3): p. 835-841.
81. Suzuki, T.e.a., *In Doping in CdTe Film by Co-Evaporation of CdTe and In.* Japanese Journal of Applied Physics, 1987. **26**(Part 1, No. 12): p. 2009-2014.
82. Fritsche, J., et al., *Band energy diagram of CdTe thin film solar cells.* Thin Solid Films, 2002. **403-404**: p. 252-257.
83. Fritsche, J., et al., *Utilization of sputter depth profiling for the determination of band alignment at polycrystalline CdTe/CdS heterointerfaces.* Applied Physics Letters, 2002. **81**(12): p. 2297-2299.

Appendix A – Powder diffraction file (PDF) of hexagonal GaN

Pattern : 01-076-0703 ***Radiation =*** 1.540598 ***Quality :*** Calculated

GaN

Gallium Nitride

2th	i	h	k	l
32.381	463	1	0	0
34.543	373	0	0	2
36.828	999	1	0	1
48.071	193	1	0	2
57.758	254	1	1	0
63.395	255	1	0	3
67.788	35	2	0	0
69.070	204	1	1	2
70.490	111	2	0	1
72.853	20	0	0	4
78.381	32	2	0	2
81.991	20	1	0	4

Lattice : Hexagonal

S.G. : P63mc (186)

a = 3.19000

c = 5.18900

Z = 2

Mol. weight = 83.73

Volume [CD] = 45.73

Dx = 6.081

I/Icor = 8.26

ICSD collection code: 034476
Temperature factor: ATF
Additional pattern: See PDF 74-243 and PDF 79-2499.
Data collection flag: Ambient.

Schulz, H., Thiemann, K.H., Solid State Commun., volume 23, page 815 (1977)
Calculated from ICSD using POWD-12++ (1997)

Radiation : CuKa1

Lambda : 1.54060

SS/FOM : F12=1000(0.0001,12)

Filter : Not specified

d-sp : Calculated spacings

Appendix B – AFM pictures of 2 μm and 10 μm squares

Sputter Deposited GaN

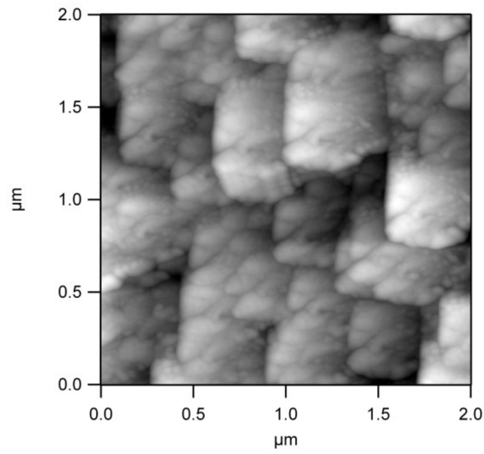

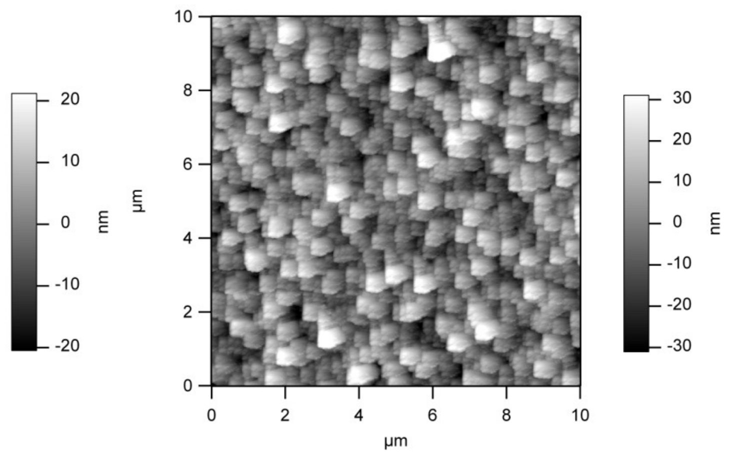

Sputter Deposited InGaN

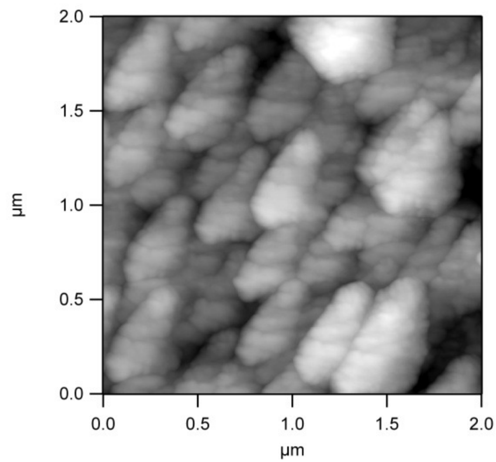

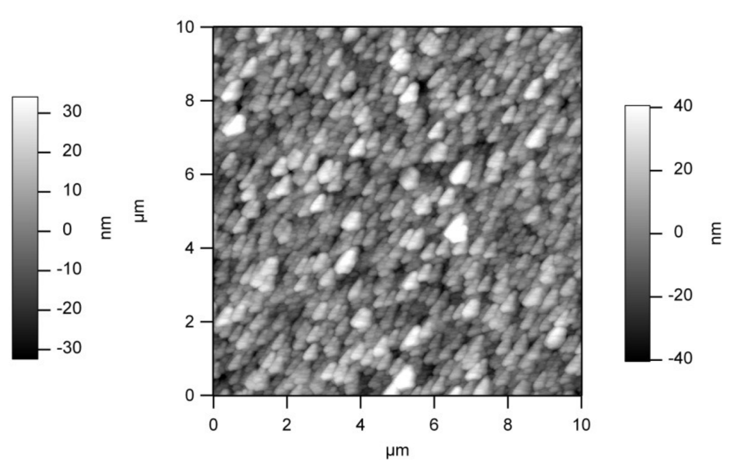

MOCVD GaN

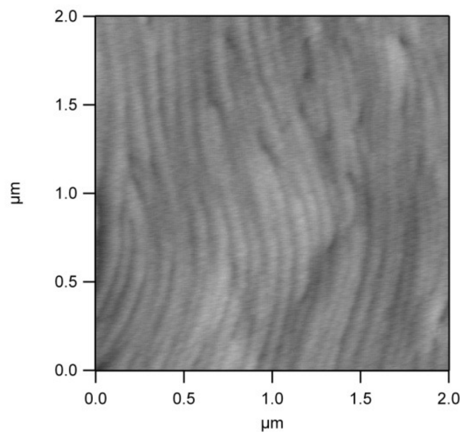

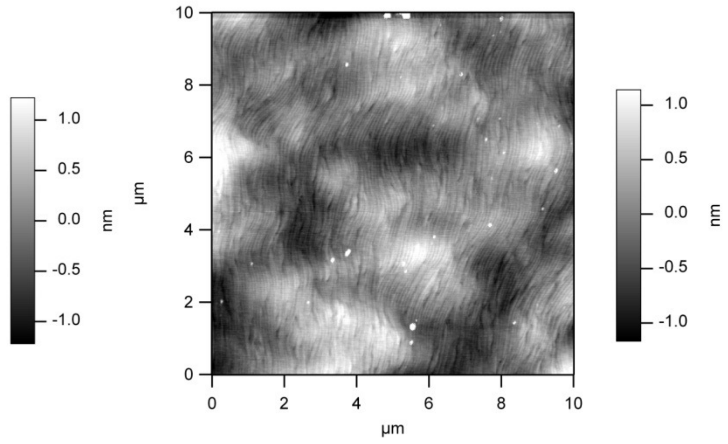

CdTe on Sputtered GaN

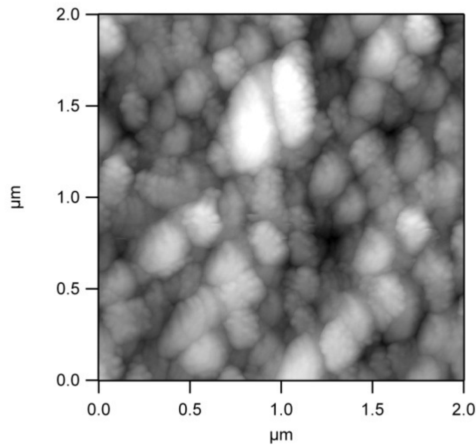

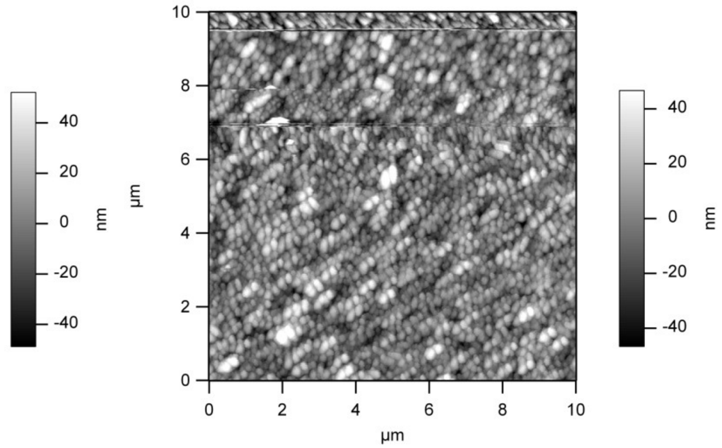

CdTe on Sputtered InGaN

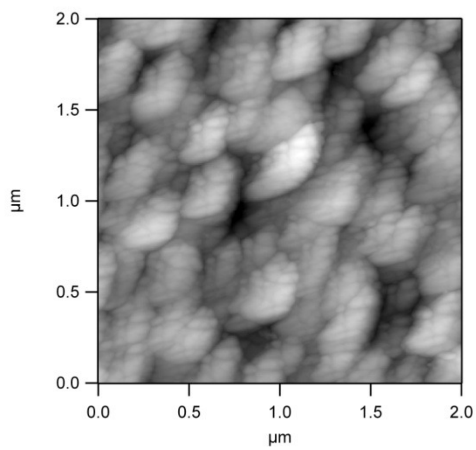

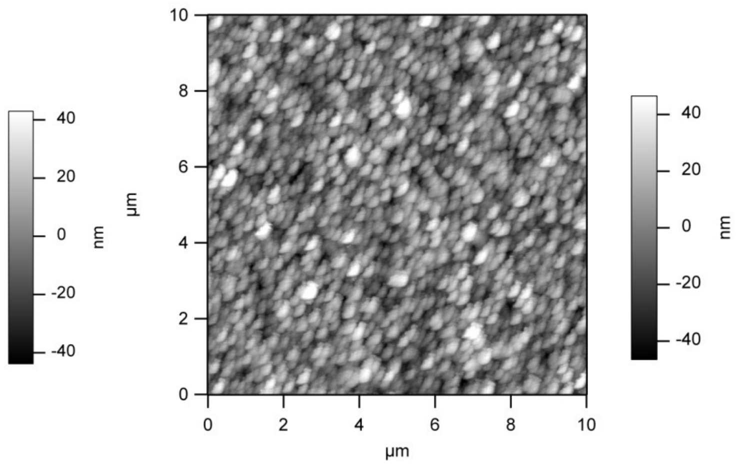

CdTe on MOCVD GaN

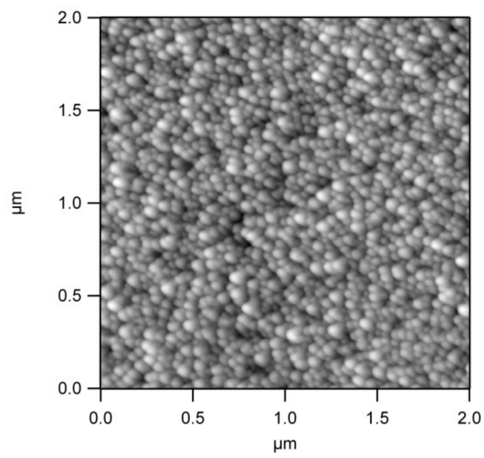

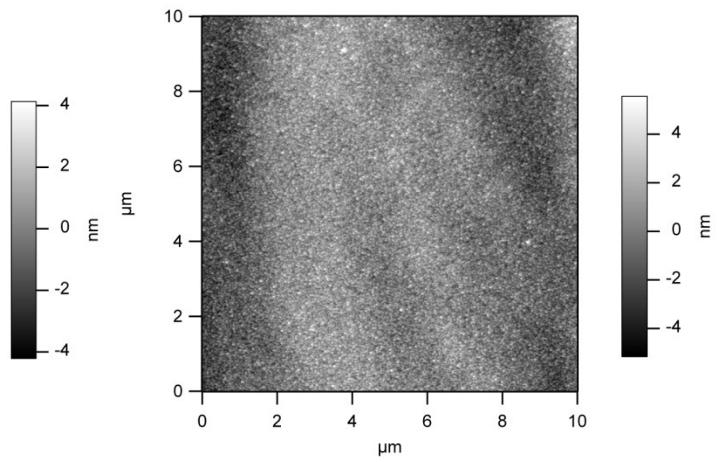

CdS on Sputtered GaN

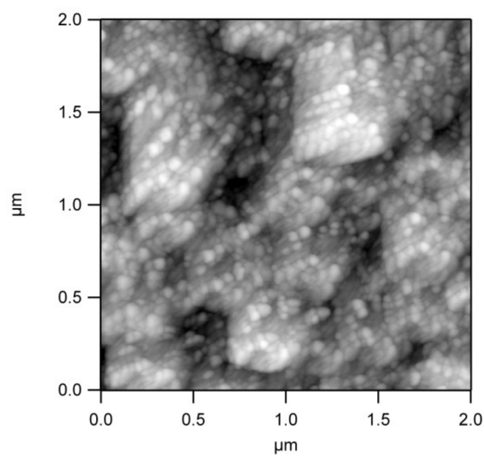

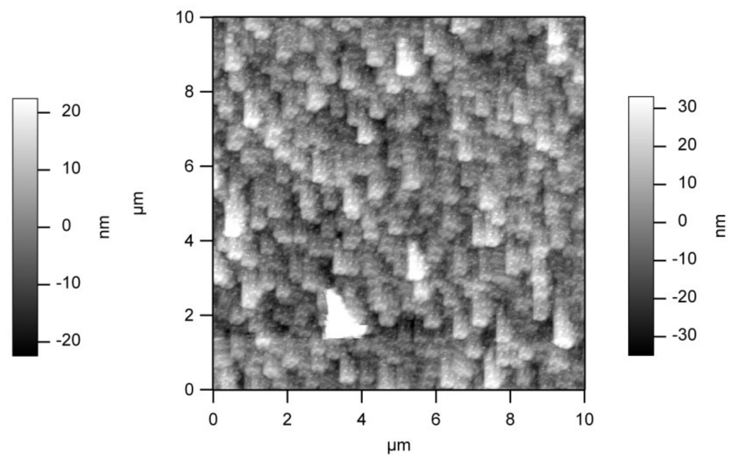

CdS on Sputtered InGaN

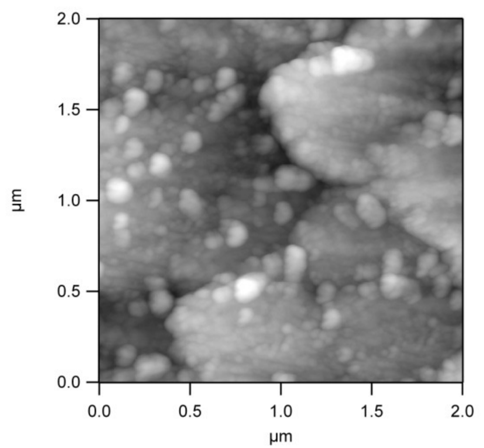

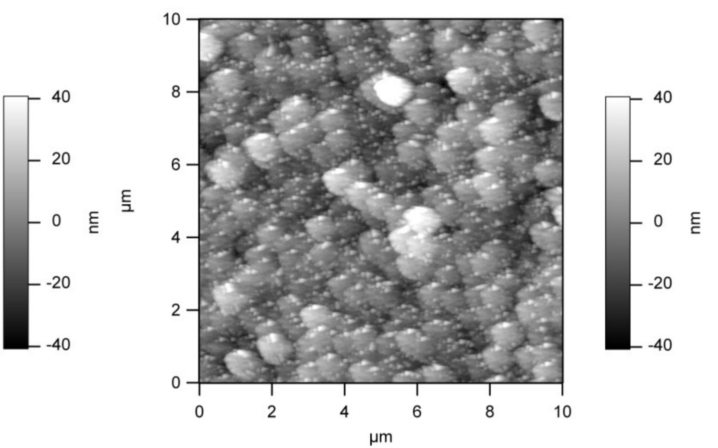

CdS on MOCVD GaN

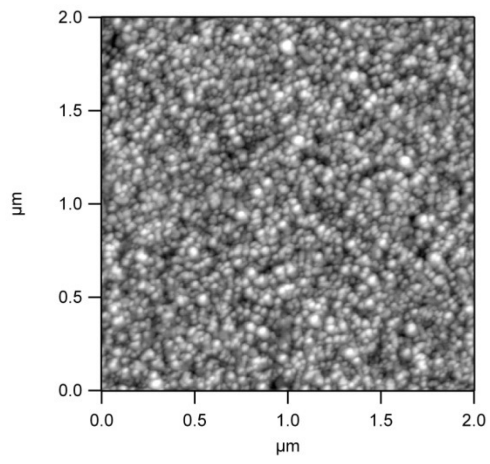

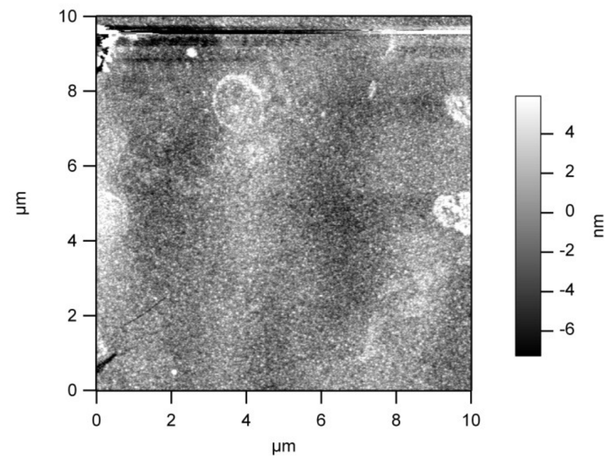

Appendix C – XPS and UPS Data for Interface Studies

Sputter Deposited GaN and CdTe Interface

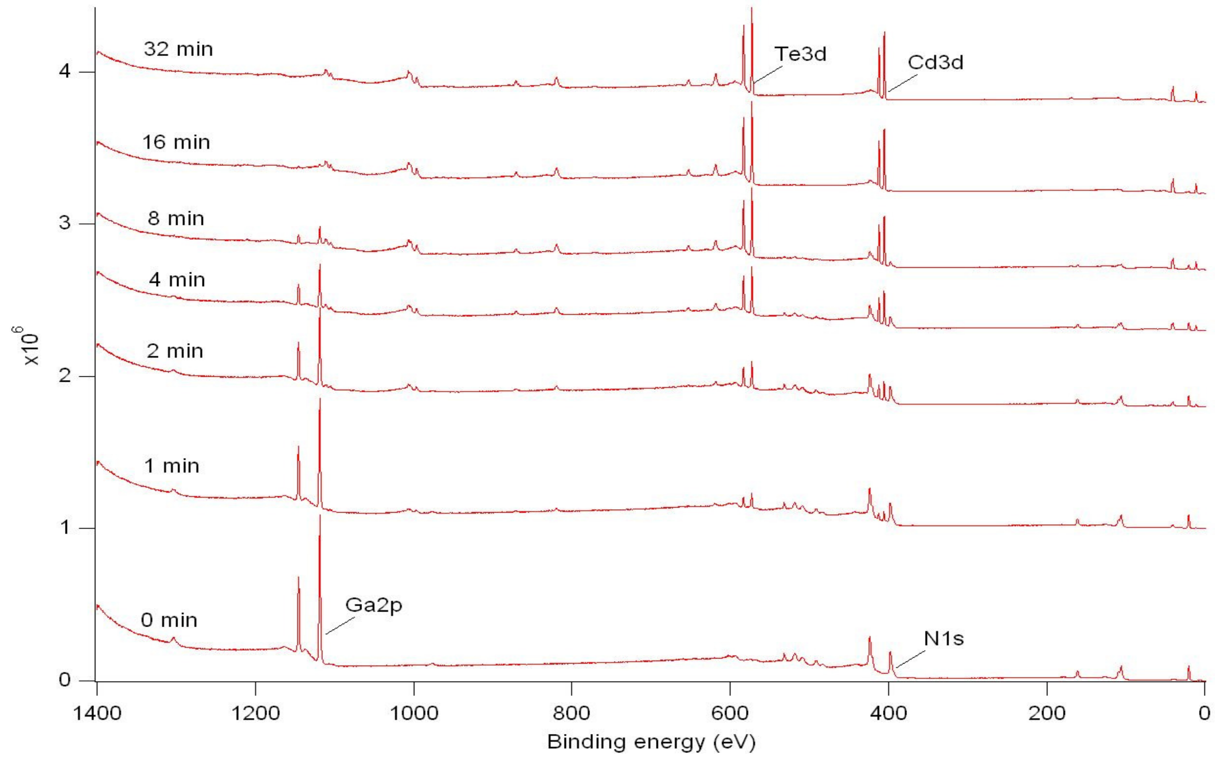

Survey XPS measurements as the sample transitions from bulk GaN (0 min) to bulk CdTe (32 min)

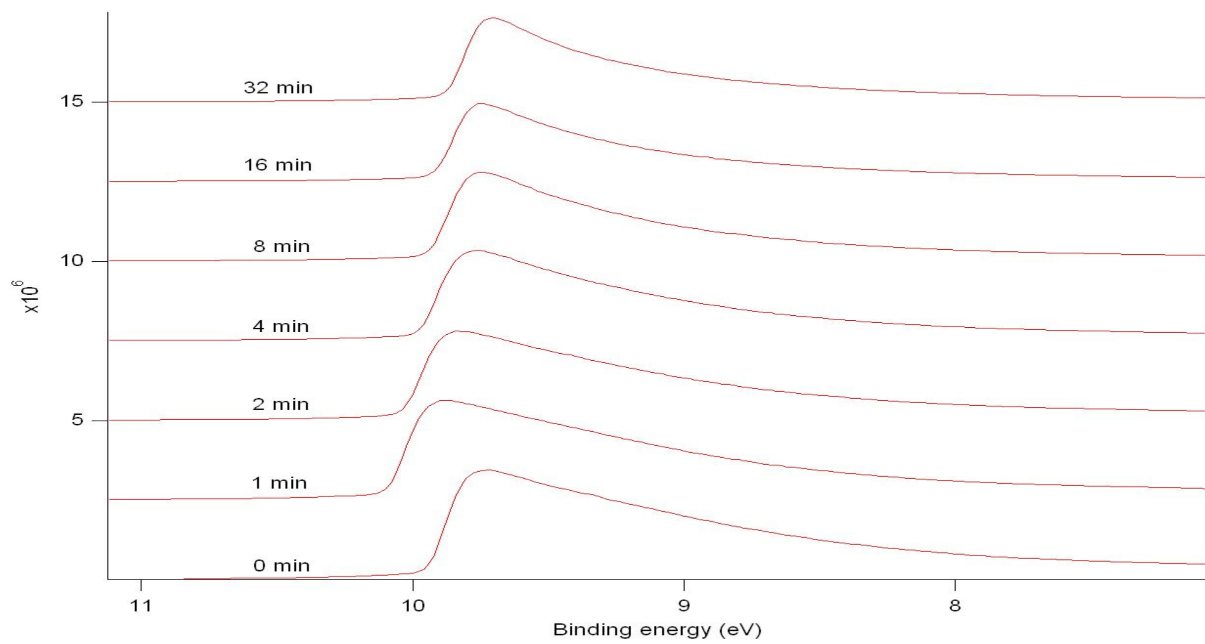

UPS measurements as the transitions from bulk GaN (0 min) to bulk CdTe (32 min)

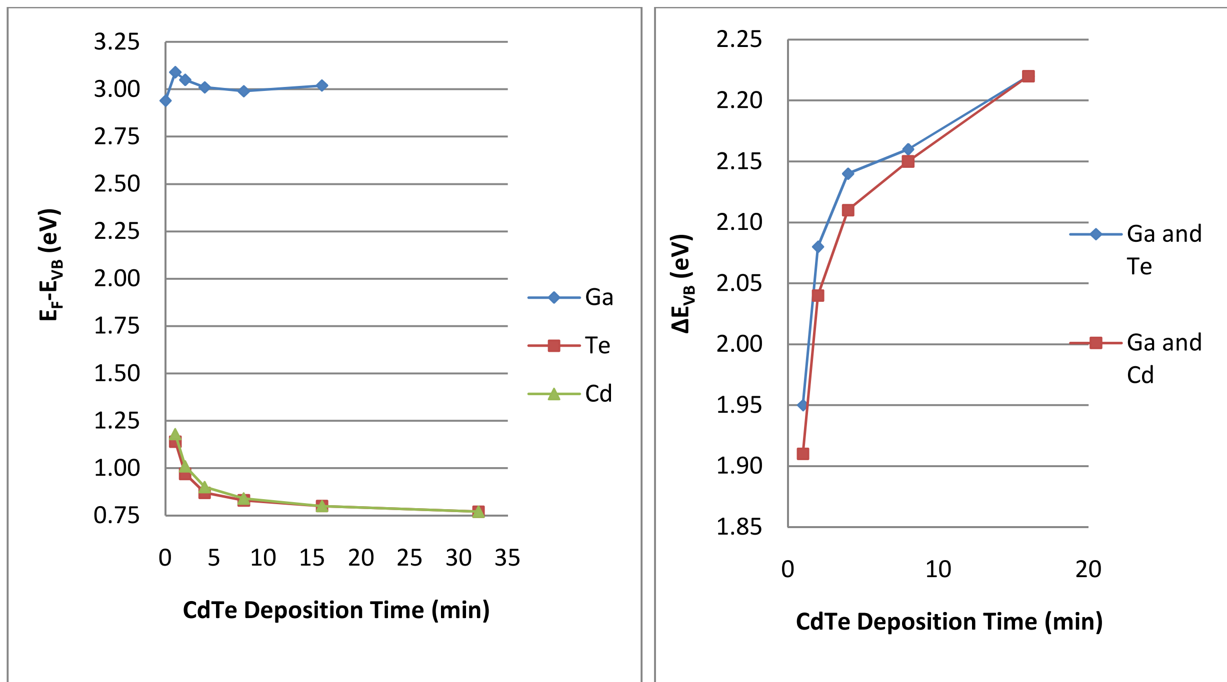

Left: The change in Fermi level position for each element as the interface study proceeds. Right: The change in valence band offset between the two materials as the interface study proceeds.

MOCVD GaN and CdTe Interface

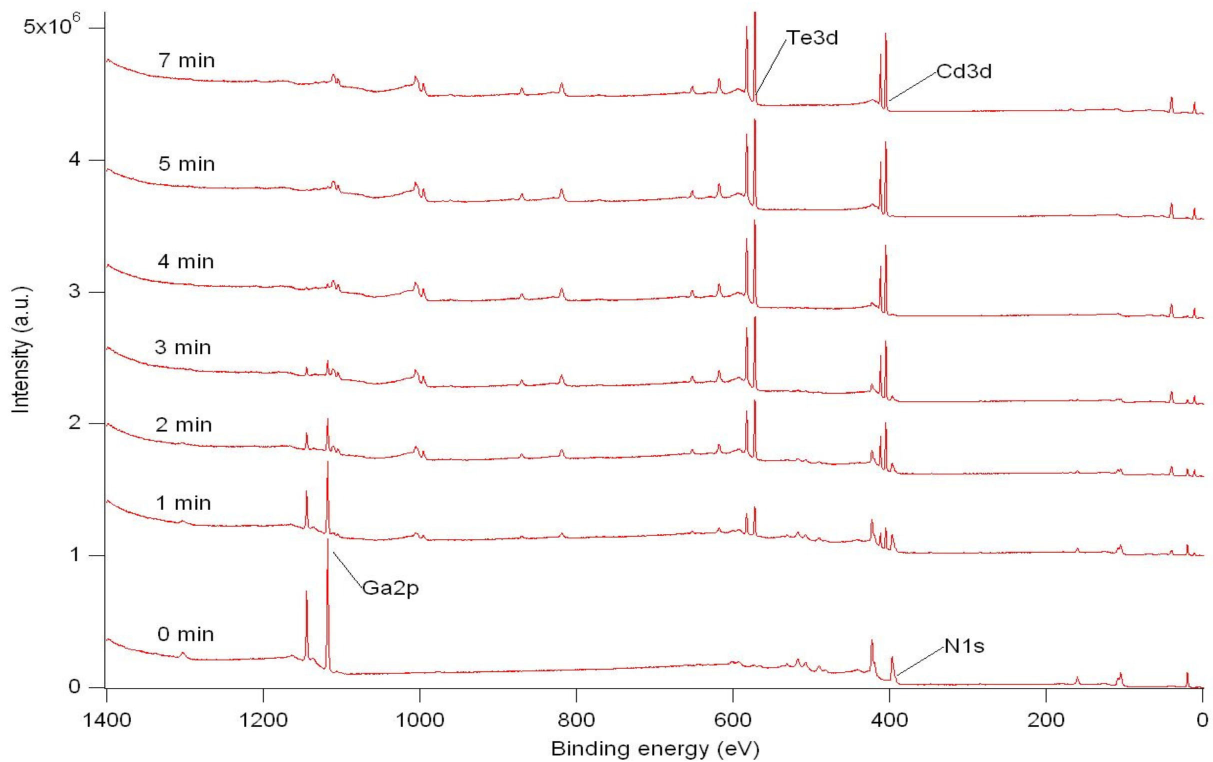

Survey XPS measurements as the sample transitions from bulk GaN (0 min) to bulk CdTe (7 min)

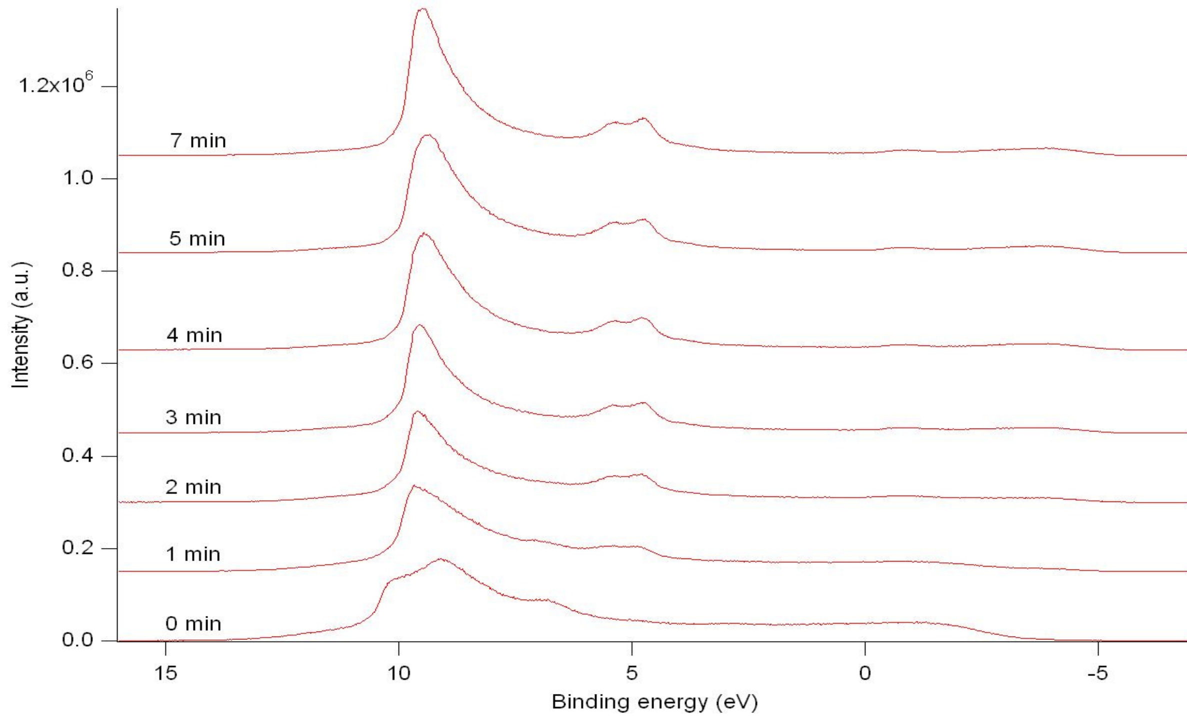

UPS measurements as the transitions from bulk GaN (0 min) to bulk CdTe (8 min)

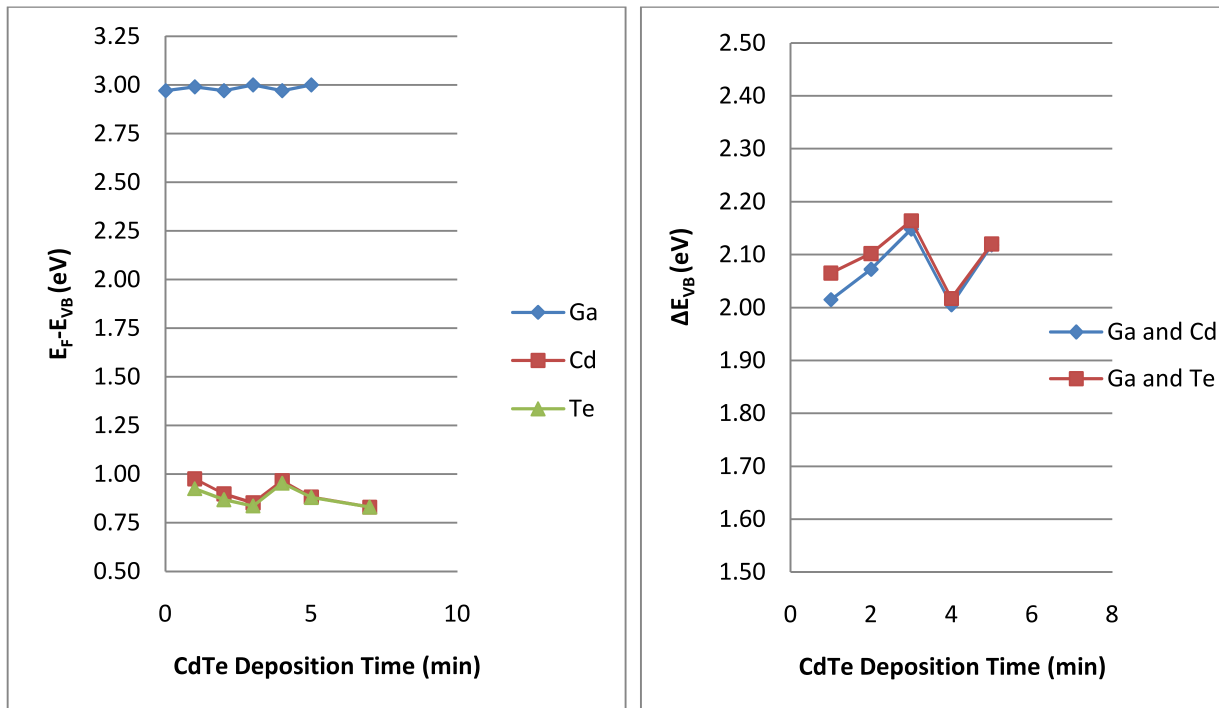

Left: The change in Fermi level position for each element as the interface study proceeds. Right: The change in valence band offset between the two materials as the interface study proceeds.

Sputter Deposited InGaN and CdTe Interface

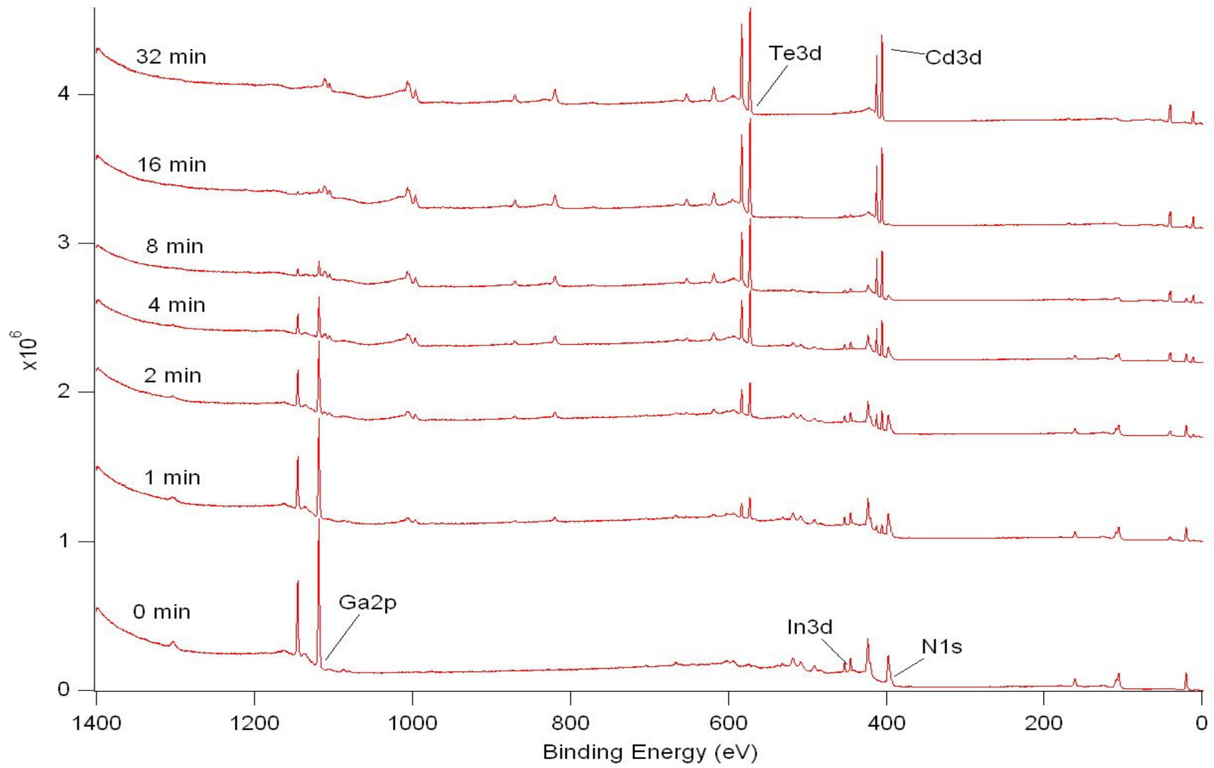

Survey XPS measurements as the sample transitions from bulk InGaN (0 min) to bulk CdTe (32 min)

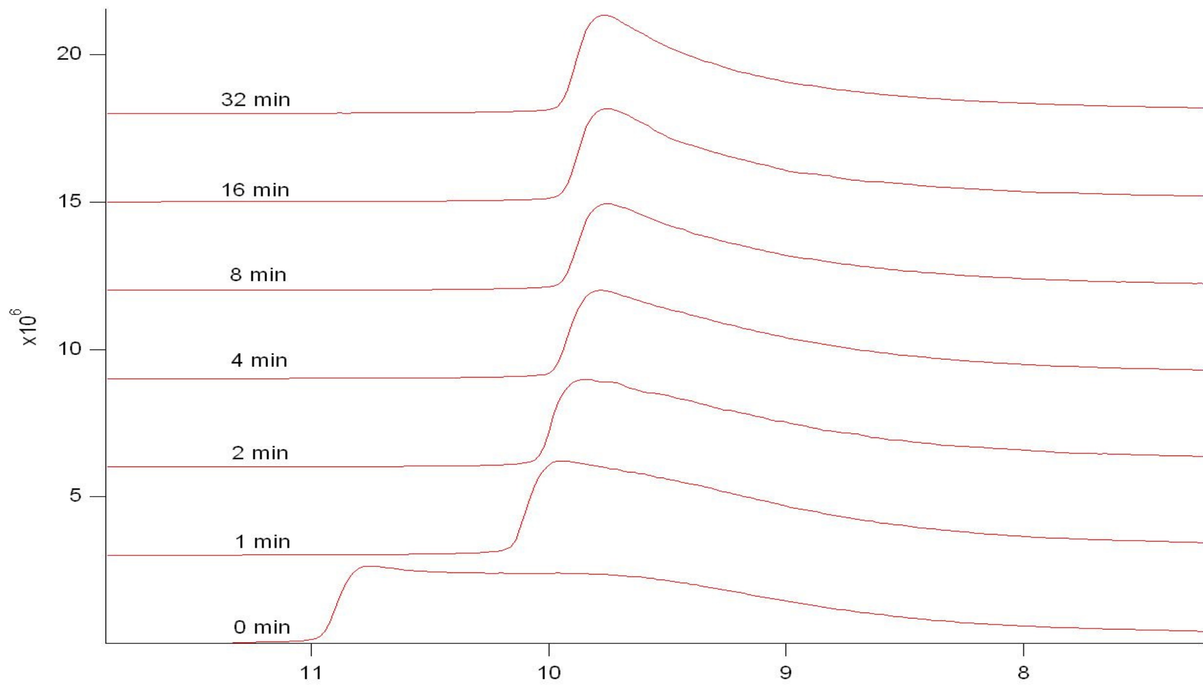

UPS measurements as the transitions from bulk InGaN (0 min) to bulk CdTe (32 min)

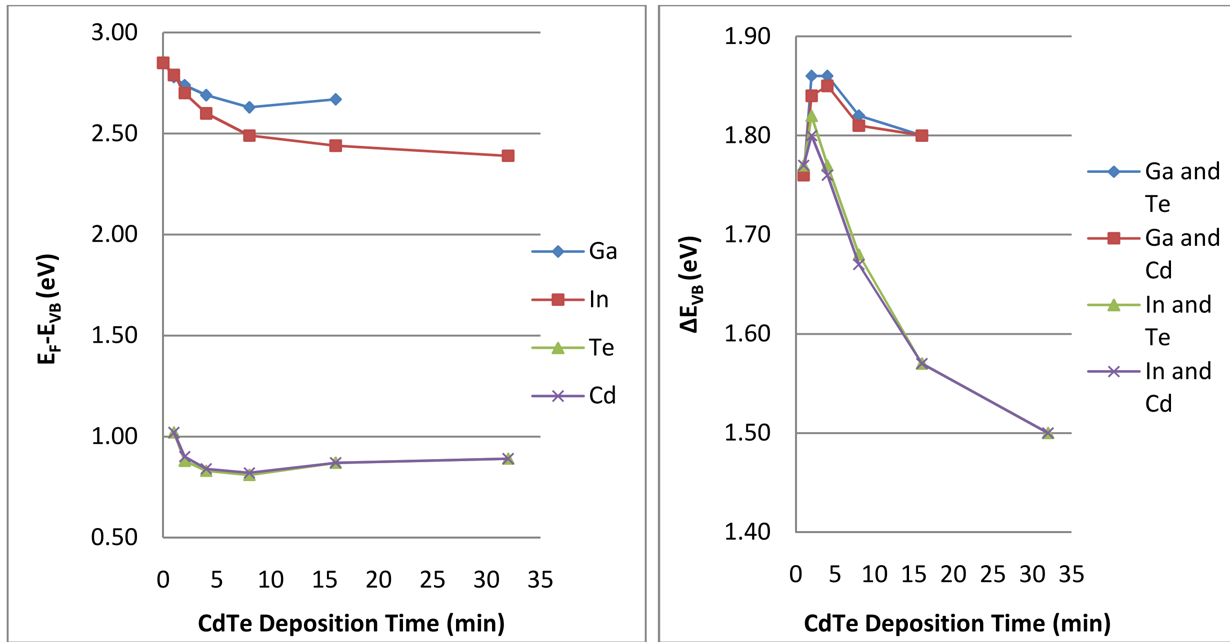

Left: The change in Fermi level position for each element as the interface study proceeds. Right: The change in valence band offset between the two materials as the interface study proceeds.

Sputter Deposited GaN and CdS Interface

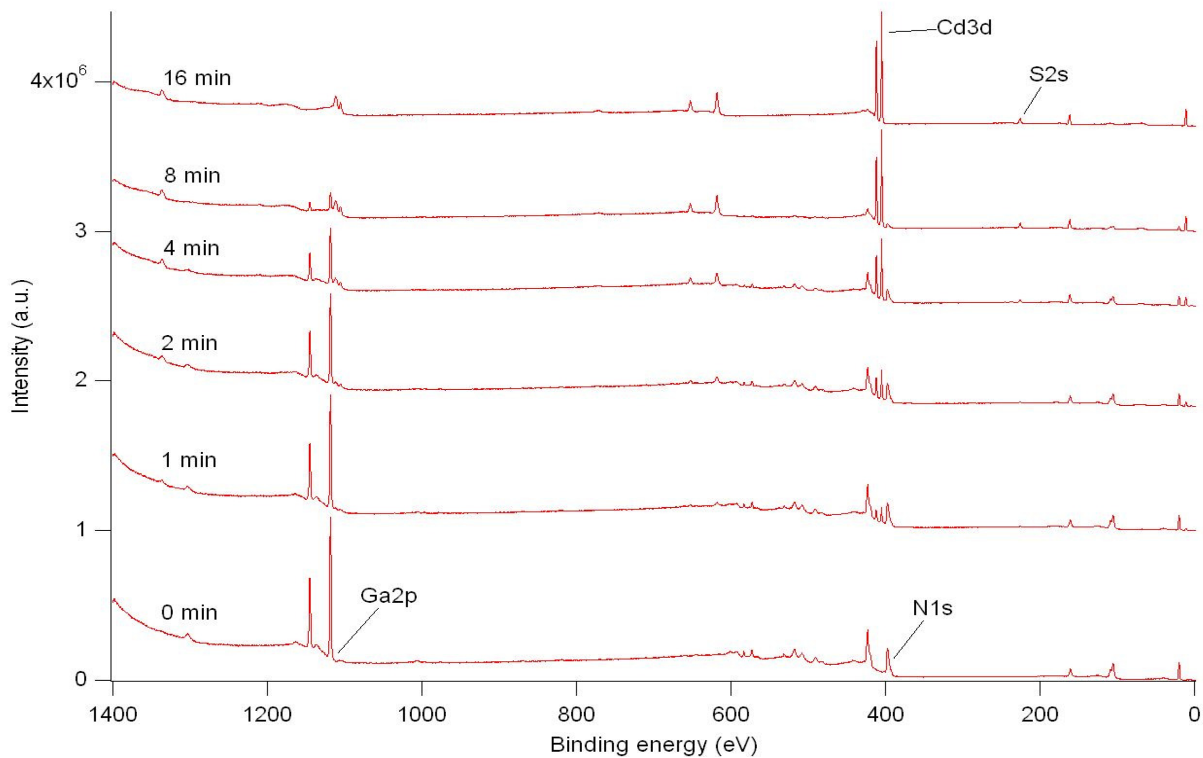

Survey XPS measurements as the sample transitions from bulk GaN (0 min) to bulk CdS (16 min)

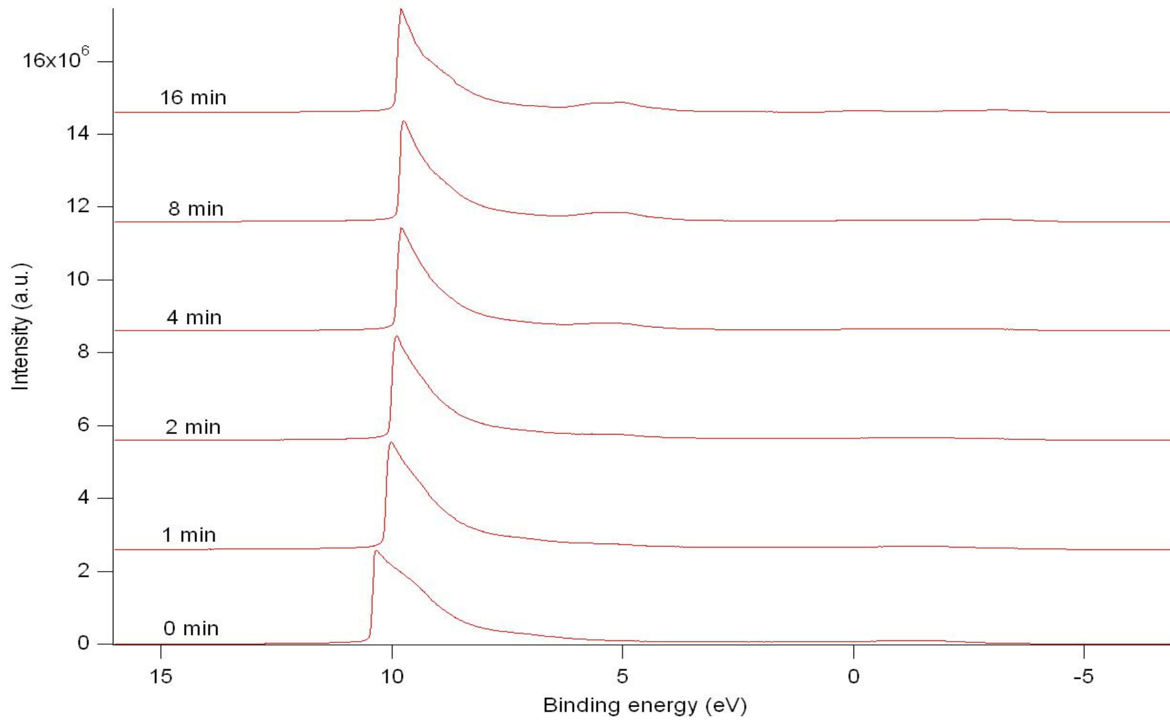

UPS measurements as the sample transitions from bulk GaN (0 min) to bulk CdS (16 min)

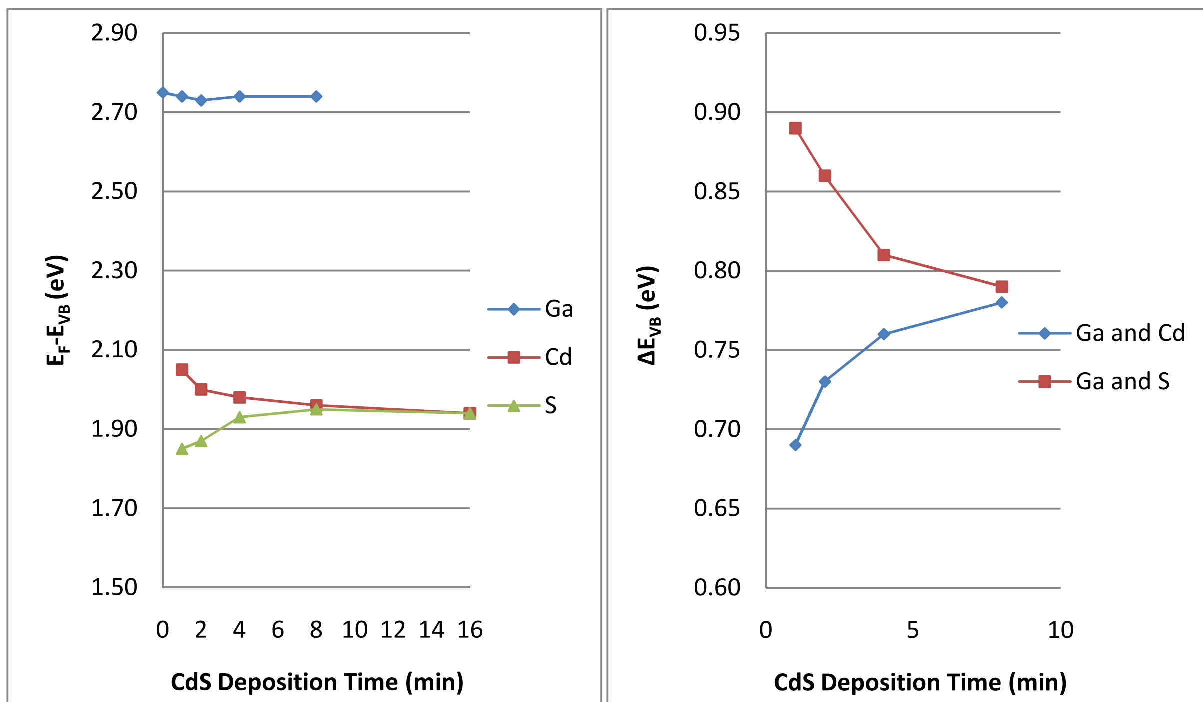

Left: The change in Fermi level position for each element as the interface study proceeds. Right: The change in valence band offset between the two materials as the interface study proceeds.

MOCVD-GaN and CdS Interface

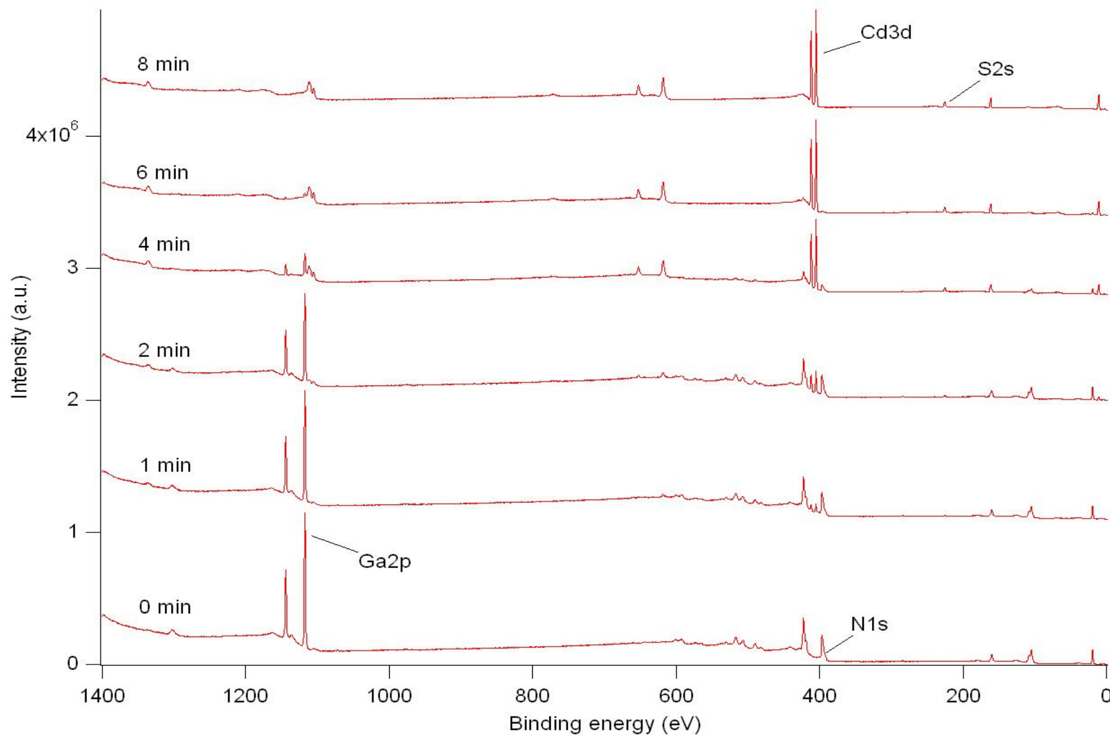

Survey XPS measurements as the sample transitions from bulk GaN (0 min) to bulk CdS (8 min)

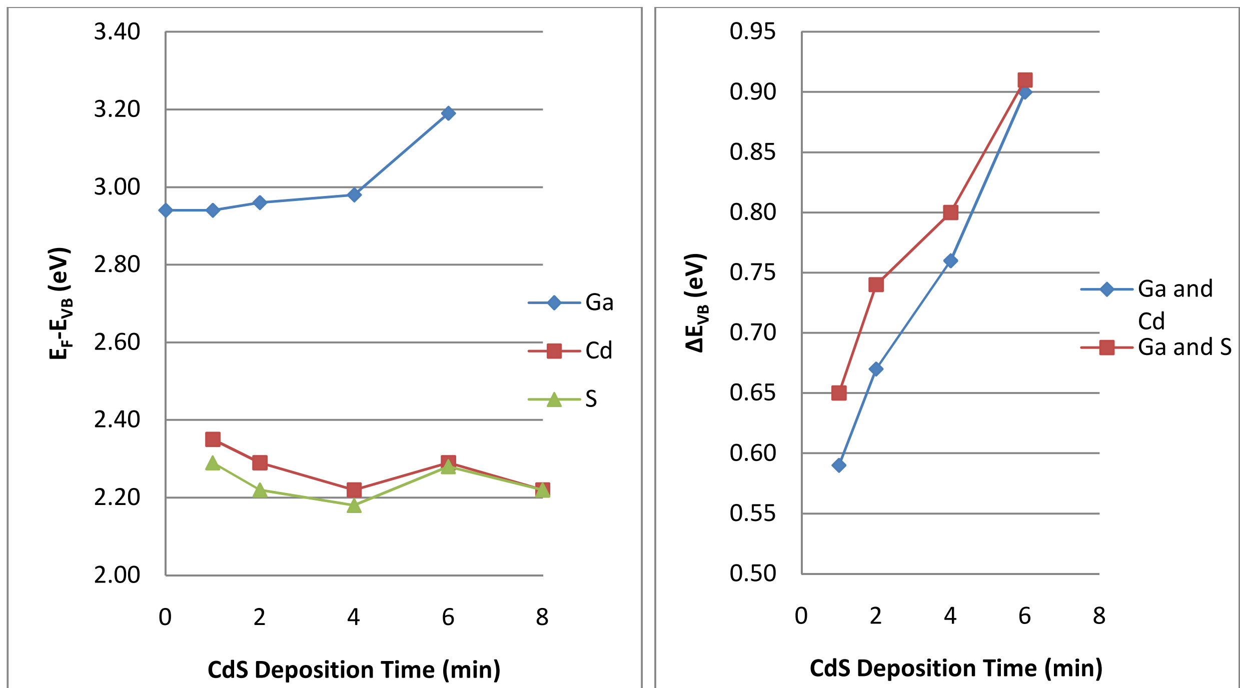

Left: The change in Fermi level position for each element as the interface study proceeds. Right: The change in valence band offset between the two materials as the interface study proceeds.

Sputter Deposited InGaN and CdS Interface

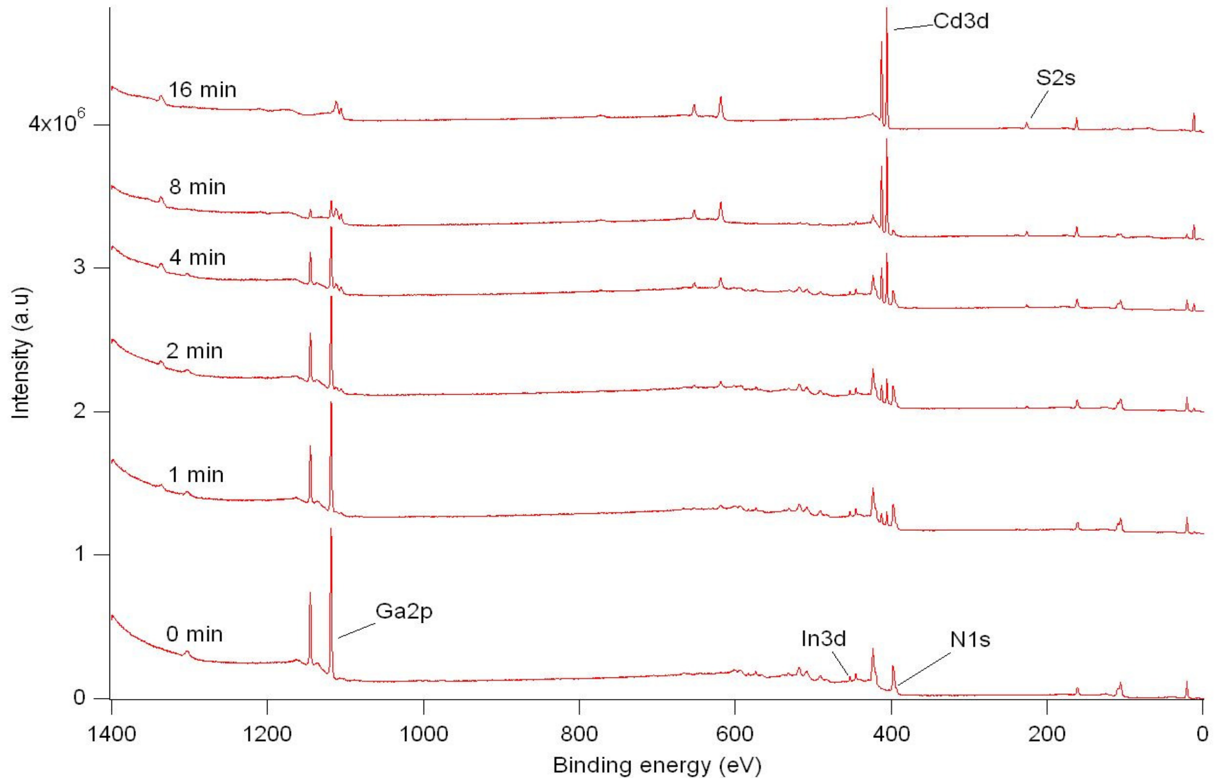

Survey XPS measurements as the sample transitions from bulk InGaN (0 min) to bulk CdS (16 min)

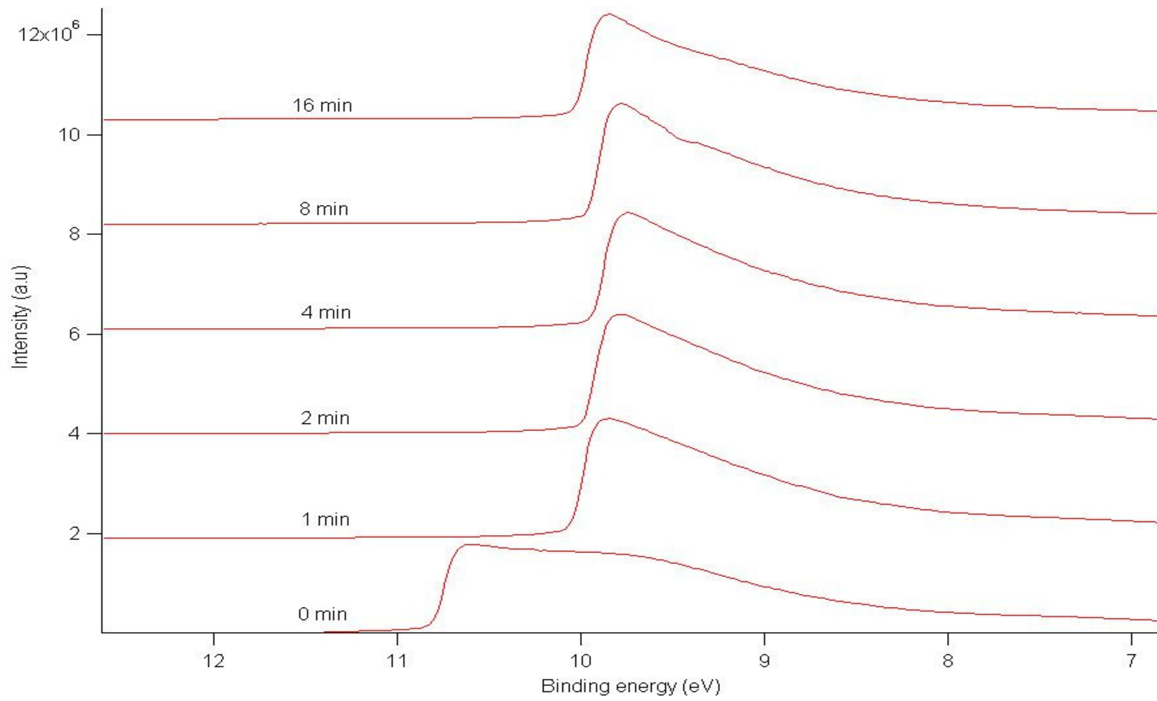

UPS measurements as the transitions from bulk InGaN (0 min) to bulk CdS (16 min)

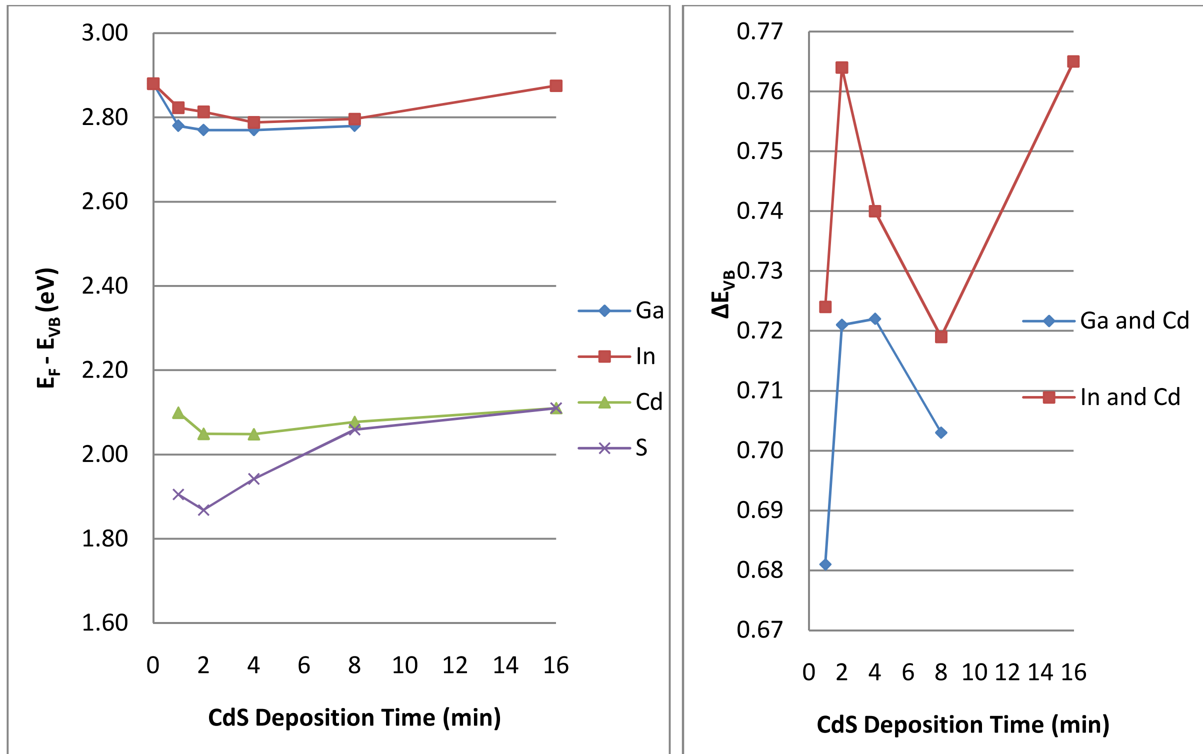

Left: The change in Fermi level position for each element as the interface study proceeds. Right: The change in valence band offset between the two materials as the interface study proceeds.